CHAPTER 19

Radar Tracking Algorithms

W. Dale Blair

Chapter Outline

19.1 INTRODUCTION

When radar systems are discussed in the literature or the remainder of this text, it is in the context of a sensor providing observations of the environment. While some of those measurements are responses from coherent waveforms of finite duration, the environment is treated as stationary with at most linear motion on the targets. Target tracking addresses the integration of measurements into a longer-term picture as illustrated in Figure 19-1. Target tracking is separated into two parts: *track filtering* and *measurement-to-track data association*.

Track filtering is the process of estimating the trajectory (i.e., position, velocity, and possibly acceleration) of a track from measurements (e.g., range, bearing, and elevation) that have been assigned to that track. As shown in Figure 19-1, a trajectory estimate always has an associated uncertainty that is characterized by the covariance of the estimate. The position and velocity estimates are used to predict the next measurement and, in the case of an electronically scanned (or phased array) radar, the position of the beam for the next measurement as illustrated in Figure 19-2.

Measurement-to-track data association (or data association) is the process of assigning a measurement to an existing track or as a detection of a newly found target or false signal. In Figure 19-2, three measurements (or threshold exceedances) occur in the dwell. Two measurements fall in the validation region (or gate) for the predicted measurement of the track, while the third measurement falls outside the validation region. Typically, the

FIGURE 19-1 ■ Tracking and prediction for a phased array radar.

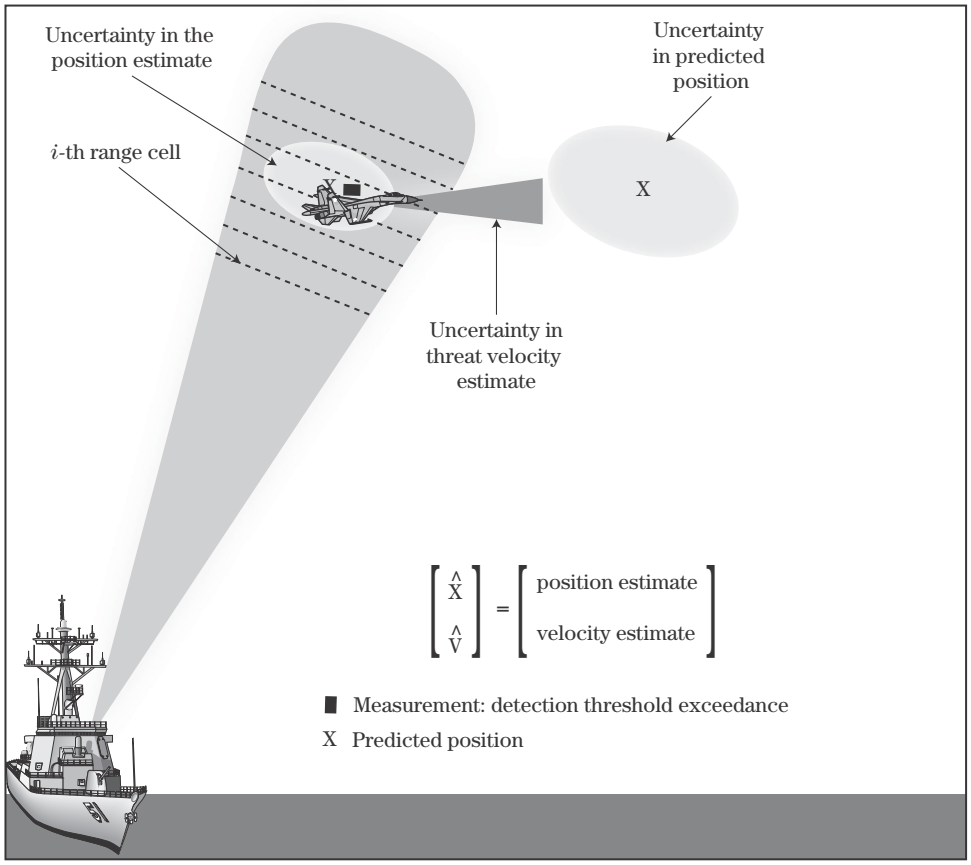

FIGURE 19-2 ■ Gating and assignment algorithms couple new measurements to a track.

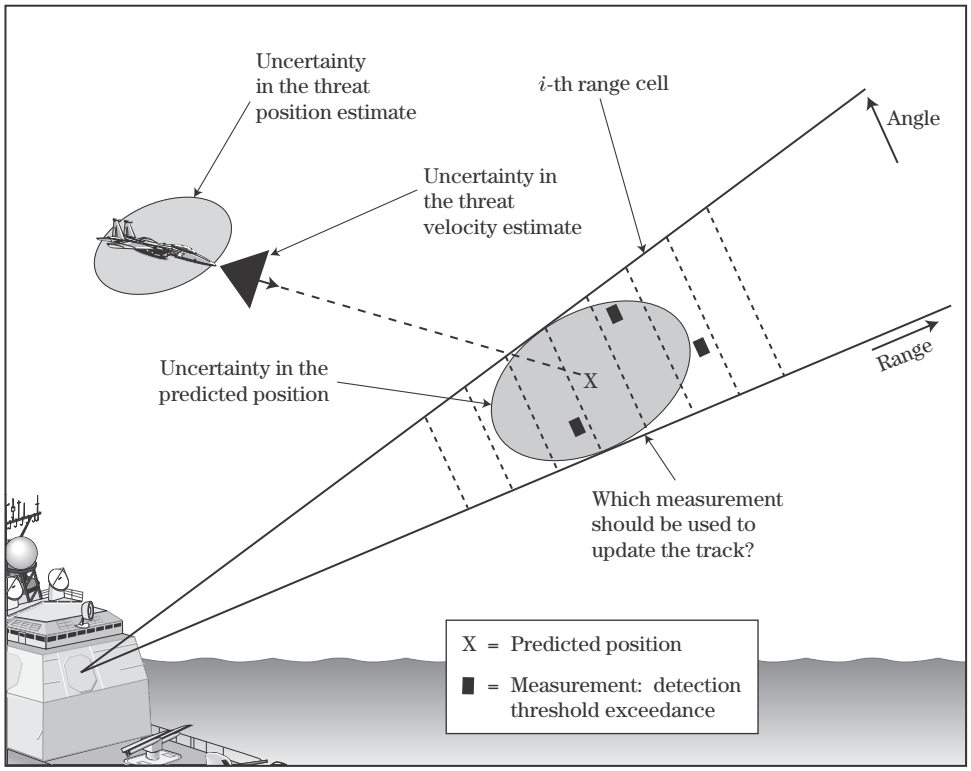

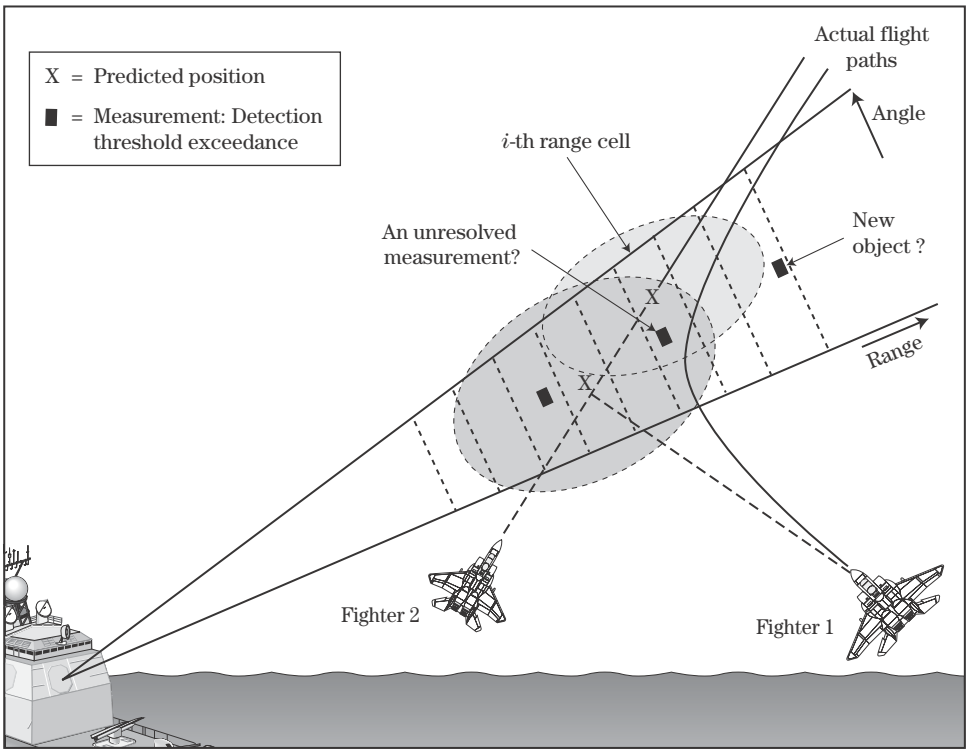

FIGURE 19-3 ■ Resolution and measurement-to-track association are critical for accurate tracking.

measurement in the validation region that is closest to the predicted measurement is used to update the estimates of position and velocity of the track, while the second measurement in the validation gate and the measurement outside the validation region are considered to be false measurement or used to initiate a new tentative track.

The track filtering and measurement-to-track association is further complicated by target maneuvers, closely spaced targets, and limited resolution of the radar. In Figure 19-2, a target maneuver could have easily switched the roles of the three measurements in the assignment. In this case, the measurement outside the validation gate is likely the target-originated measurement, while the measurements inside the gate are false alarms. Thus, validation gates that account for target maneuvers are critical. Figure 19-3 shows measurements that further illustrate the tracking and data association problems in a multitarget environment. Two fighters are shown to be entering into formation. The data association problem is complicated by the overlap in the uncertainty in the predicted positions of the two fighters at the measurement time. The track of Fighter 1 has two possible measurements, while the track of Fighter 2 has one possible measurement. Also, one of the measurements could represent a new target that is not currently under track. In the measurement-to-track assignment problem, the measurement in both gates of the predicted positions of the two targets could be a merged measurement of the two aircraft or a resolved measurement of one of the two aircraft. If this measurement is assigned as a resolved measurement to the track on Fighter 1, a misdetection of Fighter 2 will be declared. On the other hand, if the measurement is assigned as a resolved measurement to Fighter 2, the other measurement will be assigned to Fighter 1. From the actual trajectories in Figure 19-3, the correct measurement-to-track assignment is the assignment of the

measurement in both validation gates to both aircraft as a merged measurement and the other possible measurement as a false alarm. If that merged measurement is assigned to Fighter 2 and the other measurement is assigned to Fighter 1, Fighter 1 will not be found near the predicted position in the following radar dwells and the track of Fighter 1 is likely to be lost. Various approaches to data association are given in [1,2].

In much of the literature on radar systems, target tracking is viewed from a single signal or single target perspective in that a single signal is selected by time of arrival or frequency, and an error signal is generated for tracking. For example, in [3] range tracking is achieved with early and late gates, and the difference in the signal amplitudes in the two gates are used to adjust the range estimate. For a radar system to perform *multiple target tracking* (MTT), the data processing must be treated differently. The role of the target tracking in a MTT radar is illustrated in Figure 19-4. The most significant differences with the view of [3] is the presence of the measurement-to-track assignment and track management functions in which multiple measurements are considered for the assignment to multiple tracks.

Targets, clutter, and electronic countermeasurements (ECMs) from the environment and false alarms from the receiver noise can cause tracks to be formed in the radar system. In target tracking, *track* denotes the position and velocity estimate that represents

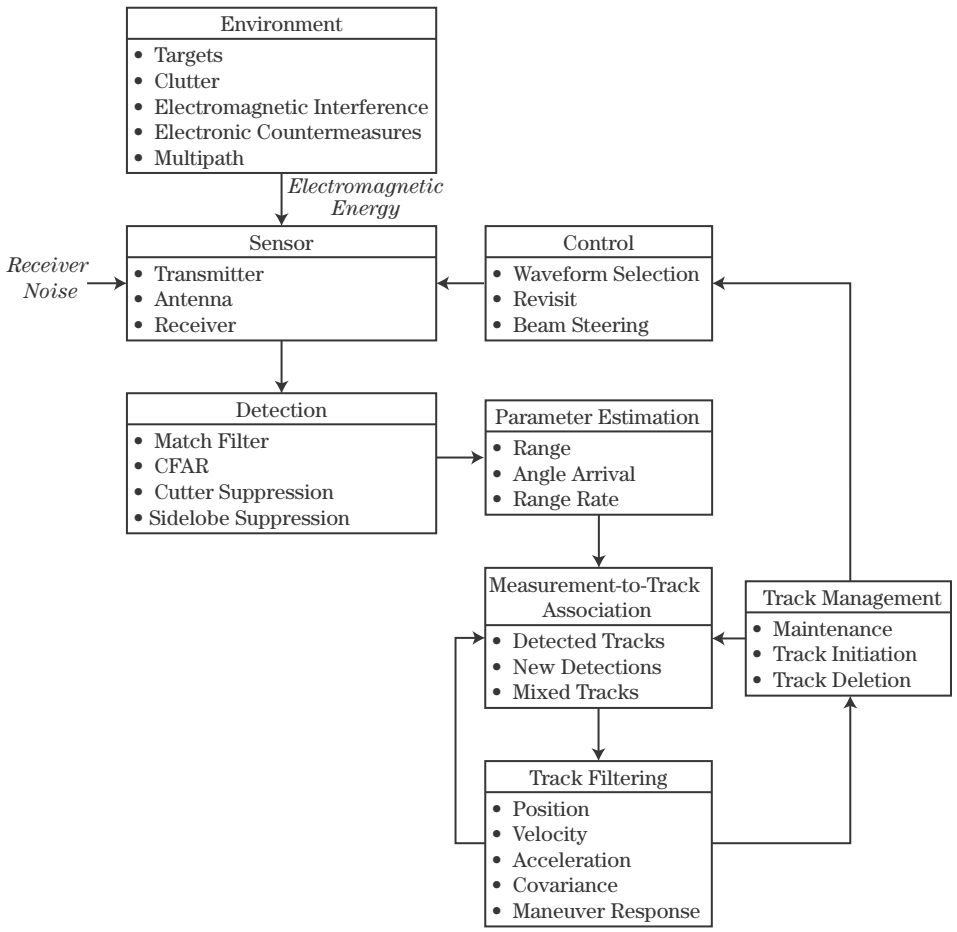

FIGURE 19-4 ■ Target tracking algorithms are highly sophisticated in modern radar systems.

something perceived to be in the environment, while *target* or *truth object* denotes something actually in the environment that should be tracked by the radar. Tracks are based solely on data collected by the radar, and the number of tracks held by a radar system can be larger (extra) or smaller (missed) than the number of targets. Ideally, the number of tracks will equal the number of targets. Clutter rejection techniques such as Doppler processing are used to reduce the clutter in a radar system. The radar returns are also monitored to detect the presence of ECM, and special processing is employed to minimize the number of false tracks introduced.

In the detection processing, signal amplitude and short time signal correlations are examined to reduce the number of false alarms and clutter detections reported to the tracker. Higher detection thresholds for a given signal-to-noise ratio (SNR) are used to the reduce the effects of false alarms. However, the higher detection thresholds also reduce the probability of detecting the true target. Constant false alarm processing (CFAR) is a classical approach to limiting the number of false detections. In CFAR processing, the detection threshold for a range cell or matched filter output is adjusted to reflect the noise level of the nearby range cells. Special processing can also be employed to prevent the declaration of threshold exceedances due to range sidelobes as detections of targets. Space-time adaptive processing (STAP) or Doppler processing can be employed to reduce the effects of clutter.

In the parameter estimation, estimates of the range, angle of arrival, and possibly range rate are produced for all of the detections and provided as measurements to the measurement-to-track association function and track filter. In the measurement-to-track association, measurements are assigned to existing tracks, and unassigned measurements are declared as a false alarms or new targets. Tracks that are not assigned a measurement are declared as missed. A track miss does not necessarily imply a missed detection, because a measurement from the target associated with the track could have been assigned incorrectly to a different track or the measurement could have failed the gating test with the correct track. Measurements that are assigned to existing tracks are provided to the track filter for updating the estimates of position and velocity. Unassigned measurements are considered with other unassigned measurements at different times for initiation of new tracks. Track misses are monitored for deleting a track or declaring a it as lost. The track management function monitors the number of measurements assigned to a track and declares the maturity of the track as a tentative or firm. It also monitors track misses and declares a track as lost for removal from the list of confirmed tracks. The control function monitors the list of tentative and firm tracks and clutter along with the track accuracies to schedules the timing and waveform for radar dwells.

As illustrated in Figure 19-5, tracking targets can be viewed as four functional areas: detection, resolution, association, and filtering. As shown in the upper left corner of Figure 19-5, detection is the first step in tracking a target. Detection of target echoes occurs in the presence of false alarms and clutter. The detection threshold that sets the false alarm rate and probability of detection also sets the performance limits of the tracker. Clutter is often countered with Doppler processing for clutter rejection, a clutter map, or tracking of moving clutter. As indicated in Figure 19-5, the second step of tracking targets is resolving the signals of closely spaced objects or nearby clutter into separate/isolated measurements. In radar systems, closely spaced targets are typically resolved in either range, angle, or range rate. Radars tend to be very effective in resolving closely spaced objects in range with waveforms of wider bandwidths and resolving targets from background clutter with Doppler processing. The third step of tracking targets is assigning measurements to tracks.

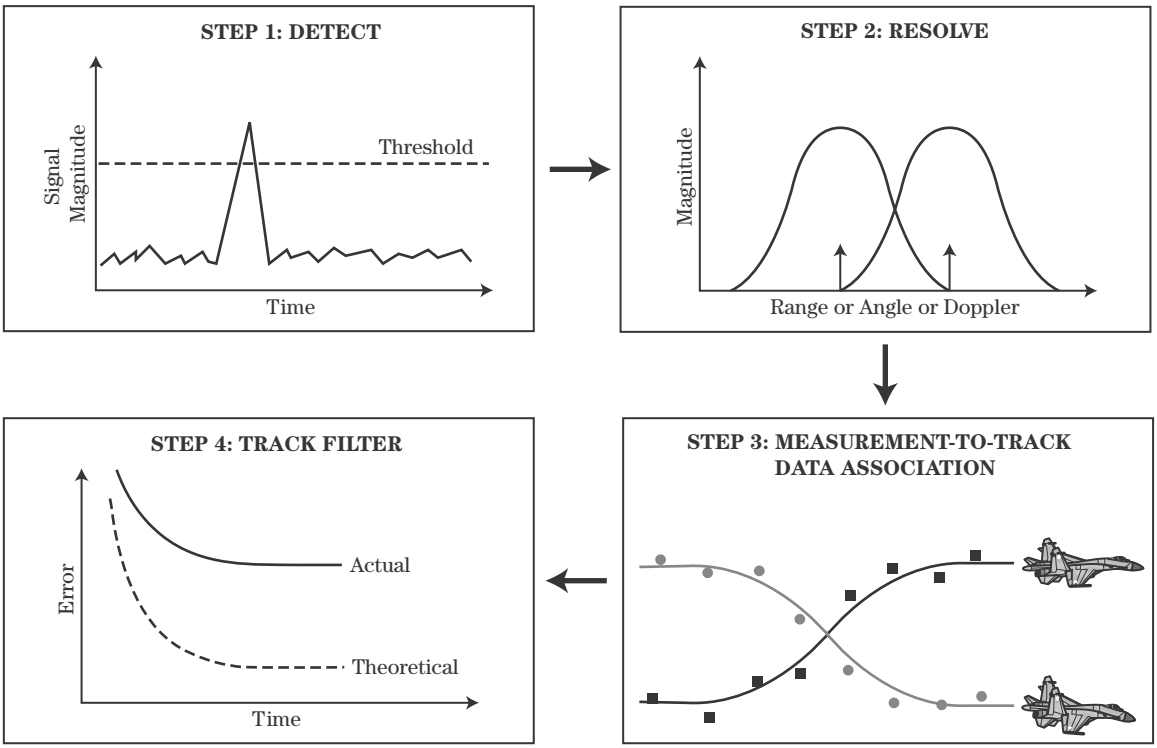

FIGURE 19-5 ■ Functional tracking components begin with detections and end with track filtering before the process repeats.

This involves assigning measurements to existing tracks, initiating new tracks, and deleting tracks that are not perceived to represent a truth object. As shown in Figure 19-5, the fourth step involves the track filtering to estimate the position, velocity, and possibly acceleration of the target. The performance of the track filter is often analyzed under ideal conditions and the performance is found to be below expectations when tested in the field.

This chapter addresses the fundamentals of tracking a single target with a radar, while the advanced topics associated with tracking multiple targets are addressed in [4]. The basics of *kinematic state estimation* (or track filtering) are discussed in Section 19.2. The section discusses the parametric and stochastic state estimation approaches to track filtering and addresses the use of least squares estimation, *Kalman filtering*, *alpha-beta filters*, and the *interacting multiple model* (IMM) estimator for tracking maneuvering targets. The kinematic models commonly used in track filtering are reviewed in Section 19.3, while the measurement models are discussed in Section 19.4. The application of the estimation methods discussed in Section 19.2 to the models presented in Sections 19.3 and 19.4 are discussed in Section 19.5. Measurement-to-track data association for a single target in the presence of false signals is discussed in Section 19.6, where the topics include measurement validation and gating, *strongest neighbor tracking*, *nearest neighbor tracking*, and the *probabilistic data association filter* (PDAF). In Section 19.7, performance assessment of track filtering algorithms is discussed. Key results and suggestions for further reading are provided in Section 19.8.

19.2 BASICS OF TRACK FILTERING

Given the decision to assign a measurement to a particular track, an update to the kinematic state estimate is performed for the track with that measurement. For most radar systems, the target motion is modeled in Cartesian coordinates, while radar measurements are typically in polar or spherical coordinates. For this basic treatment of track filtering, the kinematic state of the target will be represented in a single Cartesian coordinate, and the radar measurement will be treated as a linear observation of that kinematic state.

Let $\boldsymbol{X}_k$ denote the kinematic state vector at time t_k and $\boldsymbol{Z}_k$ denote the measurement at time t_k. The state estimate for t_k given measurements through t_j is denoted by $\boldsymbol{X}_{k|j}$. Thus, when the state vector has a single subscript, it denotes a truth or modeled value, and when it has two subscripts, it represents an estimate. The state estimate $\boldsymbol{X}_{k|k}$ is referred to as the filtered state estimate, while $\boldsymbol{X}_{k|k-1}$ is referred to as the one-step prediction of the state. The estimate $\boldsymbol{X}_{k|k+1}$ is referred to as the one-step smoothed estimate.

Track filtering algorithms typically fall into one of two groups. The first group uses a parametric estimation approach that presumes a perfect model for the target motion and the time period over which the model is applied is limited to prevent distortion of the data. In this approach, the covariance of the state estimate (or track) will approach zero as more data are processed. As the covariance of the track error approaches zero, the gain for processing new data will approach zero. When this processing gain reaches a very small number, all future data will be essentially ignored. Thus, since all motion models are imperfect in practice, the time period for which the perfect model is applied is limited to alleviate the distortion that results when new data are ignored. Least squares or maximum likelihood (ML) estimation are examples of the parametric approach to track filtering.

The second group uses a stochastic state estimation approach that presumes an imperfect model for the target motion. In this approach, the target motion model includes a random process, and a perfect estimate of the kinematic state is not possible. In other words, the covariance of the track does not approach zero as the window of data expands. As the model is applied over an expanding window of measurements, the covariance of the track settles to a stable, slowing changing value. If the measurement rate is fixed and the data quality is uniform, the filter will achieve "steady-state" conditions in which the covariance is the same value after each measurement update. The Kalman filter and alpha-beta filter are examples of the the stochastic state estimation approach.

One of the most critical items of a tracking system that supports any automatic decision system is track filter consistency. A track filter is considered to be *consistent* if the following three criteria are satisfied [5]:

1. The state errors should be acceptable as zero mean and have magnitudes commensurate with the state covariance as yielded by the filter.
2. The *innovations* (i.e., residuals or difference between the measurement and predicted measurement) should be acceptable as zero mean and have magnitudes commensurate with the innovation covariance as yielded by the filter.
3. The innovations should be acceptable as a white error process.

In other words, a track filter that is consistent produces a state error covariance that accurately represents the errors in the state estimate. Thus, track filter consistency is critical for effective fusion of data from multiple sensors with diverse accuracies. Maneuvering targets pose a particularly difficult challenge to achieving track filter consistency. In fact, [6]

includes an illustrative example that shows that more data does not necessary mean better estimates when a Kalman filter is used to track a maneuvering target. Using a Kalman filter to track a maneuvering target will not provide reliable tracking performance because the loss of track filter consistency prevents reliable decision making for simultaneously adapting the filter parameters and performing data association.

In this section, parametric and stochastic state approaches are discussed in further detail.

19.2.1 Parametric Estimation

For a typical parametric approach, the dynamical motion and measurement equations for tracking a target are given by

$$\boldsymbol{X}_{k+1} = \mathbf{F}_k \boldsymbol{X}_k \tag{19.1}$$

$$\boldsymbol{Z}_k = \mathbf{H}_k \boldsymbol{X}_k + \boldsymbol{w}_k \tag{19.2}$$

where $\boldsymbol{X}_k$ is the state vector for the target at time t_k, $\mathbf{F}_k$ defines the kinematic motion constraint between between time t_k and time t_{k+1}, $\boldsymbol{Z}_k$ is the sensor measurement vector at time t_k, $\mathbf{H}_k$ is the output matrix that relates the kinematic state to the measurement, and $\boldsymbol{w}_k$ is the sensor measurement error that is considered to be a zero-mean, Gaussian random variable with covariance $\mathbf{R}_k$, denoted $\boldsymbol{w}_k \sim \mathrm{N}(0, \mathbf{R}_k)$.

Figure 19-6 gives the position of a target trajectory in a single coordinate versus time and measurements for times t_1 through t_9. Figure 19-6 also includes an illustration of a parametric estimate based on constant velocity motion for the target. Note that the slope of the line illustrating the velocity estimate is constant indicating a velocity estimate that is fixed for all time t_k. The constant velocity estimate of the trajectory poorly represents the true trajectory near t_5 and t_9. If these errors are acceptable for the application of interest, the parametric estimator based on constant velocity is an acceptable solution. However, if the time expands beyond t_9, it is likely to become unacceptable.

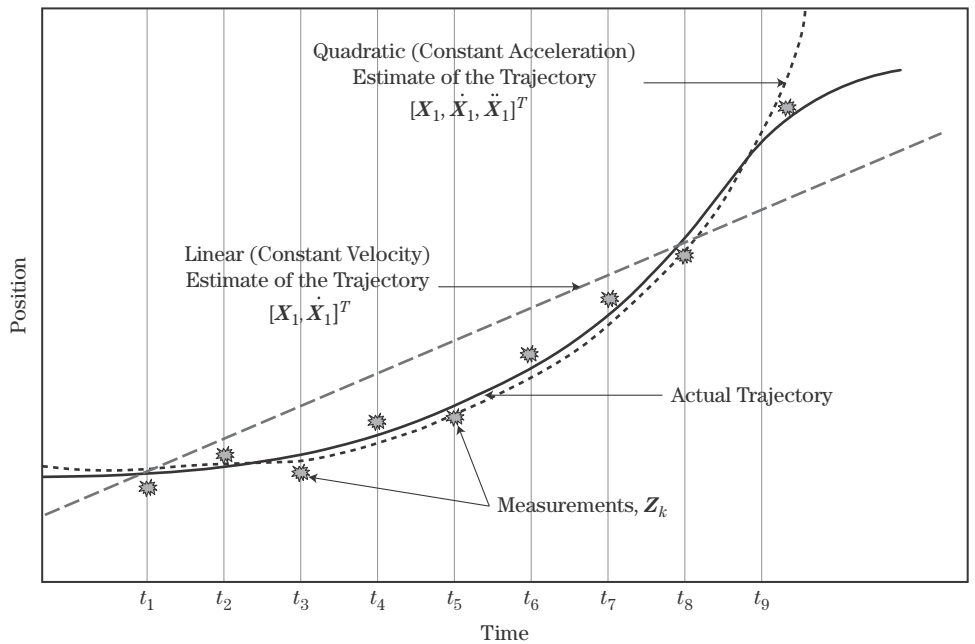

FIGURE 19-6 ■ Parametric approach to track filtering performs curve fitting to measurement data.

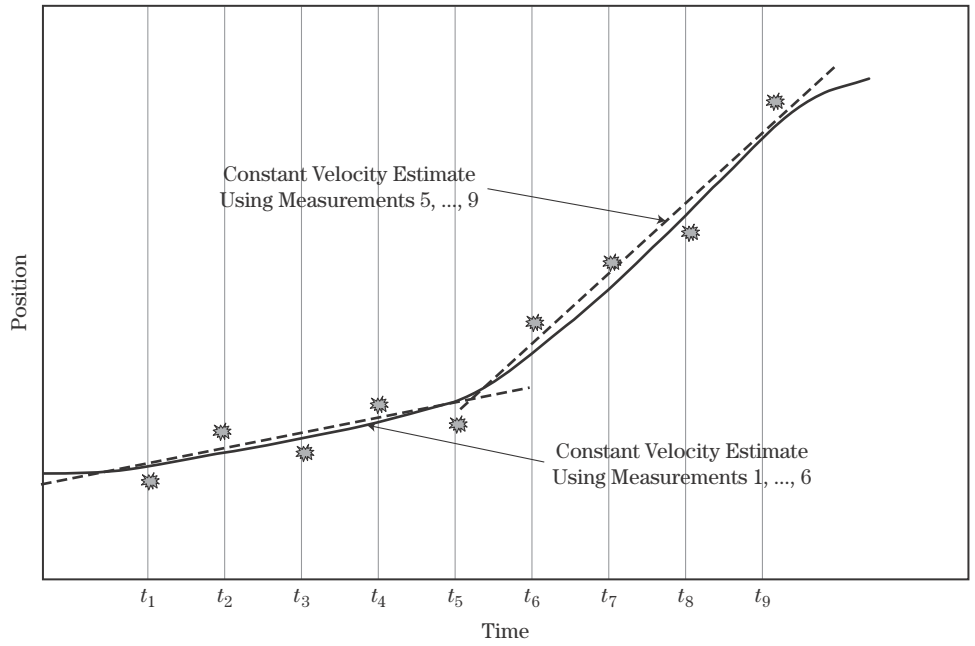

FIGURE 19-7 ■ Limiting memory in parametric approach to track filtering accommodates modeling errors.

Often, the first response to a constant velocity estimator that gives unacceptable performance is to use a higher order estimator (e.g., constant acceleration estimator). Figure 19-6 includes an illustration of a parametric estimate based on constant acceleration motion for the target. The constant acceleration estimator gives smaller errors than the constant velocity estimator near t_5 and t_9. However, estimating an additional parameter in this case results in estimates of position and velocity with higher variances. Furthermore, as the final time expands beyond t_9, the constant acceleration estimate is likely to become unacceptable.

In the application of parametric estimators, the period of time for application of the "perfect model" (i.e., the memory of the estimator) is limited to reduce the mismatch between the true trajectory and the assumed model. Figure 19-7 illustrates the application of the constant velocity estimator with a memory of five measurements. The state estimate for each time is computed from the data in a window of five measurements prior to and including the time of the estimate. This estimator is often referred to as a *sliding window estimator*. Note that the estimates based on fewer measurements will have a higher variance, but the distortions of the underlying true trajectory will be less.

Using (19.1) and (19.2), the measurement at t_N can be rewritten as

$$\boldsymbol{Z}_N = \mathbf{H}_N \boldsymbol{X}_N + \boldsymbol{w}_N = \mathbf{H}_k \mathbf{F}_{N-1} \mathbf{F}_{N-2} \ldots \mathbf{F}_1 \boldsymbol{X}_1 + \boldsymbol{w}_k \tag{19.3}$$

Given N measurements between t_1 and t_N, an augmented measurement equation can be written in terms of $\boldsymbol{X}_1$ as

$$\bar{\boldsymbol{Z}}_1^N = \begin{bmatrix} \boldsymbol{Z}_1 \\ \boldsymbol{Z}_2 \\ \vdots \\ \boldsymbol{Z}_{N-1} \\ \boldsymbol{Z}_N \end{bmatrix} = \begin{bmatrix} \mathbf{H}_1 \\ \mathbf{H}_2\mathbf{F}_1 \\ \vdots \\ \mathbf{H}_{N-1}\mathbf{F}_{N-2}\mathbf{F}_{N-3} \ldots \mathbf{F}_1 \\ \mathbf{H}_N\mathbf{F}_{N-1}\mathbf{F}_{N-2} \ldots \mathbf{F}_1 \end{bmatrix} \boldsymbol{X}_1 + \begin{bmatrix} \boldsymbol{w}_1 \\ \boldsymbol{w}_2 \\ \vdots \\ \boldsymbol{w}_{N-1} \\ \boldsymbol{w}_N \end{bmatrix} = \bar{\mathbf{H}}_N \boldsymbol{X}_1 + \bar{\boldsymbol{W}}_N \tag{19.4}$$

In this case, $\mathrm{E}\{\bar{W}_N\} = 0$, and

$$\bar{\mathbf{H}}_N = \begin{bmatrix} \mathbf{H}_1 \\ \mathbf{H}_2\mathbf{F}_1 \\ \vdots \\ \mathbf{H}_{N-1}\mathbf{F}_{N-2}\mathbf{F}_{N-3}\ldots\mathbf{F}_1 \\ \mathbf{H}_N\mathbf{F}_{N-1}\mathbf{F}_{N-2}\ldots\mathbf{F}_1 \end{bmatrix} \tag{19.5}$$

$$\bar{R}_N = \mathrm{E}\{\bar{W}_N\bar{W}_N^T\} = \begin{bmatrix} \mathbf{R}_1 & \mathbf{0} & \ldots & \mathbf{0} \\ \mathbf{0} & \mathbf{R}_2 & \ldots & \vdots \\ \vdots & & \ddots & \\ \mathbf{0} & \ldots & \mathbf{0} & \mathbf{R}_N \end{bmatrix} \tag{19.6}$$

In this case, $\bar{\mathbf{R}}_N$ is a block diagonal matrix because the measurement errors between any two times are assumed to be zero mean and independent. When the errors are correlated across time, the off-diagonal elements of the matrix are nonzero. The minimum mean squared error (MMSE) for Gaussian errors or weighted least squares estimate (LSE) [7] of $\boldsymbol{X}_1$ given measurements from t_1 to t_N is given by

$$\boldsymbol{X}_{1|N} = \left(\bar{\mathbf{H}}_N^T\bar{\mathbf{R}}_N^{-1}\bar{\mathbf{H}}_N\right)^{-1}\bar{\mathbf{H}}_N^T\bar{\mathbf{R}}_N^{-1}\bar{\boldsymbol{Z}}_1^N \tag{19.7}$$

and the covariance of the estimate is given by

$$\mathbf{P}_{1|N} = \left(\bar{\mathbf{H}}_N^T\bar{\mathbf{R}}_N^{-1}\bar{\mathbf{H}}_N\right)^{-1} \tag{19.8}$$

Note that the covariance will reflect only the actual errors in the state estimate to the degree that the kinematic model (19.1) is accurate and the measurement errors are zero-mean Gaussian with covariance $\bar{\mathbf{R}}_N$. The $\boldsymbol{X}_{1|N}$ and $\mathbf{P}_{1|N}$ are smoothed estimates. For a state estimate and covariance at time t_j, $t_1 < t_j \leq t_N$,

$$\boldsymbol{X}_{j|N} = \mathbf{F}_{j-1}\ldots\mathbf{F}_1\boldsymbol{X}_{1|N} \tag{19.9}$$

$$\mathbf{P}_{j|N} = \mathbf{F}_{j-1}\ldots\mathbf{F}_1\mathbf{P}_{1|N}\mathbf{F}_1^T\ldots\mathbf{F}_{j-1}^T \tag{19.10}$$

In this case, $\boldsymbol{X}_{j|N}$ is an MMSE estimate of $\boldsymbol{X}_j$. For the Gaussian errors, $\boldsymbol{X}_{j|N}$ is also the ML estimate of $\boldsymbol{X}_j$.

For the parametric approach, constant velocity and constant acceleration are the two most common assumptions for the motion of the target. Thus, constant velocity filtering and constant acceleration filtering are discussed here.

19.2.1.1 Constant Velocity Filtering

Let x_k denote the position of the x coordinate of the target at time t_k and $\dot{x}_k$ denote the velocity of the x coordinate of the target at time t_k. For a target moving with a constant velocity, the kinematic state at time t_{k+1} in terms of the state at time t_k is given by

$$x_{k+1} = x_k + (t_{k+1} - t_k)\dot{x}_k \tag{19.11}$$

$$\dot{x}_{k+1} = \dot{x}_k \tag{19.12}$$

This evolution of the target state can be written as

$$\boldsymbol{X}_{k+1} = \begin{bmatrix} x_{k+1} \\ \dot{x}_{k+1} \end{bmatrix} = \begin{bmatrix} 1 & (t_{k+1} - t_k) \\ 0 & 1 \end{bmatrix} \begin{bmatrix} x_k \\ \dot{x}_k \end{bmatrix} = \mathbf{F}_k \boldsymbol{X}_k \tag{19.13}$$

For a measurement of the position of the target at t_k,

$$Z_k = x_k + w_k = \begin{bmatrix} 1 & 0 \end{bmatrix} \begin{bmatrix} x_k \\ \dot{x}_k \end{bmatrix} + w_k = \mathbf{H}_k \boldsymbol{X}_k + w_k \tag{19.14}$$

where w_k is a scalar Gaussian random variable with variance σ_{wk}^2 and $\mathbf{H}_k = \begin{bmatrix} 1 & 0 \end{bmatrix}^T$. In this case, (19.5) and (19.6) are given by

$$\bar{\mathbf{H}}_N = \begin{bmatrix} 1 & 0 \\ 1 & t_2 - t_1 \\ \vdots & \vdots \\ 1 & t_{N-1} - t_1 \\ 1 & t_N - t_1 \end{bmatrix} \tag{19.15}$$

$$\bar{\mathbf{R}}_N = \begin{bmatrix} \sigma_{w1}^2 & 0 & \dots & 0 \\ 0 & \sigma_{w2}^2 & \dots & 0 \\ \vdots & & \ddots & \vdots \\ 0 & 0 & \dots & \sigma_{wN}^2 \end{bmatrix} \tag{19.16}$$

Thus, $\bar{\mathbf{H}}_N$ and $\bar{\mathbf{R}}_N$ have rather simple forms that can be easily manipulated. For N measurements with uniform sampling in time with period T and equal variances $\sigma_{wk}^2 = \sigma_w^2$,

$$\bar{\mathbf{H}}_N = \begin{bmatrix} 1 & 0 \\ \vdots & \vdots \\ 1 & (N-2)T \\ 1 & (N-1)T \end{bmatrix} \tag{19.17}$$

$$\bar{\mathbf{R}}_N = \sigma_w^2 \mathbf{I}_N \tag{19.18}$$

where $\mathbf{I}_N$ is an N dimensional identity matrix. For this case, the smoothed state estimate and covariance for t_1 are given by

$$\boldsymbol{X}_{1|N} = \frac{1}{N(N+1)} \begin{bmatrix} \displaystyle\sum_{k=1}^{N} (2N + 2 - 3k) Z_k \\ \dfrac{3}{(N-1)T} \displaystyle\sum_{k=1}^{N} (2k - N - 1) Z_k \end{bmatrix} \tag{19.19}$$

$$\mathbf{P}_{1|N} = \frac{2\sigma_w^2}{N(N+1)} \begin{bmatrix} 2N - 1 & -\dfrac{3}{T} \\ -\dfrac{3}{T} & \dfrac{6}{(N-1)T^2} \end{bmatrix} \tag{19.20}$$

The filtered state estimate and covariance for t_N are given by

$$\boldsymbol{X}_{N|N} = \frac{1}{N(N+1)} \begin{bmatrix} \sum_{k=1}^{N} (3k - N - 1) Z_k \\ \frac{3}{(N-1)T} \sum_{k=1}^{N} (2k - N - 1) Z_k \end{bmatrix} \tag{19.21}$$

$$\mathbf{P}_{N|N} = \frac{2\sigma_w^2}{N(N+1)} \begin{bmatrix} 2N-1 & \frac{3}{T} \\ \frac{3}{T} & \frac{6}{(N-1)T^2} \end{bmatrix} \tag{19.22}$$

Comparing the equations for the velocity estimates in (19.19) and (19.21) shows that they are identical for both times. However, the position estimates are different. A comparison of the expressions for the elements of the covariances in (19.20) and (19.22) shows that they are almost identical. The variances of the position and velocity estimates are identical. However, the covariance in the (1,2) or (2,1) elements of (19.20) for the smoothed position and velocity estimates in (19.19) is negative, while the covariance in the (1,2) or (2,1) elements of (19.22) for the filtered position and velocity estimates in (19.21) is positive.

A scalar coordinate of the trajectory of a maneuvering target is given in Figure 19-8 along with 120 measurements at integer times. The measurement errors have a standard deviation of 120 m. The trajectory starts at t_0 seconds with a initial position of $x_0 = 150$ m and initial velocity of $\dot{x}_0 = -20$ m/s and it moves with constant velocity until $t = 20$ s. From $t = 20$ until $t = 30$ s, the target maneuvers with acceleration of $\ddot{x} = 10$ m/s^2. From $t = 30$ until $t = 70$ s, the target moves with constant velocity motion. Then, the target maneuvers with acceleration of $\ddot{x} = -10$ m/s^2 from $t = 70$ until $t = 80$ s. Then, the target moves with constant velocity motion until $t = 120$ s. A constant velocity (CV) estimate based on all 120 measurements is also given in Figure 19-8. Note that the position estimates make a perfectly straight line and the velocity estimate (i.e., the slope of the line) is a constant for all time. The position estimates poorly match the true position near times of 0, 25, 75, and 120 s. On the other hand, the position estimates closely match the true position near times of 10, 50, and 90 s. The velocity estimates poorly match the true velocity

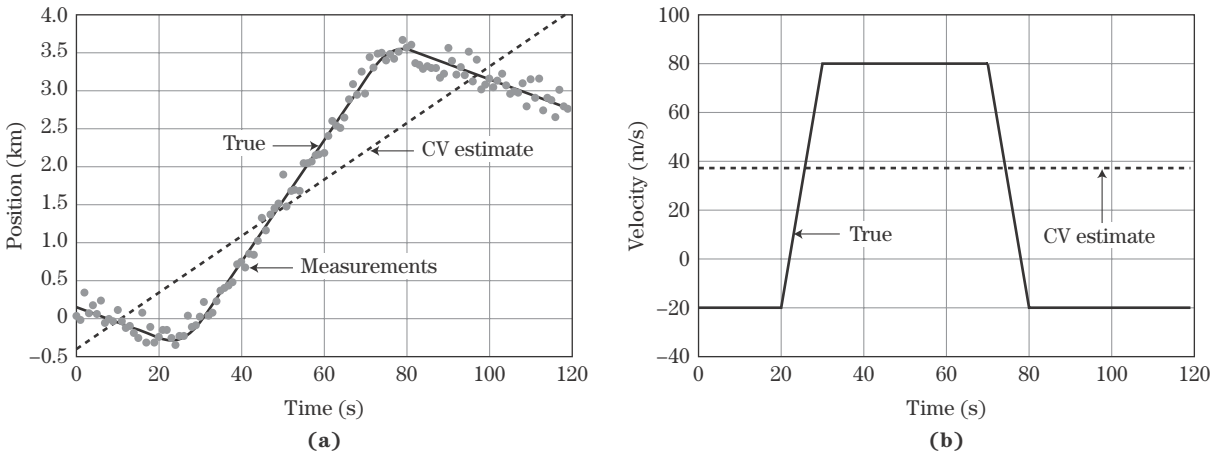

FIGURE 19-8 ■ Trajectory with measurements and the average constant velocity (CV) estimate. (a) Position. (b) Velocity.

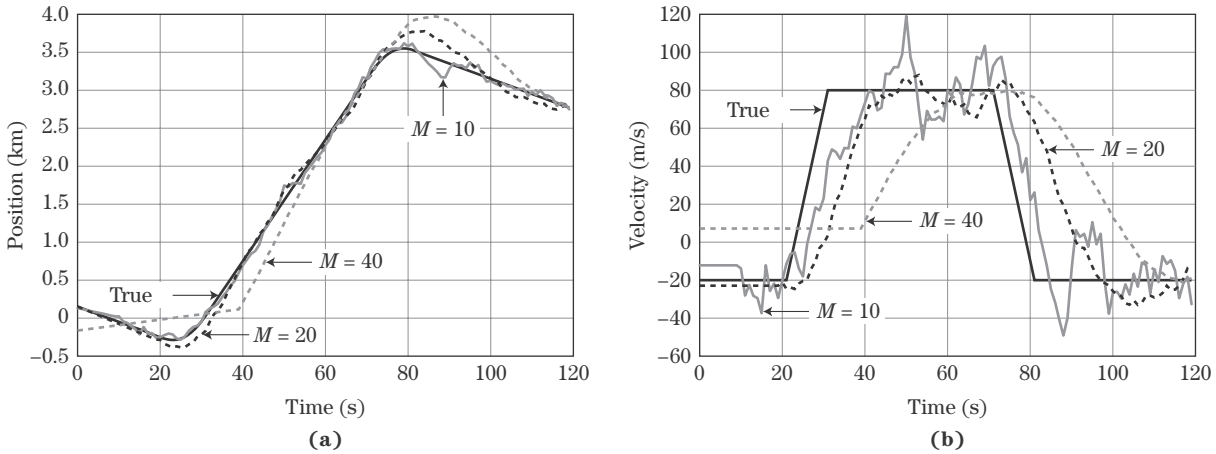

FIGURE 19-9 ■ Average CV position (a) and velocity (b) estimates with true values for memory of 10, 20, and 40 measurements.

at all times except those times near 25 and 75 s. The errors in the CV estimates will grow as the target maneuvers and continues to move beyond $t = 120$ s with a constant velocity. Thus, the number of measurements M (or memory) of the estimator must be limited.

If the distortions of the trajectory that are present in the estimates are unacceptable, the memory is limited to reduce the distortion or model mismatch. The averages of the CV estimates with memory of $M = 10, 20$, and 40 measurements over 2,000 Monte Carlo runs are shown in Figure 19-9. The first M measurements are used to initialize the tracking and the estimate at $t_k = t_{M-1}$ is a filtered estimate, while all of the estimates for $t_k < t_{M-1}$ are smoothed estimates. For $t_k \geq t_{M-1}$, the CV estimates are filtered estimates based on the current and $M-1$ previous measurements. In other words, the velocity estimate for the CV estimator with $M = 40$ is the same for $0 \leq t_k \leq 39$ s, and it will change value at $t_k = 40$ s. Note that the distortion or error in the position and velocity estimates as the maneuvers increase as M increases. For $M = 10$, distortion in the estimates is very little, while the distortion for $M = 40$ is large for the first 40 s and near 85 s. The *root mean squared error* (RMSE) of the CV estimator with $M = 10, 20$, and 40 measurements is given in Figure 19-10. Note that the smallest values of RMSE are achieved by the CV estimator with $M = 40$ after the maneuver has been expunged from the memory of the filter (i.e., $t = 70$ and 115 s). Also, note that the values of the RMSE of the CV estimator with $M = 10$ are the largest at those times. However, the values of RMSE of the CV estimator with $M = 10$ are the smallest during the maneuvers. Thus, the implementation or design of the CV estimator involves selecting the memory that best meets the requirements of the application.

A key aspect of a track filter is the accuracy of the covariance estimate. Generation of an accurate covariance is a challenge for maneuvering targets because most all estimation algorithms poorly model the acceleration and the uncertainty in the presence or absence of a maneuver. The accuracy of the covariance is measured through the normalized estimation error squared at time t_k given measurements through t_j by

$$C_{k|j} = (\boldsymbol{X}_{k|j} - \boldsymbol{X}_k)^T \mathbf{P}_{k|j}^{-1} (\boldsymbol{X}_{k|j} - \boldsymbol{X}_k) \tag{19.23}$$

For Gaussian errors in the state estimate with respect to the true state $\boldsymbol{X}_k$ and an accurate covariance $\mathbf{P}_{k|j}$, $C_{k|j}$ is chi-square distributed [7] with n degrees of freedom, where n is the size of the state vector. The average *normalized estimation error squared* (NEES)

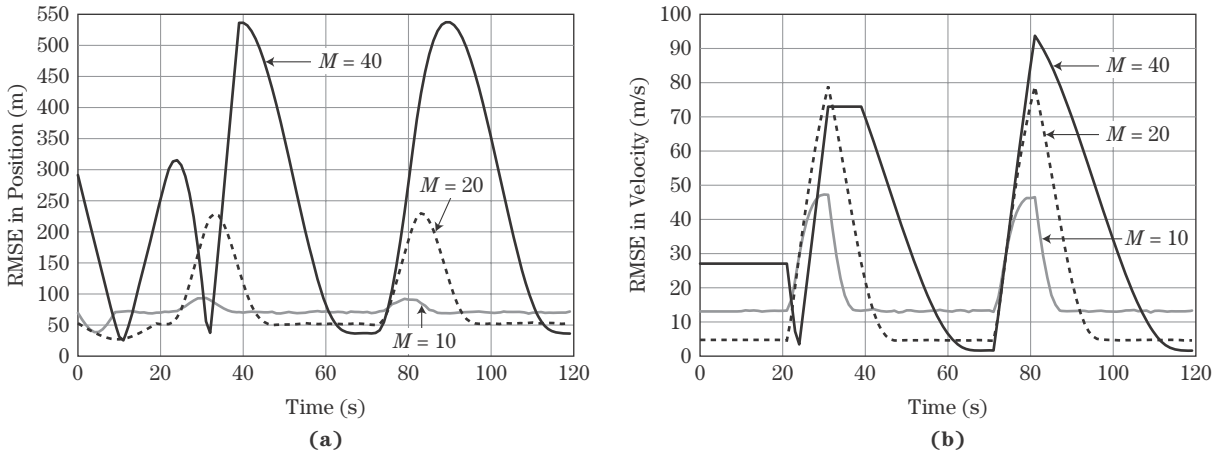

FIGURE 19-10 ■ RMSE of CV estimates with memory of 10, 20, and 40 measurements. (a) Position RMSE. (b) Velocity RMSE.

for the CV estimator with $M = 10$, 20, and 40 and 2,000 Monte Carlo runs is shown in Figure 19-11. For a single sample of the NEES for the CV estimate, it should be chi-square distributed with two degrees of freedom. The average value for $C_{k|k}$ should be two, and the chi-square tables in [7] give the 95% containment region for the NEES as $0.54 \leq C_{k|k} \leq 7.38$. According, in Figure 19-11, the average NEES of all three CV estimators closely matches two when the maneuver has been expunged from it memory. When more than a few seconds of target maneuver are included in the memory of the CV estimator, the average NEES is greater than 7.38 and falls outside the 95% confidence region for a two degree of freedom chi-square random variable. Thus, the presence of the maneuver significantly degrades the quality of the covariance estimate, and the quality degrades as M grows.

19.2.1.2 Constant Acceleration Filtering

Let $\ddot{x}_k$ denote the acceleration of the x coordinate of the target at time t_k. For a target moving with a constant acceleration, the kinematic state at time t_{k+1} given in terms of the state at time t_k is given by

$$x_{k+1} = x_k + (t_{k+1} - t_k)\dot{x}_k + \frac{1}{2}(t_{k+1} - t_k)^2\ddot{x}_k \tag{19.24}$$

$$\dot{x}_{k+1} = \dot{x}_k + (t_{k+1} - t_k)\ddot{x}_k \tag{19.25}$$

$$\ddot{x}_{k+1} = \ddot{x}_k \tag{19.26}$$

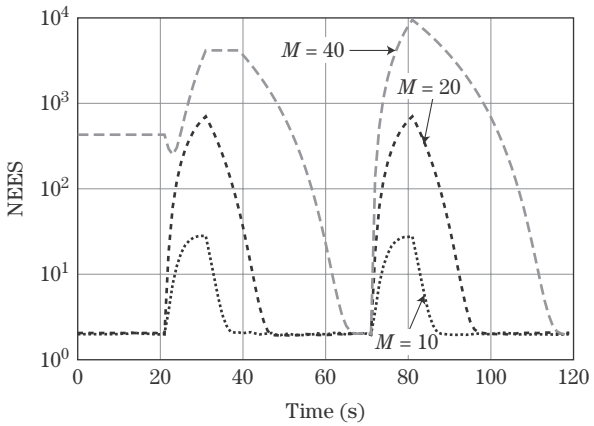

FIGURE 19-11 ■ Average NEES of CV estimates with memory of 10, 20, and 40 measurements.

This evolution of the target state can be written as

$$\boldsymbol{X}_{k+1} = \begin{bmatrix} x_{k+1} \\ \dot{x}_{k+1} \\ \ddot{x}_{k+1} \end{bmatrix} = \begin{bmatrix} 1 & (t_{k+1} - t_k) & \frac{1}{2}(t_{k+1} - t_k)^2 \\ 0 & 1 & (t_{k+1} - t_k) \\ 0 & 0 & 1 \end{bmatrix} \begin{bmatrix} x_k \\ \dot{x}_k \\ \ddot{x}_k \end{bmatrix} = \mathbf{F}_k \boldsymbol{X}_k \quad (19.27)$$

For measurements of the position of the target at t_k,

$$Z_k = x_k + w_k = \begin{bmatrix} 1 & 0 & 0 \end{bmatrix} \begin{bmatrix} x_k \\ \dot{x}_k \\ \ddot{x}_k \end{bmatrix} + w_k = \mathbf{H}_k \boldsymbol{X}_k + w_k \quad (19.28)$$

where w_k is a scalar Gaussian random variable with variance σ_{wk}^2. In this case, the smoothed estimate $\boldsymbol{X}_{1|N}$ is given by (19.7) and (19.8) with $\bar{\boldsymbol{Z}}_1^N$ given by (19.4), and $\mathbf{R}_N$ and $\bar{\mathbf{H}}_N$ are given by

$$\bar{\mathbf{H}}_N = \begin{bmatrix} 1 & 0 & 0 \\ 1 & t_2 - t_1 & \frac{1}{2}(t_2 - t_1)^2 \\ \vdots & \vdots & \vdots \\ 1 & t_{N-1} - t_1 & \frac{1}{2}(t_{N-1} - t_1)^2 \\ 1 & t_N - t_1 & \frac{1}{2}(t_N - t_1)^2 \end{bmatrix} \quad (19.29)$$

$$\bar{\mathbf{R}}_N = \begin{bmatrix} \sigma_{w1}^2 & 0 & \dots & 0 \\ 0 & \sigma_{w2}^2 & \dots & 0 \\ \vdots & \vdots & \ddots & \\ \vdots & 0 & \dots & \sigma_{wN}^2 \end{bmatrix} \quad (19.30)$$

For N measurements with uniform sampling with period T and equal variances $\sigma_{wk}^2 = \sigma_w^2$,

$$\bar{\mathbf{H}}_N = \begin{bmatrix} 1 & 0 & 0 \\ 1 & T & \frac{1}{2}T^2 \\ \vdots & \vdots & \vdots \\ 1 & (N-2)T & \frac{1}{2}(N-2)^2T^2 \\ 1 & (N-1)T & \frac{1}{2}(N-1)^2T^2 \end{bmatrix} \quad (19.31)$$

$$\bar{\mathbf{R}}_N = \sigma_w^2 \mathbf{I}_N \quad (19.32)$$

The estimate of the filtered state estimate and covariance are expressed in a form similar to (19.21) and (19.22) in [7]. However, the covariance is a 3×3 matrix and the variances of position and velocity are larger for a given N than in the case of the constant velocity estimator.

A constant acceleration estimate based on all 120 measurements could be envisioned for Figure 19-8. Note that the position estimates would form a perfectly quadratic line, the velocity would change linearly, and the acceleration estimate would be a constant for all time. The position and velocity estimates would poorly match the true values at one of the two ends of the trajectory. Thus, the number of measurements (or memory) of the estimator would have to be limited in order ensure reasonable performance.

19.2.2 Stochastic State Estimation

For stochastic state estimation, measurements are defined by (19.2) and the dynamical motion model is given by

$$\boldsymbol{X}_{k+1} = \mathbf{F}_k \boldsymbol{X}_k + \mathbf{G}_k \boldsymbol{v}_k \tag{19.33}$$

where

$\boldsymbol{v}_k$ = error in the system processes at time t_k with $v_k \sim \mathrm{N}(0, \mathbf{Q}_k)$.
$\mathbf{G}_k$ = relates the system errors to the target state at time t_k.

For a nearly constant velocity motion model, the state vector of the target in a scalar coordinate is given by

$$\boldsymbol{X}_k = \begin{bmatrix} x_k & \dot{x}_k \end{bmatrix}^T \tag{19.34}$$

where x_k represents the position of the target at time t_k, and $\dot{x}_k$ represents the velocity of the target. Process noise is included to account for the uncertainty associated with unknown maneuvers and unmodeled dynamics of the target under track. Since the evolution of the state includes a stochastic process, the state estimates are a stochastic process, and the covariance of the estimate will not achieve zero and grow in the absence of measurements.

The Kalman filter gives the MMSE and minimum variance estimate of the stochastic state $\boldsymbol{X}_k$. Since the random processes $\boldsymbol{v}_k$ and $\boldsymbol{w}_k$ are additive Gaussian and the Kalman filter is a linear filter, the state estimation error of the Kalman filter will be Gaussian. Thus, only the mean and covariance are needed to fully characterize the state estimation error. The Kalman filter is a predictor-corrector algorithm with the predictor accounting for changes in time and the corrector accounting for the measurement processing. The Kalman algorithm is defined by the following equations, where $\boldsymbol{X}_{k|j}$ denotes the state estimate at t_k given measurements through t_j, and $\mathbf{P}_{k|j}$ denotes the state error covariance at t_k given measurements through t_j:

Prediction of the state estimate and covariance to the next time:

$$\boldsymbol{X}_{k|k-1} = \mathbf{F}_{k-1} \boldsymbol{X}_{k-1|k-1} \tag{19.35}$$

$$\mathbf{P}_{k|k-1} = \mathbf{F}_{k-1} \mathbf{P}_{k-1|k-1} \mathbf{F}_{k-1}^T + \mathbf{G}_{k-1} \mathbf{Q}_{k-1} \mathbf{G}_{k-1}^T \tag{19.36}$$

Update of the state estimate and covariance with the measurement:

$$\boldsymbol{X}_{k|k} = \boldsymbol{X}_{k|k-1} + \mathbf{K}_k [\mathbf{Z}_k - \mathbf{H}_k \boldsymbol{X}_{k|k-1}] = \boldsymbol{X}_{k|k-1} + \mathbf{K}_k \widetilde{\mathbf{Z}}_k \tag{19.37}$$

$$\mathbf{P}_{k|k} = [\mathbf{I} - \mathbf{K}_k \mathbf{H}_k] \mathbf{P}_{k|k-1} \tag{19.38}$$

$$\mathbf{K}_k = \mathbf{P}_{k|k-1} \mathbf{H}_k^T \mathbf{S}_k^{-1} \tag{19.39}$$

$$\mathbf{S}_k = \mathbf{H}_k \mathbf{P}_{k|k-1} \mathbf{H}_k^T + \mathbf{R}_k \tag{19.40}$$

where $\mathbf{K}_k$ is referred to as the Kalman filter gain, $\widetilde{\mathbf{Z}}_k$ denotes the filter residual vector, and the $\mathbf{S}_k$ is the covariance of the measurement residual.

The processing of the Kalman filter for nearly constant velocity filtering is illustrated in Figure 19-12. The state estimate at time t_1 is predicted with constant velocity motion to t_2. The predicted state estimate $\boldsymbol{X}_{2|1}$ is then updated with measurement $\boldsymbol{Z}_2$ to produce the filtered state estimate $\boldsymbol{X}_{2|2}$. The filtered state estimate is an optimal weighting of the predicted measurement and the measurement. The filtered state estimate will tend to

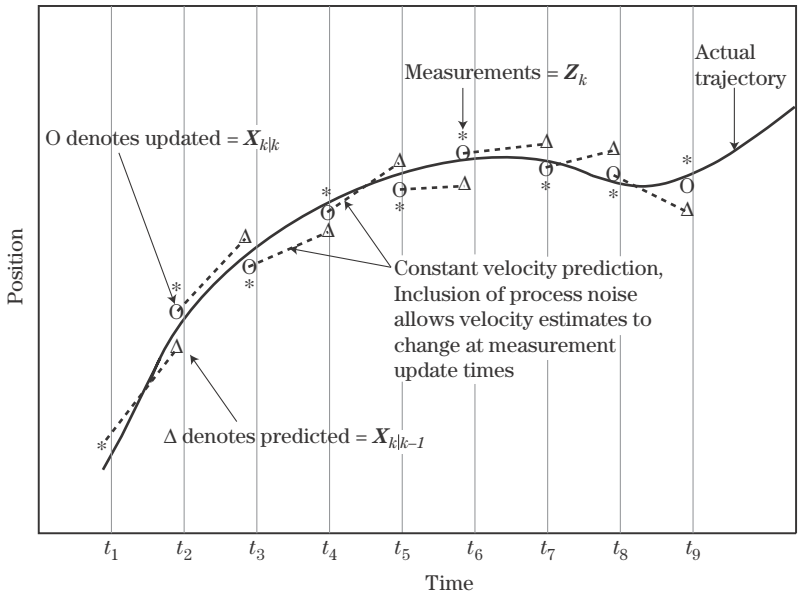

FIGURE 19-12 ■ Kalman filter process performs track filtering by correcting the predicted state with measurements.

"favor" the one with the smaller covariance. Note that the filtered state estimate lies on a line connecting the measurement and the position of the predicted measurement. This filter step is repeated for each measurement. Note that the velocity estimates (i.e., the slope of the prediction lines) are not constant over the window of data. In fact, it changes after every measurement update. The higher the process noise covariance is set, the more the velocity will change between measurement updates. For example, tracking a highly maneuvering air target will involve a large covariance for the process noise acceleration and the velocity estimate will make large changes between updates. For tracking ballistic targets above the atmosphere, the process noise covariance will be smaller and the velocity estimate will change much more slowly over time.

An alternate depiction of the processing of the Kalman filter is shown in Figure 19-13 as a predictor-corrector algorithm. The filter process is recursive. It starts with the initial

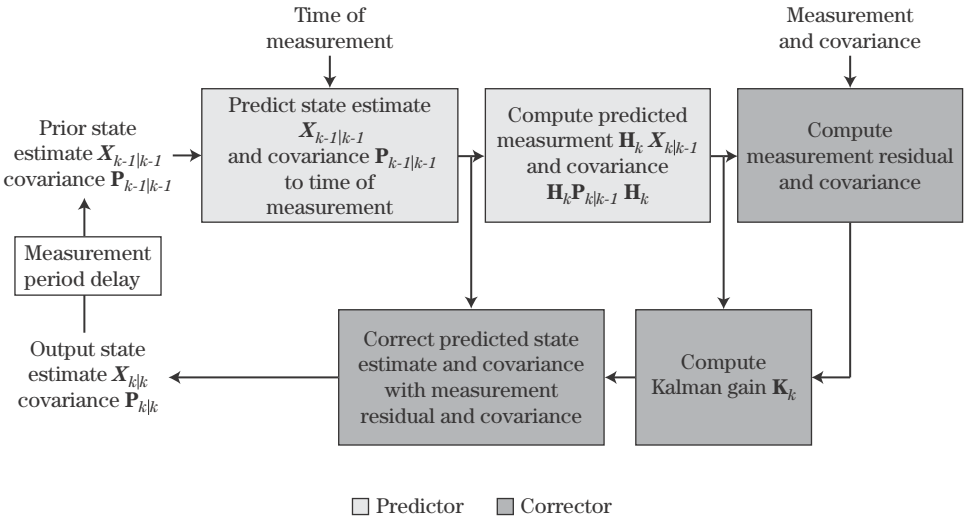

FIGURE 19-13 ■ Kalman filter is a predictor-corrector algorithm.

state estimate $\boldsymbol{X}_{k-1|k-1}$ and covariance $\mathbf{P}_{k-1|k-1}$ at time t_{k-1}. The filtered state estimate and covariance are predicted to the time of the measurement t_k to obtain $\boldsymbol{X}_{k|k-1}$ and $\mathbf{P}_{k|k-1}$. The predicted measurement and its covariance are then computed to complete the predictor. The measurement and its covariance are then used to compute the measurement residual and its covariance. Then the Kalman gain is computed and the predicted state is updated with the measurement residual and the Kalman gain to form the new filtered state estimate $\boldsymbol{X}_{k|k}$. The predicted covariance is updated with the Kalman gain to form the new filtered covariance $\mathbf{P}_{k|k}$. The new filtered state estimate $\boldsymbol{X}_{k|k}$ and covariance $\mathbf{P}_{k|k}$ are then retained until the next filter cycle in which they become the new initial state estimate and covariance.

Nearly constant velocity and *nearly constant acceleration* are the most commonly used motion models [2,7]. The choice of a model is governed by the maximum acceleration of the target, the quality of the sensor measurements, and the measurement rate. Since no algorithm exists for predicting the best model, experience in the design process and Monte Carlo simulations are typically used to assess the best model for a tracking system. If the quality of the measurements and the measurement rate are not sufficient to estimate acceleration during a maneuver, models that do not include acceleration in the target state will be the better models. For example, if only two or three measurements are taken during maneuvers, accurate estimation of the acceleration will not be possible and the acceleration should not be included in the target state. If the quality of the measurements and the measurement rate allow for estimation of the acceleration during a maneuver and the bias in the position estimates of the nearly constant velocity filter during the maximum acceleration of the target [8] is larger than the measurement errors, then acceleration should be included the target state.

Process noise is included to account for the uncertainty associated with the unknown maneuvers of the target. The process noise for nearly constant velocity motion is typically treated as *discrete white noise acceleration* (DWNA) errors or discretized *continuous-time white noise acceleration* (CWNA) [7]. Nearly constant velocity filtering with the two different models for process noise and two different models for measurements is discussed in the next three sections. The measurement models reflect standard radar measurements of position with linear frequency modulation (LFM) waveforms and fixed frequency waveforms. Nearly constant acceleration tracking and multiple model tracking for highly maneuvering targets are addressed to complete this section on stochastic state estimation.

19.2.2.1 Nearly Constant Velocity Filtering with DWNA

Nearly constant velocity motion with DWNA in a single coordinate is given by (19.33) with

$$\boldsymbol{X}_k = \begin{bmatrix} x_k & \dot{x}_k \end{bmatrix}^T \tag{19.41}$$

$$\mathbf{F}_k = \begin{bmatrix} 1 & \delta_k \\ 0 & 1 \end{bmatrix} \tag{19.42}$$

$$\boldsymbol{G}_k = \begin{bmatrix} \dfrac{\delta_k^2}{2} \\ \\ \delta_k \end{bmatrix} \tag{19.43}$$

$$Q_k = \sigma_{vk}^2 \tag{19.44}$$

where $\delta_k = t_k - t_{k-1}$. The v_k is a white noise acceleration error that is constant or fixed between t_k and t_{k-1} in the state process with $v_k \sim \mathrm{N}(0, \sigma_{vk}^2)$. For the nearly constant

velocity motion model, the process noise covariance matrix for DWNA is given by

$$\boldsymbol{G}_k Q_k \boldsymbol{G}_k^T = \sigma_{vk}^2 \begin{bmatrix} \frac{\delta_k^4}{4} & \frac{\delta_k^3}{2} \\ \frac{\delta_k^3}{2} & \delta_k^2 \end{bmatrix} \tag{19.45}$$

The σ_{vk} is the design parameter for the nearly constant velocity (NCV) filter with DWNA errors. Typically, the filter design process begins by setting σ_{vk} greater than one half of the maximum acceleration of the target and less than the maximum acceleration, and Monte Carlo simulations are conducted to further refine the selection of σ_{vk}. Further guidelines on the selection of σ_{vk} are developed in [9] and summarized next. Typically, the measurements are the position of the target. In this case, the measurement equation of (19.2) is defined by

$$\boldsymbol{H}_k = \begin{bmatrix} 1 & 0 \end{bmatrix} \tag{19.46}$$

When the error processes v_k and w_k are stationary (i.e., zero mean and constant variances) and the data rate is constant, the Kalman filter will achieve steady-state conditions in which the filtered state covariance and Kalman gain are constant. While these conditions are seldom satisfied in practice, the steady-state form of the filter can be used to predict average or expected tracking performance. The design and performance of the filter is characterized by the *maneuver index* or *random tracking index*

$$\Gamma_{DWNA} = \frac{\sigma_v T^2}{\sigma_w} = \frac{\beta}{\sqrt{1-\alpha}} \tag{19.47}$$

where $\sigma_v = \sigma_{vk}$, $\sigma_w = \sigma_{wk}$, and $T = t_k - t_{k-1}$ for all k. Under steady-state conditions, the NCV Kalman filter is equivalent to an alpha-beta filter. For the alpha-beta filter, the steady-state gains that occur after the transients associated with filter initialization diminish are given by

$$\boldsymbol{K}_k = \begin{bmatrix} \alpha & \frac{\beta}{T} \end{bmatrix}^T \tag{19.48}$$

where α and β are the optimal gains for DWNA given in [7,10]. The alpha-beta filter is rather simple and computationally efficient to implement because online real-time calculation of neither the state covariance nor gain is needed. The alpha-beta filter for a scalar coordinate is given by

$$x_{k|k-1} = x_{k-1|k-1} + T\dot{x}_{k-1|k-1} \tag{19.49}$$

$$\dot{x}_{k|k-1} = \dot{x}_{k-1|k-1} \tag{19.50}$$

$$x_{k|k} = x_{k|k-1} + \alpha[Z_k - x_{k|k-1}] \tag{19.51}$$

$$\dot{x}_{k|k} = \dot{x}_{k|k-1} + \frac{\beta}{T}[Z_k - x_{k|k-1}] \tag{19.52}$$

The steady-state error covariance of the alpha-beta filter is given by

$$\mathbf{P}_{\alpha\beta} = \sigma_w^2 \begin{bmatrix} \alpha & \frac{\beta}{T} \\ \frac{\beta}{T} & \frac{\beta(2\alpha-\beta)}{2(1-\alpha)T^2} \end{bmatrix} \tag{19.53}$$

Given the maneuver or tracking index, the steady-state filter gains are specified according to

$$\alpha = -\frac{1}{8}\Gamma_{DWNA}^2 - \Gamma_{DWNA} + \frac{1}{8}(\Gamma_{DWNA} + 4)\sqrt{\Gamma_{DWNA}^2 + 8\Gamma_{DWNA}} \tag{19.54}$$

$$\beta = \frac{1}{4}\Gamma_{DWNA}^2 + \Gamma_{DWNA} - \frac{1}{4}\Gamma_{DWNA}\sqrt{\Gamma_{DWNA}^2 + 8\Gamma_{DWNA}} \tag{19.55}$$

Figure 19-14 gives the gains versus the random tracking index, and also includes the corresponding CWNA case to be discussed in Section 19.2.2.3. Note that α approaches 1 and β approaches 2 for large values of the random tracking index. An additional relationship between α and β for DWNA [7,10] is given by

$$\beta = 2(2 - \alpha) - 4\sqrt{1 - \alpha} \tag{19.56}$$

While the alpha-beta filter can be implemented efficiently for steady-state conditions, poor tracking will be experienced if the steady-state gains are used for the settling of the alpha-beta filter from track initiation to steady state. Least squares techniques can be used to develop an effective gain scheduling method. Given $k = 0$ for the first measurement, the alpha and beta gains can be scheduled as a function of the measurement number according to

$$\alpha_k = \max\left\{\frac{2(2k+1)}{(k+1)(k+2)}, \alpha_{SS}\right\} \tag{19.57}$$

$$\beta_k = \max\left\{\frac{6}{(k+1)(k+2)}, \beta_{SS}\right\} \tag{19.58}$$

where $x_{0|-1} = 0$, and $\dot{x}_{0|-1} = 0$, and α_{SS} and β_{SS} are the steady-state values for α and β, respectively. Using these gains through N measurements gives a parametric least squares estimate of the position and velocity for constant velocity filtering for the first N measurements.

When a target undergoes a deterministic maneuver (i.e., a constant acceleration maneuver), the estimates are biased and the covariance matrix tends to be a biased estimate of track filter performance. When a target undergoes no maneuver (i.e., zero acceleration), the covariance matrix tends to also be a biased estimate of track filter performance, because

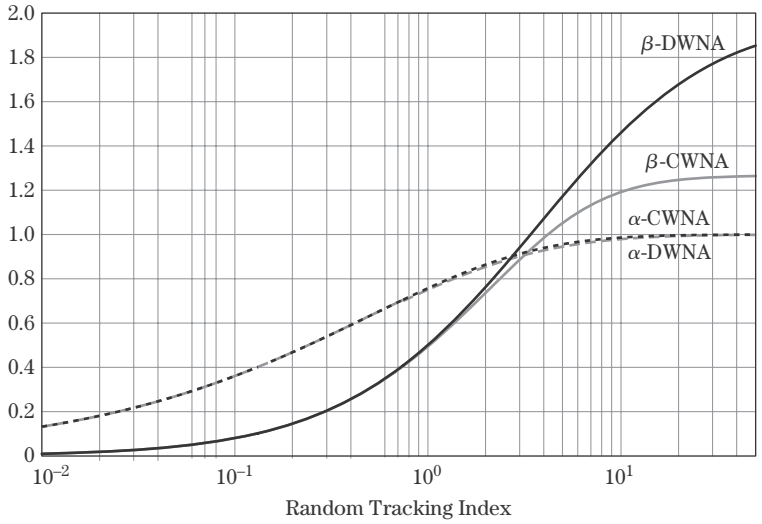

FIGURE 19-14 ■ α and β gains versus random tracking index for DWNA and CWNA models for maneuvers.

process noise is included in the filter for maneuver response, when there is no maneuver. Thus, to address both conditions of the performance prediction, the MSE can be written in terms of a sensor-noise only (SNO) covariance for no maneuver and a bias or maneuver lag for the constant acceleration maneuver. Let Γ_D denote the deterministic tracking index given by

$$\Gamma_D = \frac{A_{max} T^2}{\sigma_w} \tag{19.59}$$

where A_{max} denotes the maximum acceleration of the target. Then the maximum MSE (MMSE) in the filtered position estimates of the alpha-beta filter can be written as

$$MMSE^p = \sigma_w^2 \left[\frac{2\alpha^2 + \beta(2 - 3\alpha)}{\alpha(4 - 2\alpha - \beta)} + (1 - \alpha)^2 \frac{\Gamma_D^2}{\beta^2} \right] \tag{19.60}$$

The MMSE in the velocity estimates can be expressed as

$$MMSE^v = \frac{\sigma_w^2}{T^2} \left[\frac{2\beta^2}{\alpha(4 - 2\alpha - \beta)} + \left(\frac{\alpha - 0.5\beta}{\beta} \right)^2 \Gamma_D^2 \right] \tag{19.61}$$

For a given value of Γ_D, a unique α and β minimize (19.60) in conjunction with (19.56). These α and β define a unique Γ_{DWNA} given by (19.47) for the given Γ_D. Let the random tracking index be expressed in terms of the deterministic tracking index as

$$\Gamma_{DWNA} = \kappa_1(\Gamma_D)\Gamma_D \tag{19.62}$$

Using (19.47) and (19.59) in (19.62) gives

$$\sigma_v = \kappa_1(\Gamma_D) A_{max} \tag{19.63}$$

The $\kappa_1(\Gamma_D)$ that corresponds to minimizing (19.60) is given versus Γ_D in Figure 19-15 and denoted by the line labeled "MMSE". It is given approximately by

$$\kappa_1(\Gamma_D) = 1.67 - 0.74 \log(\Gamma_D) + 0.26[\log(\Gamma_D)]^2, \quad 0.01 \le \Gamma_D \le 10 \tag{19.64}$$

Thus, (19.64) along with (19.63) and the maximum acceleration of the target defines the process noise variance for the NCV Kalman filter so that the MMSE is minimized.

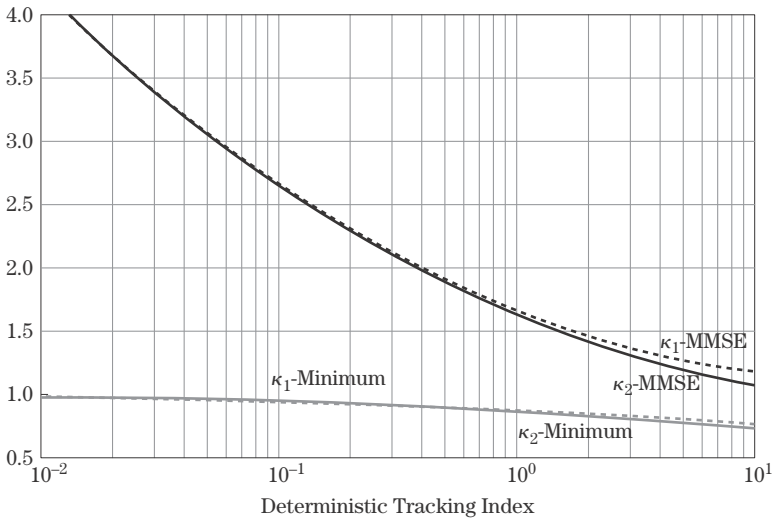

FIGURE 19-15 ■ Values for $\kappa_1(\Gamma_D)$ and $\kappa_2(\Gamma_D)$ for defining the process noise variance in terms of the maximum acceleration.

Using the constraint that the MMSE in the filtered position estimate should not exceed the measurement error variance gives that $MMSE^p \leq \sigma_w^2$ or

$$\frac{2\alpha^2 + \beta(2 - 3\alpha)}{\alpha(4 - 2\alpha - \beta)} + \frac{(1 - \alpha)^2}{\beta^2}\Gamma_D^2 \leq 1 \tag{19.65}$$

For a given value of Γ_D, unique α and β satisfy (19.65) with equality in conjunction with (19.56). These α and β are the minimum gains and define the minimum Γ_{DWNA} (or σ_v) that is related to Γ_D by $\kappa_1(\Gamma_D)$. The κ_1 that defines the minimum σ_v is given versus Γ_D in Figure 19-15 and is denoted by the line labeled "MINIMUM". It is given approximately by

$$\kappa_1^{\min}(\Gamma_D) = 0.87 - 0.09\log(\Gamma_D) - 0.02[\log(\Gamma_D)]^2 \tag{19.66}$$

Thus, Figure 19-15 shows that the constraint is most always satisfied if the process noise variance is chosen to minimize the MMSE. For $\Gamma_D < 1.0$, Figure 19-15 shows that a wide range of values for κ_1 satisfy the constraint in (19.65) and the filter designer has freedom in their selection of σ_v.

When designing NCV filters for deterministic maneuvers, the question of the duration of a typical maneuver arises. Figure 19-16 gives the approximate time period in measurement samples for the maneuver lag to achieve 90% of the steady-state lag in position [11]. Thus, for $\Gamma_D \approx 1$, the method presented here for selecting the process noise variance is valid for maneuvers lasting three measurements or longer. For $\Gamma_D \approx 0.1$, this method for selecting the process noise variance is valid for maneuvers lasting six measurements or longer. For targets with maximum maneuvers that are not sustained so that the maximum bias in the estimate is achieved, an alternate design procedure should be considered.

For illustrating the filter design methodology, consider a target that maneuvers with 40 m/s^2 of acceleration from 40 to 60 s. The sensor measures the target position at a 1 Hz rate with errors defined by $\sigma_w = 120$ m. Thus, $\Gamma_D = 0.33$. Since the maneuver is sustained for more than four measurements, considering the maximum lag for design is acceptable. Then, (19.66) gives $\kappa_1^{\min} = 0.91$ and $\sigma_v = 36.4$ as the minimum acceptable

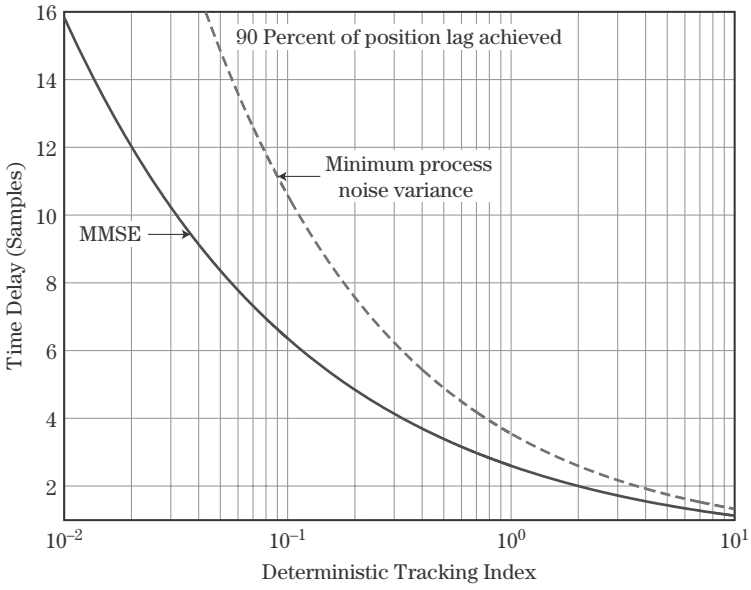

FIGURE 19-16 ■ Approximate time delay in filters achieving 90% of steady-state lag in position.

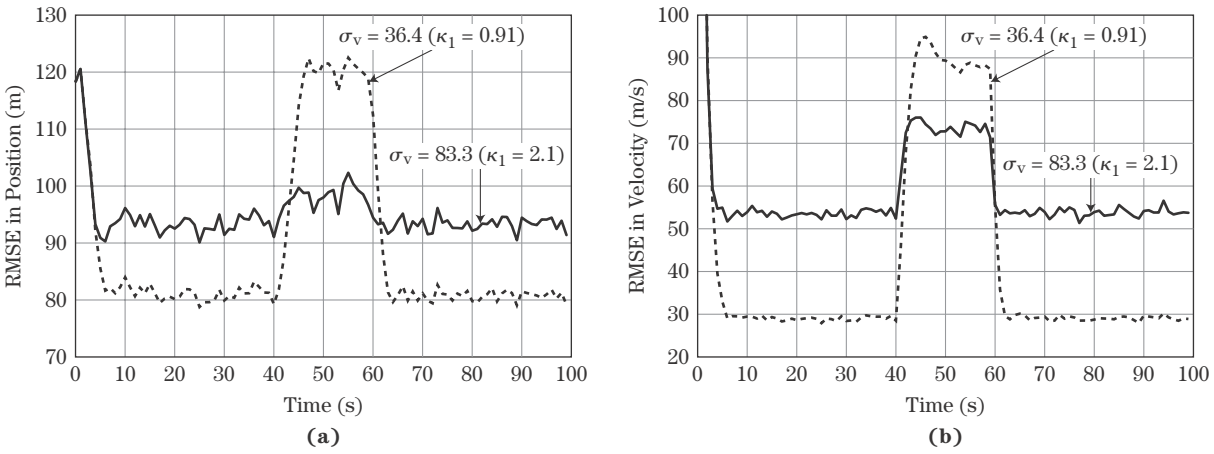

FIGURE 19-17 ■ RMSE in state estimates of two NCV filter designs for tracking maneuvering target. (a) RMSE in position. (b) RMSE in velocity.

value for σ_v. The design for minimizing MMSE gives $\kappa_1(0.33) = 2.1$ from (19.64) and $\sigma_v = 83.3$ as the process noise standard deviation that minimizes the MSE. Figure 19-17 shows the RMSE results of Monte Carlo simulations with 2,000 experiments for the two filter designs. Note that the RMSE in position during the maneuver for $\kappa_1 = 0.91$ and $\sigma_v = 36.4$ is closely matched to the standard deviation of the measurements of 120 m as anticipated. Also, note for $\kappa_1 = 2.1$ and $\sigma_v = 83.3$, the maximum RMSE in position is minimized and is only slightly larger than the RMSE in the absence of a maneuver.

Figure 19-18 gives the NEES as defined in (19.23) for the two filter designs. If the errors in the state estimates are zero-mean Guassian with covariance $\mathbf{P}_{k|k}$, then the NEES

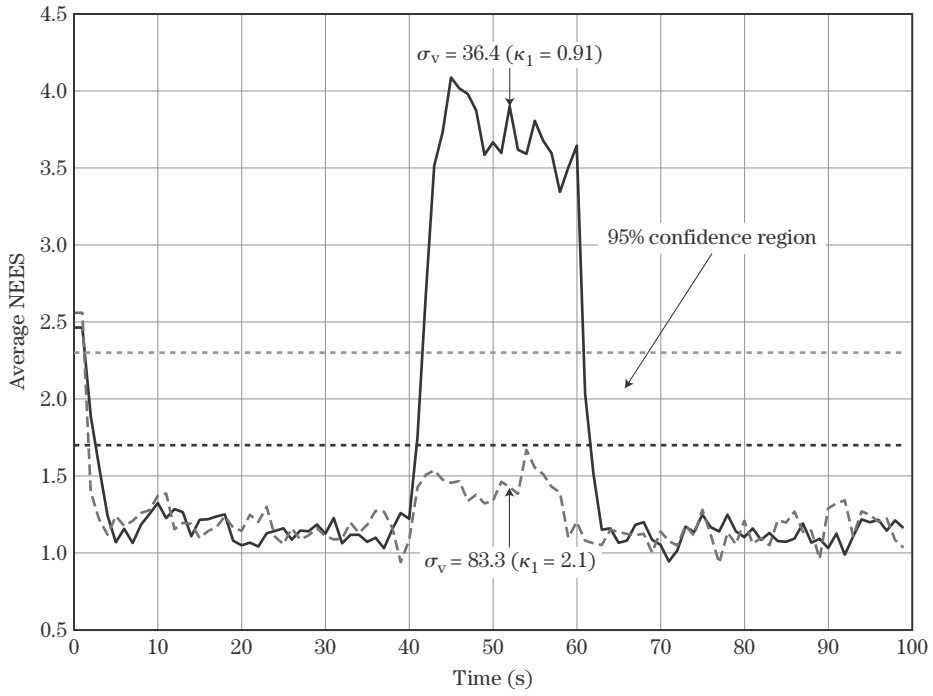

FIGURE 19-18 ■ Covariance consistency of state estimates of two NCV filter designs for tracking a maneuvering target.

is a chi-square random variable with two degrees of freedom. For a two degree of freedom chi-square random variable, the sample average should be two. In Figure 19-18, the two dotted lines denote the 95% confidence region for a 200 sample average of a two degree of freedom chi-square random variable. Thus, results indicate that the covariances for both filter designs are too large when the target is not maneuvering. For the design with $\kappa_1 = 2.1$, the covariance is also too large during the maneuver. For the design with $\kappa_1 = 0.91$, the covariance is too small during maneuver. Thus, Figure 19-18 illustrates the challenge with the error covariance that results from modeling deterministic-like maneuvers with a random acceleration model.

19.2.2.2 Nearly Constant Velocity Tracking with LFM Waveforms

When radars use an LFM waveform, the range measurement is coupled to the range rate-induced Doppler of the target [12]. For an LFM waveform, DWNA, and fixed track rate, the system for tracking in the range coordinate is given by (19.41) through (19.46) with the changes given by

$$\boldsymbol{X}_k = [\, r_k \quad \dot{r}_k \,]^T \tag{19.67}$$

$$\mathbf{H}_k = \mathbf{H} = [\, 1 \quad \Delta t \,] \tag{19.68}$$

where r_k and $\dot{r}_k$ are the range and range rate of the target, respectively, and Δt is the range-Doppler coupling coefficient. The range-Doppler coupling coefficient is defined by

$$\Delta t = \frac{f_1 \tau}{f_2 - f_1} \tag{19.69}$$

with f_1 denoting the initial frequency of the transmitted waveform, τ denoting the duration of the transmitted waveform, and f_2 denoting the final frequency in the waveform modulation.

As noted in [12] and shown analytically in [13], the range-Doppler coupling of the waveform affects the tracking accuracy. For example, an up-chirp waveform (i.e., $f_2 > f_1$ or $\Delta t > 0$) gives lower steady-state tracking errors than an equivalent down-chirp waveform (i.e., $f_2 < f_1$ or $\Delta t < 0$). The steady-state gains and covariance for tracking the range and range rate with LFM waveforms are derived in [13].

Figure 19-19 shows that the variances of range and range rate estimates decrease with increasing Δt for a given maneuver index Γ_{DWNA}. The correlation coefficients for the range and range rate estimates are between 0 and 1. As Δt becomes more positive, the correlation coefficient for range and range rate goes to zero at higher values of Γ_{DWNA}. This means that the range and range rate estimates are less correlated at higher values of Γ_{DWNA}. Thus, the accuracy of the predicted measurements will be improved at more positive Δt. Thus, α decreases with increasing Δt.

19.2.2.3 Nearly Constant Velocity Filtering with CWNA

Nearly constant velocity motion with continuous acceleration errors is described in a scalar coordinate by

$$\begin{bmatrix} \dot{x}(t) \\ \ddot{x}(t) \end{bmatrix} = \begin{bmatrix} 0 & 1 \\ 0 & 0 \end{bmatrix} \begin{bmatrix} x(t) \\ \dot{x}(t) \end{bmatrix} + \begin{bmatrix} 0 \\ 1 \end{bmatrix} \tilde{v}(t) \tag{19.70}$$

where $\tilde{v}(t)$ is a continuous time, zero-mean white noise process with $\mathrm{E}\{\tilde{v}(t)\tilde{v}(\tau)\} = \tilde{q}\delta_D(t - \tau)$, where $\mathrm{E}\{\cdot\}$ denotes the expected value, $\delta_D(\cdot)$ is the Dirac delta function.

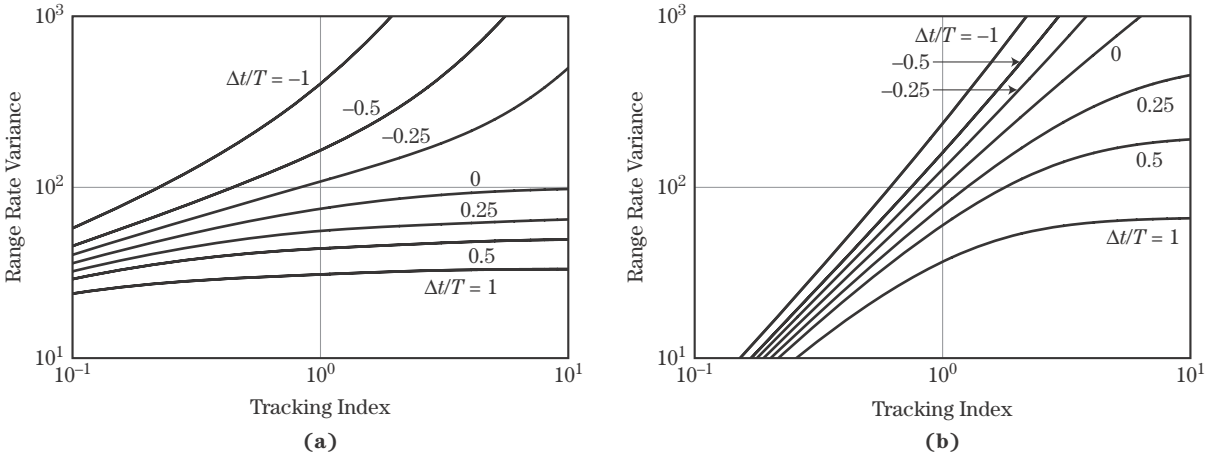

FIGURE 19-19 ■ Variances of the range and range rate estimates for tracking with LFM waveforms versus Γ_{DWNA}.

For time-invariant system, $\tilde{q}$ is the power spectral density. The discretized version of the motion model in a single coordinate is given by (19.33) with

$$\boldsymbol{X}_k = \begin{bmatrix} x_k & \dot{x}_k \end{bmatrix}^T \tag{19.71}$$

$$\mathbf{G}_k = \begin{bmatrix} \frac{1}{2\sqrt{3}}(\sqrt{\delta_k})^3 & \frac{1}{2}(\sqrt{\delta_k})^3 \\ 0 & \sqrt{\delta_k} \end{bmatrix} \tag{19.72}$$

$$\mathbf{Q}_k = \begin{bmatrix} \tilde{q} & 0 \\ 0 & \tilde{q} \end{bmatrix} \tag{19.73}$$

For the nearly constant velocity motion model, the process noise covariance matrix for CWNA is given by

$$\mathbf{G}_k \mathbf{Q}_k \mathbf{G}_k^T = \tilde{q} \begin{bmatrix} \frac{1}{3}\delta_k^3 & \frac{1}{2}\delta_k^2 \\ \frac{1}{2}\delta_k^2 & \delta_k \end{bmatrix} \tag{19.74}$$

where $\tilde{q}$ is the design parameter for the NCV Kalman filter. Typically, the filter design process begins by setting $\sqrt{\tilde{q}}/T$ greater than one half of the maximum acceleration of the target and less than the maximum acceleration, where T is a nominal sample period. Monte Carlo simulations are conducted to further refine the selection of $\tilde{q}$. Further guidelines on the selection of $\tilde{q}$ are developed in [9] and summarized below. Typically, the measurements are the position of the target and the measurement equation of (19.2) is defined by (19.46).

When the error processes $\tilde{v}(t)$ and w_k are stationary and the data rate is constant, the Kalman filter will achieve steady-state conditions in which the filtered state covariance and Kalman gain are constant. The design and performance of the filter is characterized by the maneuver index

$$\Gamma_{CWNA}^2 = \frac{\tilde{q}T^3}{\sigma_w^2} = \frac{\beta^2}{1-\alpha} \tag{19.75}$$

where $\sigma_w = \sigma_{wk}$, and $T = t_k - t_{k-1}$ for all k. Under steady-state conditions, the NCV filter is equivalent to an alpha-beta filter, where α and β are the optimal gains for CWNA

model given in [7]. The steady-state error covariance of the alpha-beta filter is given as a function of α and β by (19.53). Given the random tracking index, the steady-filter gains are specified by

$$u = \frac{1}{3} + \sqrt{\frac{1}{12} + \frac{4}{\Gamma_{CWNA}^2}} \tag{19.76}$$

$$\alpha = \frac{12}{6(u + \sqrt{u}) + 1} \tag{19.77}$$

$$\beta = \frac{12\sqrt{u}}{6(u + \sqrt{u}) + 1} \tag{19.78}$$

Figure 19-14 gives the gains versus the random tracking index. Note that α approaches 1 and β approaches 1.3 for large values of the random tracking index. An additional relationship between α and β [7] is given by

$$\beta = 3(2 - \alpha) - \sqrt{3(\alpha^2 - 12\alpha + 12)} \tag{19.79}$$

While the alpha-beta filter can be implemented efficiently for steady-state conditions, poor tracking will be experienced if the steady-state gains are used for the settling of the alpha-beta filter from track initiation to steady-state. The filter initialization and settling can be accomplished by the gains in (19.57) and (19.58) for the first N measurements.

The MMSE in the filtered position and velocity estimates of the alpha-beta filter are given by (19.60) and (19.61). For a given value of Γ_D, a unique α and β minimize (19.60) in conjunction with (19.79). The α and β define a unique Γ_{CWNA} for the given Γ_D. Let the random tracking index be expressed in terms of the deterministic tracking index as

$$\Gamma_{CWNA} = \kappa_2(\Gamma_D)\Gamma_D \tag{19.80}$$

Using (19.75) and (19.59) in (19.80) gives

$$\tilde{q} = T\kappa_2^2(\Gamma_D)A_{max}^2 \tag{19.81}$$

where κ_2 that corresponds to minimizing (19.60) is given versus Γ_D in Figure 19-15 and denoted by the line labeled with MMSE. It is given approximately by

$$\kappa_2(\Gamma_D) = 1.62 - 0.79\log(\Gamma_D) + 0.24(\log(\Gamma_D))^2, \quad 0.01 \le \Gamma_D \le 10 \tag{19.82}$$

Thus, (19.82) along with (19.81) and the maximum acceleration of the target defines the process noise variance for the NCV filter. Using the constraint that the MMSE in the filtered position estimate should not exceed the measurement error variance gives that $MMSE^p \le \sigma_w^2$ or (19.65). For a given value of Γ_D, unique α and β satisfy (19.65) with equality in conjunction with (19.79). These values α and β are the minimum gains and define the minimum Γ_{CWNA} that is related to Γ_D by κ_2. The κ_2 that defines the minimum Γ_{CWNA} is given versus Γ_D in Figure 19-15, denoted by the line labeled "MINIMUM," and given approximately by

$$\kappa_2^{\min}(\Gamma_D) = 0.87 - 0.11\log(\Gamma_D) - 0.03[\log(\Gamma_D)]^2 \tag{19.83}$$

Thus, Figure 19-15 shows that the constraint is most always satisfied if the process noise variance is chosen to minimize the MMSE. For $\Gamma_D < 1.0$, Figure 19-15 shows that a wide range of values for κ_2 satisfy the constraint in (19.65) and the filter designer has freedom in the selection of σ_v. When designing NCV Kalman filters for deterministic

maneuvers, the question of duration of a typical maneuver arises. Figure 19-16 gives the approximate time period in measurement samples for the maneuver lag to achieve 90% of the steady-state value. For targets with maximum maneuvers that are not sustained such that the maximum bias in the estimate is attained, an alternate design procedure should be considered.

19.2.2.4 Nearly Constant Acceleration Filtering

Nearly constant acceleration motion with piecewise constant acceleration errors in a scalar coordinate is defined by (19.33) with

$$\boldsymbol{X}_k = \begin{bmatrix} x_k & \dot{x}_k & \ddot{x}_k \end{bmatrix}^T \tag{19.84}$$

$$\mathbf{F}_k = \begin{bmatrix} 1 & \delta_k & \frac{1}{2}\delta_k^2 \\ 0 & 1 & \delta_k \\ 0 & 0 & 1 \end{bmatrix} \tag{19.85}$$

$$\boldsymbol{G}_k = \begin{bmatrix} \frac{1}{2}\delta_k^2 & \delta_k & 1 \end{bmatrix}^T \tag{19.86}$$

where v_k is a discrete Wiener process acceleration (DWPA) error that is constant between t_k and t_{k-1} in the state process with $v_k \sim \mathrm{N}(0, \sigma_{vk}^2)$ For the nearly constant acceleration motion model, the process noise covariance matrix for DWPA is given by

$$\boldsymbol{G}_k Q_k \boldsymbol{G}_k^T = \sigma_{vk}^2 \begin{bmatrix} \frac{1}{4}\delta_k^4 & \frac{1}{2}\delta_k^3 & \frac{1}{2}\delta_k^2 \\ \frac{1}{2}\delta_k^3 & \delta_k^2 & \delta_k \\ \frac{1}{2}\delta_k^2 & \delta_k & 1 \end{bmatrix} \tag{19.87}$$

where σ_{vk} is the design parameter for the nearly constant acceleration (NCA) filter with DWPA. Typically, the filter design process begins by setting σ_{vk} greater than one half of the maximum change in acceleration between t_{k-1} and t_k and less than the maximum change in acceleration. Monte Carlo simulations are conducted to further refine the selection of σ_{vk}. Typically, the measurements are of the position of the target. In this case, the measurement equation of (19.2) is defined by

$$\mathbf{H}_k = \begin{bmatrix} 1 & 0 & 0 \end{bmatrix} \tag{19.88}$$

When the error processes v_k and w_k are stationary (i.e., zero mean and constant variances) and the data rate is constant, the Kalman filter will achieve steady-state conditions in which the filtered state covariance and Kalman gain are constant. While these conditions are seldom satisfied in practice, the steady-state form of the filter can be used to predict average or expected tracking performance. The design and performance of the filter is characterized by the maneuver index or random tracking index

$$\Gamma_{DWPA} = \frac{\sigma_v T^2}{\sigma_w} \tag{19.89}$$

where $\sigma_v = \sigma_{vk}$, $\sigma_w = \sigma_{wk}$, and $T = t_k - t_{k-1}$ for all k. Under steady-state conditions, the NCA filter is equivalent to an alpha-beta-gamma filter. For the alpha-beta-gamma filter, the steady-state gains that occur after the transients associated with filter initialization diminish are given by

$$\boldsymbol{K}_k = \begin{bmatrix} \alpha & \frac{\beta}{T} & \frac{\gamma}{2T^2} \end{bmatrix}^T \tag{19.90}$$

where α, β, and γ are the optimal gains for DWPA given in [7,10]. The alpha-beta-gamma filter is rather simple and computationally efficient to implement because online real-time calculation of the filtered state covariance and gains is not needed. The alpha-beta-gamma filter for a scalar coordinate is given by

$$x_{k|k-1} = x_{k-1|k-1} + T\dot{x}_{k-1|k-1} + \frac{T^2}{2}\ddot{x}_{k-1|k-1} \tag{19.91}$$

$$\dot{x}_{k|k-1} = \dot{x}_{k-1|k-1} + T\ddot{x}_{k-1|k-1} \tag{19.92}$$

$$\ddot{x}_{k|k-1} = \ddot{x}_{k-1|k-1} \tag{19.93}$$

$$x_{k|k} = x_{k|k-1} + \alpha[Z_k - x_{k|k-1}] \tag{19.94}$$

$$\dot{x}_{k|k} = \dot{x}_{k|k-1} + \frac{\beta}{T}[Z_k - x_{k|k-1}] \tag{19.95}$$

$$\ddot{x}_{k|k} = \ddot{x}_{k|k-1} + \frac{\gamma}{2T^2}[Z_k - x_{k|k-1}] \tag{19.96}$$

where Z_k is the measured position of the target. The steady-state error covariance of the alpha-beta-gamma filter is given in [7,10] as

$$\mathbf{P}_{\alpha\beta} = \sigma_w^2 \begin{bmatrix} \alpha & \dfrac{\beta}{T} & \dfrac{\gamma}{2T^2} \\ \dfrac{\beta}{T} & \dfrac{8\alpha\beta + \gamma(\beta - 2\alpha - 4)}{8(1-\alpha)T^2} & \dfrac{\beta(2\beta - \gamma)}{4(1-\alpha)T^3} \\ \dfrac{\gamma}{2T^2} & \dfrac{\beta(2\beta - \gamma)}{4(1-\alpha)T^3} & \dfrac{\gamma(2\beta - \gamma)}{4(1-\alpha)T^4} \end{bmatrix} \tag{19.97}$$

Given the maneuver index, the steady-filter gains are found by solving three simultaneous equations given by

$$\Gamma_{DWPA} = \frac{\gamma^2}{4(1-\alpha)} \tag{19.98}$$

$$\beta = 2(2-\alpha) - 4\sqrt{1-\alpha} \tag{19.99}$$

$$\gamma = \frac{\beta^2}{\alpha} \tag{19.100}$$

For a given tracking index, the gains are found by the use of a table. The table is constructed by varying α from a small value to a value near 1 and for each value of α, values for β, γ, and Γ_{DWPA} are computed. These gains are plotted versus the tracking index in Figure 19-20. Note that for a given tracking index, alpha is larger for the alpha-beta-gamma filter than for the alpha-beta filter. Thus, according to (19.53) and (19.97), the position estimate of the alpha-beta filter will have a smaller variance than that of the alpha-beta-gamma filter for a given tracking index.

While the alpha-beta-gamma filter can be implemented efficiently for steady-state conditions, poor tracking will be experienced if the steady-state gains are used for the settling of the alpha-beta-gamma filter from track initiation to steady-state. Least squares techniques can be used to develop and effective gain scheduling method. Given $k = 0$ for the first measurement, the alpha, beta, and gamma gains can be scheduled as a function

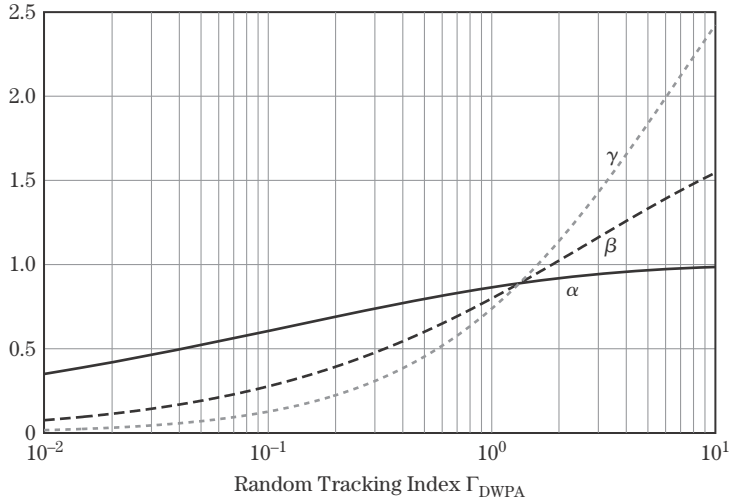

FIGURE 19-20 ■ Alpha, beta, and gamma gains versus random tracking index.

of the measurement number according to

$$\alpha_k = \max\left\{\frac{3(3k^2+3k+2)}{(k+1)(k+2)(k+3)}, \alpha_{SS}\right\} \tag{19.101}$$

$$\beta_k = \max\left\{\frac{18(2k+1)}{(k+1)(k+2)(k+3)}, \beta_{SS}\right\} \tag{19.102}$$

$$\gamma_k = \max\left\{\frac{60}{(k+1)(k+2)(k+3)}, \gamma_{SS}\right\} \tag{19.103}$$

where $x_{0|-1} = 0$, $\dot{x}_{0|-1} = 0$, and $\ddot{x}_{0|-1} = 0$, and α_{SS}, β_{SS}, and γ_{SS} are the steady-state values. Using these gains through N measurements gives a parametric least squares estimate of the position, velocity, and acceleration for constant acceleration filtering for the first N measurements.

To illustrate NCA filter tracking, consider the target trajectory and sensor used to generate the results in Figure 19-17. The target maneuvers with 40 m/s^2 of acceleration from 40 to 60 s, and the sensor measures the target position at a 1 Hz rate with errors defined by $\sigma_w = 120$ m. Let $\sigma_v = 7$ m/s^2 for the NCA filter design. Figure 19-21 shows the RMSE results of Monte Carlo simulations with 2000 runs. Note that the RMSE in both position and velocity have peaks at the beginning and end of the maneuver and this behavior is indicative of a second-order model with acceleration estimation. Also, note that the peak of the RMSE in position remains lower than the measurement error during the maneuver. However, the RMSE in position is significantly higher than that of the NCV filters in Figure 19-17, when the target is not maneuvering. Also, when the target is not maneuvering, the RMSE in velocity is higher than that of the NCV filter with $\sigma_v = 36.4$ and less than that for the NCV filter with $\sigma_v = 83.3$. Figure 19-22 gives the NEES as defined in (19.23) for the NCA filter. In Figure 19-22, the two dotted lines denote the 95% confidence region for a 200 sample average of a two degree of freedom chi-square random variable. Thus, results indicate that the covariance for NCA filter is too large when the target is not maneuvering. This is a result of modeling deterministic-like maneuvers with a random acceleration model.

19.2.2.5 Multiple Model Filtering for Highly Tracking Maneuvering Targets

Techniques for adapting the Kalman filter for target maneuvers have been studied for many years with very little success. Adaptive Kalman filtering is based on monitoring in real time

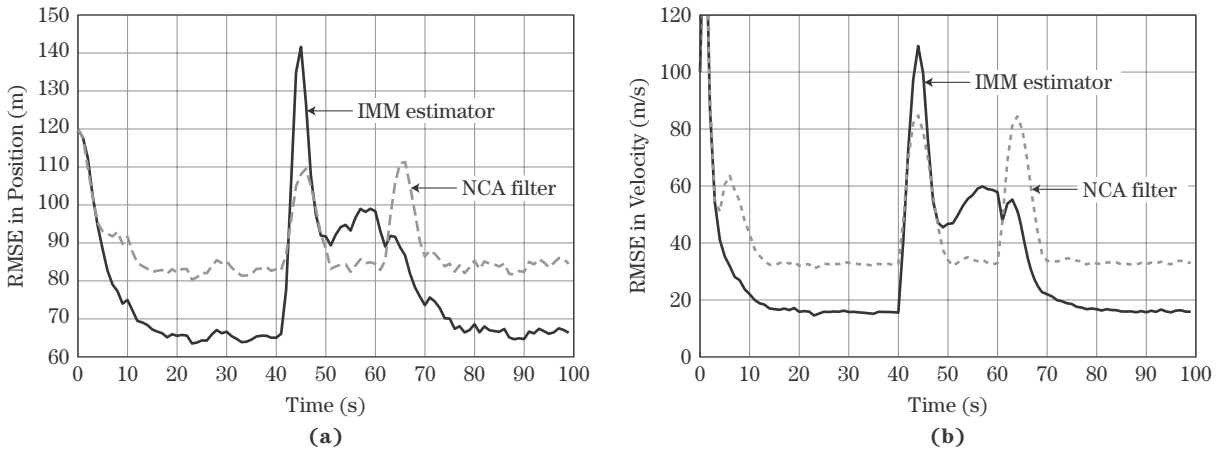

FIGURE 19-21 ■ RMSE in state estimates of NCA filter and IMM estimator for tracking a maneuvering target. (a) Position errors. (b) Velocity errors.

FIGURE 19-22 ■ Covariance consistency of state estimates of NCA filter and IMM estimator for tracking maneuvering target.

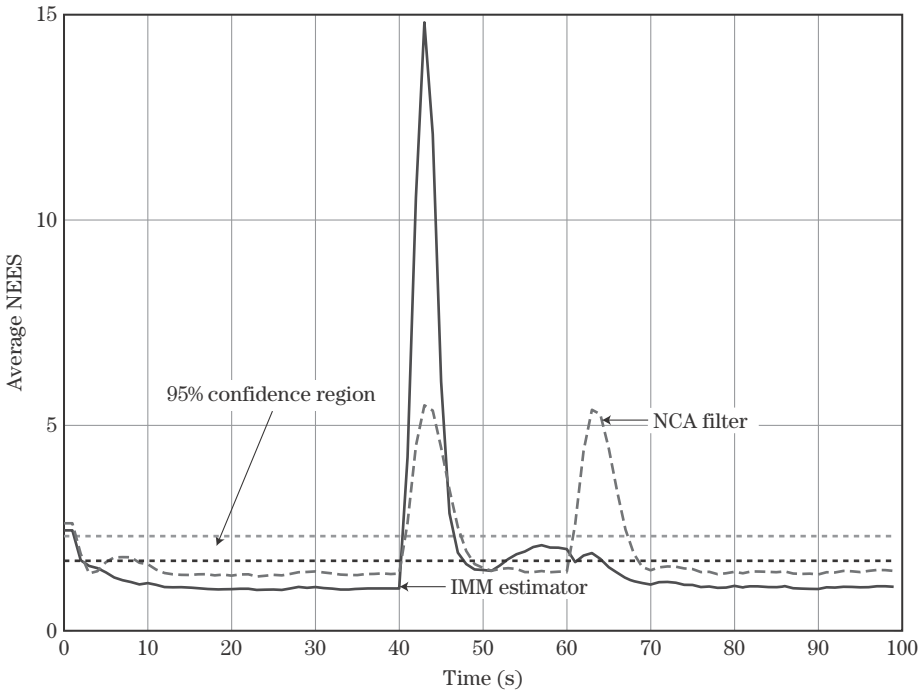

the whiteness of the residuals or the agreement of the magnitude of the innovations with their yielded error covariances. Thus, adaptive Kalman filtering for tracking maneuvering targets is based on detecting a breakdown in filter consistency and adjusting the filter parameters to regain filter consistency. Therefore, using an adaptive Kalman filter to track maneuvering targets will not provide reliable tracking performance because the loss of track filter consistency prevents reliable decision making for simultaneously adapting the filter parameters and performing data association.

As an alternative to adaptive Kalman filtering, the tracking of a maneuvering target can be treated as the state estimation of a system with Markovian switching coefficients.

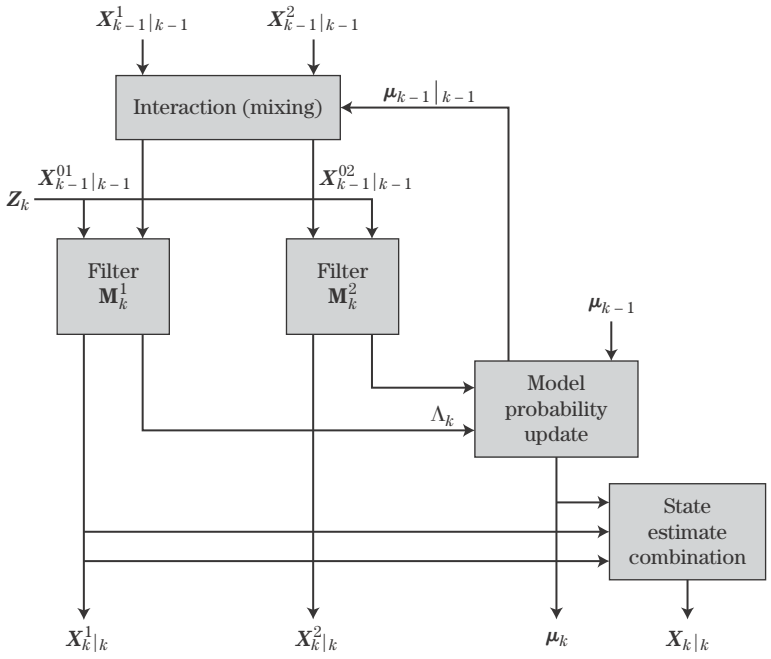

FIGURE 19-23 ■ Typical IMM estimator with two modes.

The dynamical motion and measurement equations for a system with Markovian switching coefficients are given by

$$\boldsymbol{X}_{k+1} = \mathbf{F}_k(\theta_{k+1})\boldsymbol{X}_k + \boldsymbol{G}_k(\theta_k)\boldsymbol{v}_k(\theta_k) \tag{19.104}$$

$$\boldsymbol{Z}_k = \mathbf{H}(\theta_k)\boldsymbol{X}_k + \boldsymbol{w}_k \tag{19.105}$$

where θ_k is a finite-state Markov chain taking values in $\{1, \ldots, N\}$ according to the transition probabilities p_{ij} of switching from mode i to mode j. The interacting multiple model (IMM) estimator has become the well-accepted method for state and mode estimation of such multiple-mode systems with Markov switching between the modes [7]. Also, the IMM estimator is a nearly consistent estimator for the state of a maneuvering target.

The IMM estimator consists of a filter for each model, a model probability evaluator, an estimate mixer at the input of the filters, and an estimate combiner at the output of the filters. Figure 19-23 shows a flow diagram of the IMM estimator for two modes, where $\boldsymbol{X}_{k|k}$ is the state estimate at time k based on both models, $\boldsymbol{X}^j_{k|k}$ is the state estimate based on model j, $\boldsymbol{\Lambda}_k$ is the vector of mode likelihoods, and $\boldsymbol{\mu}_k$ is the vector of mode probabilities when all the likelihoods have been considered. With the assumption that the mode switching is governed by an underlying Markov chain, the mixing uses the mode probabilities and mode switching probabilities to compute a mixed state estimate for each filter. At the beginning of a filtering cycle, each filter uses a mixed estimate and a measurement to compute a new estimate and likelihood for the model within the filter. The likelihoods, the prior mode probabilities, and the mode switching probabilities are used to compute new mode probabilities. The overall state estimate is then computed with the new state estimates and their mode probabilities. In many applications, the IMM algorithm provides a 25% reduction of error in the position estimates and a 50% reduction of error in the velocity estimates that are produced by a Kalman filter. An illustrative example that compares the performances of the Kalman filter and the IMM estimator for tracking a maneuvering target is described in the introduction of [8]. The effectiveness of the IMM

algorithm has been thoroughly documented in the literature and confirmed in a real-time tracking experiments [1,5,6,14–19].

Let $\mathbf{F}_k^i = \mathbf{F}_k(\theta_{k+1} = i)$, $\mathbf{G}_k^i = \mathbf{G}_k(\theta_{k+1} = i)$, and $\mathbf{H}_k^i = \mathbf{H}_k(\theta_k = i)$. Also, let $\boldsymbol{X}_{k|j}^i$ and $\mathbf{P}_{k|j}^i$ denote the state estimate and covariance at time t_k given data through time t_j under the condition that mode i, denoted as $\mathbf{M}_k^i$, is the true mode. The implementation of the IMM estimator involves the following five steps.

Step 1: State Mixing

Starting with $\boldsymbol{X}_{k-1|k-1}^i$ and the mode probability μ_{k-1}^i for each of r modes, compute the mixed estimate for each mode according

$$\boldsymbol{X}_{k-1|k-1}^{0i} = \sum_{j=1}^{r} \boldsymbol{X}_{k-1|k-1}^{j} \mu_{k-1|k-1}^{j|i} \tag{19.106}$$

where

$$\mu_{k-1|k-1}^{j|i} = \frac{\mu_{k-1}^{j}}{\mu_{k-1|k-1}^{i}} p_{ji}, \qquad \mu_{k-1|k-1}^{i} = \sum_{j=1}^{r} \mu_{k-1}^{j} p_{ji} \tag{19.107}$$

The covariance of the mixed estimate is given by

$$\mathbf{P}_{k-1|k-1}^{0i} = \sum_{j=1}^{r} \mu_{k-1|k-1}^{j|i} \left[\mathbf{P}_{k-1|k-1}^{j} + \left(\boldsymbol{X}_{k-1|k-1}^{j} - \boldsymbol{X}_{k-1|k-1}^{0i} \right) \left(\boldsymbol{X}_{k-1|k-1}^{j} - \boldsymbol{X}_{k-1|k-1}^{0i} \right)^T \right] \tag{19.108}$$

Step 2: Mode Conditioned Estimates

Starting with $\boldsymbol{X}_{k-1|k-1}^{0i}$ and $\mathbf{P}_{k-1|k-1}^{0i}$ for each of r modes, compute the mode-conditioned estimate for each mode according to the following.

Prediction of the mode-conditioned estimate to the next time:

$$\boldsymbol{X}_{k|k-1}^{i} = \mathbf{F}_{k-1}^{i} \boldsymbol{X}_{k-1|k-1}^{0i} \tag{19.109}$$

$$\mathbf{P}_{k|k-1}^{i} = \mathbf{F}_{k-1}^{i} \mathbf{P}_{k-1|k-1}^{0i} \left(\mathbf{F}_{k-1}^{i} \right)^T + \mathbf{G}_{k-1}^{i} Q_{k-1}^{i} \left(\mathbf{G}_{k-1}^{i} \right)^T \tag{19.110}$$

Update of the mode-conditioned estimate with the measurement:

$$\boldsymbol{X}_{k|k}^{i} = \boldsymbol{X}_{k|k-1}^{i} + \mathbf{K}_k^i \left[\mathbf{Z}_k - H_k^i \boldsymbol{X}_{k|k-1}^{i} \right] = \boldsymbol{X}_{k|k-1}^{i} + \mathbf{K}_k^i \widetilde{\mathbf{Z}}_k^i \tag{19.111}$$

$$\mathbf{P}_{k|k}^{i} = \left[\mathbf{I} - \mathbf{K}_k^i \mathbf{H}_k^i \right] \mathbf{P}_{k|k-1}^{i} \tag{19.112}$$

$$\mathbf{K}_k^i = \mathbf{P}_{k|k-1}^{i} \left(\mathbf{H}_k^i \right)^T \left(\mathbf{S}_k^i \right)^{-1} \tag{19.113}$$

$$\mathbf{S}_k^i = \mathbf{H}_k^i \mathbf{P}_{k|k-1}^{i} \left(\mathbf{H}_k^i \right)^T + \mathbf{R}_k \tag{19.114}$$

$\mathbf{K}_k^i$ is referred to as the Kalman filter gain for mode i, $\widetilde{\mathbf{Z}}_k^i$ denotes the filter residual vector for mode i, and $\mathbf{S}_k^i$ is the covariance of the measurement residual for mode i.

Step 3: Model Likelihood Computations

The likelihood of mode i at time t_k is computed according to

$$\Lambda_k^i = \frac{1}{\sqrt{|2\pi \mathbf{S}_k^i|}} \exp\left[-\frac{1}{2} \left(\widetilde{\mathbf{Z}}_k^i \right)^T \left[S_k^i \right]^{-1} \widetilde{\mathbf{Z}}_k^i \right] \tag{19.115}$$

where $\exp[\cdot]$ denotes the exponential function and $|\cdot|$ denotes the matrix determinant.

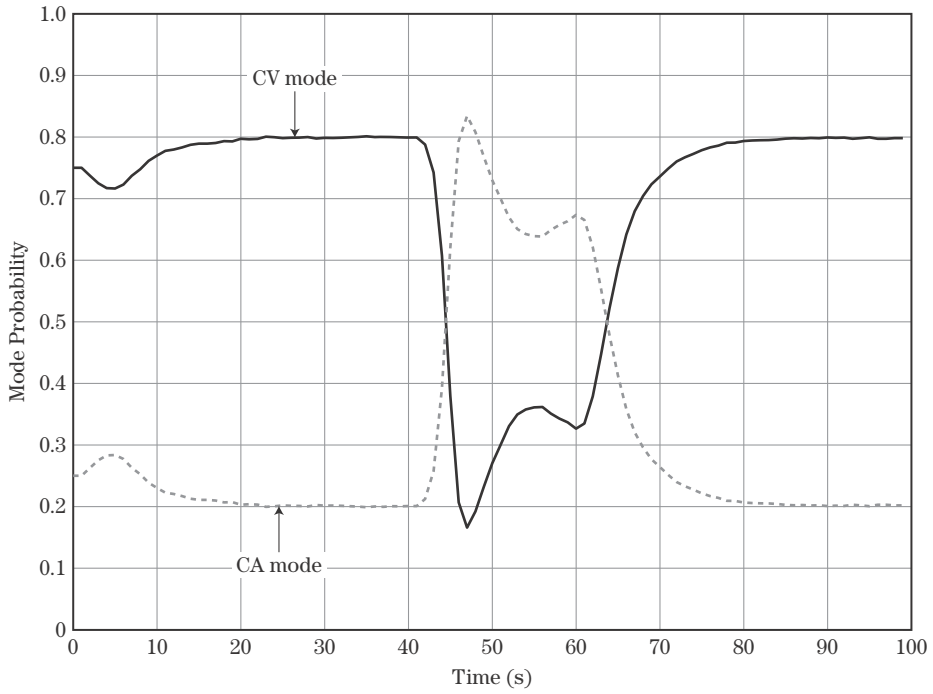

FIGURE 19-24 ■ Mode probabilities of two mode (i.e., NCV and NCA) IMM estimator for tracking a maneuvering target.

Step 4: Mode Probability Update

The probability of mode i at time t_k is computed according to

$$\mu_k^i = \frac{\Lambda_k^i}{\sum_{j=1}^r \mu_{k-1|k-1}^j} \mu_{k-1|k-1}^i \tag{19.116}$$

Step 5: Combination of State Estimates

The filtered state estimate at time t_k is computed for output according to

$$\boldsymbol{X}_{k|k} = \sum_{j=1}^r \mu_k^j \boldsymbol{X}_{k|k}^j \tag{19.117}$$

$$\mathbf{P}_{k|k} = \sum_{j=1}^r \mu_k^j \left[\mathbf{P}_{k|k}^j + \left(\boldsymbol{X}_{k|k}^j - \boldsymbol{X}_{k|k}\right)\left(\boldsymbol{X}_{k|k}^j - \boldsymbol{X}_{k|k}\right)^T\right] \tag{19.118}$$

To illustrate the tracking performance of the IMM estimator, consider the target trajectory and sensor used to generate the results in Figures 19-17 and 19-21. The target maneuvers with 40 m/s^2 of acceleration from 40 to 60 s, and the sensor measures the target position at a 1 Hz rate with errors defined by $\sigma_w = 120$ m. Consider an IMM estimator with NCV and NCA models. Let $\sigma_v^1 = 1$ m/s^2 for the NCV model and $\sigma_v^2 = 12$ m/s^2 for the NCA model. Let the mode switching probabilities be given by $p_{11} = 0.95$ with $p_{12} = 0.05$ and $p_{22} = 0.9$ with $p_{21} = 0.1$. Figure 19-24 illustrates the calculated probabilities of the CA and CV modes, showing that target acceleration causes the CA mode to be recognized as more likely, while the CV mode is deemed more likely when the target is not accelerating. Figure 19-21 shows the RMSE results of Monte Carlo simulations with 2,000 experiments. When the target is not maneuvering, the RMSE in position

and velocity are significantly lower than that of the NCA filter and the NCV filters in Figure 19-17. Note that the RMSE in both position and velocity have peaks at the beginning of the maneuver. Also, note that the peak of the RMSE in position raises slightly above the measurement error at the beginning of the maneuver. During the maneuvering, the RMSE of the IMM estimator is similar to the that of the better design of the NCV filter and that of the NCA filter. In this simulation, the target acceleration moves instantly from 0 to 40 m/s^2 and this is almost unavoidable. In practice, targets require a system response time of a few seconds to achieve maximum acceleration from a nonmaneuver state. Figure 19-22 gives the NEES as defined in (19.23) for the IMM estimator. The results indicate that the covariance for IMM estimator is too large when the target is not maneuvering and adapts to the maneuvering after the initial peak. Figure 19-24 gives the mode probabilities of the IMM estimator for this example.

The IMM estimator can also play a key role in the allocation of radar resources of phased radars when tracking maneuvering targets. Instead of setting a quasiperiodic data radar for surveillance tracking [20], the time at which the next measurement is required to maintain the track is computed after every measurement, and then a radar dwell is scheduled for the required time. Thus, the sample period between consecutive measurements is adapted giving rise to aperiodic data. The near consistency of the IMM estimator allows for reliable computation of the next required revisit time for the radar [15,21]. The next required revisit time is computed as the latest time at which the target can be expected to be in the predicted track gate, which is defined by the radar beamwidth, the length of the range window used in track mode, and maximum acceleration of the target. The revist time is determined by selecting the minimum of the required revisit times for range, bearing, and elevation and applying an upper limit on the revisit period that is based on the maximum acceleration of the target. For the angles, the revisit times are computed to be the times at which the standard deviations of the predicted angles exceeds a fraction of the beamwidth. For the range, the revisit time is computed to be the time at which the standard deviation of the predicted range exceeds a fraction of the range window. Using the output of the IMM estimator to compute the next required revisit time gives revisit intervals that automatically reflect target maneuvers, target range, missed detections, fluctuating signal amplitudes, the length of the range window, and the radar beamwidth at the predicted location of the target. Analysis of the results from simulation studies and real-time experiments [15] indicate that the IMM estimator with adaptive revisit times provides a 50% reduction in radar time and energy required for surveillance tracking by a conventional approach.

19.3 KINEMATIC MOTION MODELS

For most tracking systems, the target state is modeled in Cartesian coordinates and maintained in a reference frame that is stabilized relative to the location of the platform. The dynamical equation that is commonly used to represent the motion of the target relative to the platform is given by

$$\boldsymbol{X}_{k+1} = \mathbf{F}_k \boldsymbol{X}_k + \boldsymbol{G}_k \boldsymbol{v}_k \tag{19.119}$$

The state vector for a NCV motion model is given by

$$\boldsymbol{X}_k = \begin{bmatrix} x_k & \dot{x}_k & y_k & \dot{y}_k & z_k & \dot{z}_k \end{bmatrix}^T \tag{19.120}$$

where (x_k, y_k, z_k) represents the position of the target in Cartesian coordinates at time t_k and $(\dot{x}_k, \dot{y}_k, \dot{z}_k)$ represents the velocity of the target. When tracking with an early warning surveillance radar that measures only the range and bearing of the target, the state vector may be of a reduced Cartesian space and include only the four elements associated with x_k and y_k. Note that in this case, x_k and y_k are in a tilted frame relative to the horizontal plane and that tilt angle changes as the target moves. Thus, the x_k and y_k in the tilted frame is certainly different from those in the stabilized frame. The state vector for an NCA motion model in full Cartesian space is given by

$$\boldsymbol{X}_k = \begin{bmatrix} x_k & \dot{x}_k & \ddot{x}_k & y_k & \dot{y}_k & \ddot{y}_k & z_k & \dot{z}_k & \ddot{z}_k \end{bmatrix}^T \tag{19.121}$$

The dynamical constraint for NCV or NCA motion in full Cartesian space is given by

$$\mathbf{F}_k = \begin{bmatrix} \mathbf{A}_k & \mathbf{0}_{m\times m} & \mathbf{0}_{m\times m} \\ \mathbf{0}_{m\times m} & \mathbf{A}_k & \mathbf{0}_{m\times m} \\ \mathbf{0}_{m\times m} & \mathbf{0}_{m\times m} & \mathbf{A}_k \end{bmatrix} \tag{19.122}$$

where $\mathbf{0}_{m\times m}$ denotes an m by m matrix of zeros. For NCV motion, $m = 2$, while $m = 3$ for NCA motion. The process noise is included to account for the uncertainty associated with the unknown maneuvers of the targets. The input process noise is characterized by $\boldsymbol{G}_k\mathbf{Q}_k\boldsymbol{G}_k^T$ that is given by

$$\boldsymbol{G}_k\mathbf{Q}_k\boldsymbol{G}_k^T = \begin{bmatrix} q_k^x \boldsymbol{B}_k\boldsymbol{B}_k^T & \mathbf{0}_{m\times m} & \mathbf{0}_{m\times m} \\ \mathbf{0}_{m\times m} & q_k^y \boldsymbol{B}_k\boldsymbol{B}_k^T & \mathbf{0}_{m\times m} \\ \mathbf{0}_{m\times m} & \mathbf{0}_{m\times m} & q_k^z \boldsymbol{B}_k\boldsymbol{B}_k^T \end{bmatrix} \tag{19.123}$$

The choice of a motion model is governed by the maximum acceleration of the target, the quality of the sensor measurements, and the measurement rate. Since no algorithm exists for predicting the best model, Monte Carlo simulations are typically used to assess the best model for a tracking system. If the quality of the measurements and the measurement rate are not sufficient to estimate acceleration, models that do not include acceleration in the target state will provide better tracking performance. If only two or three measurements are taken during maneuvers, accurate estimation of the acceleration will not be possible, and the acceleration should not be included in the target state. If the quality of the measurements and the measurement rate allow for estimation of the acceleration, and the bias in the position estimates of the nearly constant velocity filter during the maximum acceleration of the target [22] is larger than the measurement errors, then acceleration should be included the target state. In this section, the motion models for NCV, NCA, Singer correlated acceleration, and constant speed turns are summarized [2,5,7,17,23].

19.3.1 Nearly Constant Velocity Motion Model

The dynamical constraint for NCV motion is given by (19.122) with

$$\mathbf{A}_k = \begin{bmatrix} 1 & \delta_k \\ 0 & 1 \end{bmatrix} \tag{19.124}$$

where $\delta_k = t_k - t_{k-1}$ denotes the sample period and t_k denotes the time of measurement k. The process noise is typically treated as DWNA or CWNA [7].

For the NCV motion model, the process noise covariance matrix for DWNA is given by (19.123) with

$$\boldsymbol{B}_k \boldsymbol{B}_k^T = \begin{bmatrix} \frac{\delta_k^4}{4} & \frac{\delta_k^3}{2} \\ \frac{\delta_k^3}{2} & \delta_k^2 \end{bmatrix} \tag{19.125}$$

The random tracking index is often used to characterize the filter design. While expressing the process noise variances in the Cartesian coordinates is straightforward, expressing the measurement variances in Cartesian coordinates is more difficult because the measurement errors are typically characterized in spherical or polar coordinates. The maneuver index for the NCV filter with DWNA [7] is given by

$$\Gamma_{DWNA} = \frac{\sigma_v T^2}{\sigma_w} \tag{19.126}$$

where σ_v^2 denotes the variance of the acceleration errors, T is the nominal measurement period, and σ_w^2 is the variance of the measurement errors in the corresponding coordinate. The σ_w^2 in each coordinate will vary with the target location. An appropriate σ_w is identified for a radar tracking problem by picking the maximum or average over the three coordinates or computing it with target location. Once an appropriate σ_w^2 and the maximum acceleration of the target have been identified, the methods in Section 19.2.2.1 can be used for the filter design. The key item of that design is to select the appropriate scaling $\kappa_1(\Gamma_D)$ between maximum acceleration of the target and σ_v.

For the NCV motion model with CWNA, the process noise covariance matrix is given by (19.123) with

$$\boldsymbol{B}_k \boldsymbol{B}_k^T q_k = \tilde{q} \begin{bmatrix} \frac{\delta_k^3}{3} & \frac{\delta_k^2}{2} \\ \frac{\delta_k^2}{2} & \delta_k \end{bmatrix} \tag{19.127}$$

The square of the random tracking index for the NCV filter with CWNA [7] is given by

$$\Gamma_{CWNA}^2 = \frac{\tilde{q} T^3}{\sigma_w^2} \tag{19.128}$$

where $\tilde{q}$ denotes the power spectral density of the CWNA. Once an appropriate σ_w^2 and the maximum acceleration of the target have been identified, the methods in Section 19.2.2.3 can be used to design the filter. The key step in the design is to select the appropriate scaling $\kappa_2(\Gamma_D)$ between maximum acceleration of the target and $\tilde{q}$.

In the case of DWNA, the acceleration errors are assumed to be fixed during each sample period and independent between any two sample periods. Thus, if the time periods between measurements vary widely, the CWNA is more appropriate, because the basic target motion model is independent of the sampling interval. This is supported by the fact that the maneuver index of DWNA is a higher order function of sample period T than the maneuver index for CWNA. Also, if the process noise for CWNA is used for the illustrative example in [6], better tracking is achieved by doubling the data rate. Thus, the process noise based on CWNA is more appropriate for tracking with multiple radars because the sample periods between measurements tend to vary significantly. However,

the DWNA model leads to simpler equations and it is most often used for illustration and publications.

19.3.2 Nearly Constant Acceleration Motion Model

The dynamical constraint for NCA motion is given by (19.122) with

$$\mathbf{A}_k = \begin{bmatrix} 1 & \delta_k & \frac{1}{2}\delta_k^2 \\ 0 & 1 & \delta_k \\ 0 & 0 & 1 \end{bmatrix} \tag{19.129}$$

For the NCA model, the process noise covariance matrix for DWPA is given by (19.123) with

$$\boldsymbol{B}_k \boldsymbol{B}_k^T = \begin{bmatrix} \frac{1}{4}\delta_k^4 & \frac{1}{2}\delta_k^3 & \frac{1}{2}\delta_k^2 \\ \frac{1}{2}\delta_k^3 & \delta_k^2 & \delta_k \\ \frac{1}{2}\delta_k^2 & \delta_k & 1 \end{bmatrix} \tag{19.130}$$

The maneuver index for the NCA filter with DWPA [7] is given by

$$\Gamma_{DWPA} = \frac{\sigma_v T^2}{\sigma_w} \tag{19.131}$$

where σ_v^2 denotes the variance of the acceleration errors. The σ_w^2 in each coordinate will vary with the target location. An appropriate value of σ_w is identified for a radar tracking problem by picking the maximum or average over the three coordinates or computing it with target location. The maneuver index is often used to characterize the filter design. However, selection of σ_v^2 presents a challenge. One design method begins by setting σ_v equal to the maximum incremental change in acceleration of the target between any two measurements. Then, Monte Carlo simulations are conducted to characterize performance and refine the selection of σ_v.

19.3.3 Singer Motion Model

The Singer motion model represents the acceleration errors as an auto-correlated sequence of accelerations. The autocorrelation decays exponentially with the time period between the measurements. The dynamical constraint for the Singer model is given by (19.122) with

$$\mathbf{A}_k = \begin{bmatrix} 1 & \delta_k & \tau_m^2 \left[\dfrac{\delta_k}{\tau_m} + \exp\left[-\dfrac{\delta_k}{\tau_m} \right] - 1 \right] \\ 0 & 1 & \tau_m \left[1 - \exp\left[-\dfrac{\delta_k}{\tau_m} \right] \right] \\ 0 & 0 & \exp\left[-\dfrac{\delta_k}{\tau_m} \right] \end{bmatrix} \tag{19.132}$$

where τ_m is the time constant for the maneuver. For the Singer model, the process noise covariance matrix is given in [24] by (19.123) with

$$\boldsymbol{B}_k \boldsymbol{B}_k^T = \sigma_v^2 \begin{bmatrix} b_{11} & b_{12} & b_{13} \\ b_{12} & b_{22} & b_{23} \\ b_{13} & b_{23} & b_{33} \end{bmatrix} \tag{19.133}$$

where

$$b_{11} = \tau_m^4 \left[1 + \frac{2\delta_k}{\tau_m} - \exp\left[-2\frac{\delta_k}{\tau_m}\right] - 2\frac{\delta_k^2}{\tau_m^2} + \frac{2\delta_k^3}{3\tau_m^3} - 4\frac{\delta_k}{\tau_m}\exp\left[-\frac{\delta_k}{\tau_m}\right] \right] \tag{19.134}$$

$$b_{12} = \tau_m^3 \left[1 - \frac{2\delta_k}{\tau_m} + \exp\left[-2\frac{\delta_k}{\tau_m}\right] - 2\left(1 - \frac{\delta_k}{\tau_m}\right)\exp\left[-\frac{\delta_k}{\tau_m}\right] + \frac{\delta_k^2}{\tau_m^2} \right] \tag{19.135}$$

$$b_{13} = \tau_m^2 \left[1 - \exp\left[-2\frac{\delta_k}{\tau_m}\right] - 2\frac{\delta_k}{\tau_m}\exp\left[-\frac{\delta_k}{\tau_m}\right] \right] \tag{19.136}$$

$$b_{22} = \tau_m^2 \left[\frac{2\delta_k}{\tau_m} - 3 - \exp\left[-2\frac{\delta_k}{\tau_m}\right] + 4\exp\left[-\frac{\delta_k}{\tau_m}\right] \right] \tag{19.137}$$

$$b_{23} = \tau_m \left[1 + \exp\left[-2\frac{\delta_k}{\tau_m}\right] - 2\exp\left[-\frac{\delta_k}{\tau_m}\right] \right] \tag{19.138}$$

$$b_{33} = 1 - \exp\left[-2\frac{\delta_k}{\tau_m}\right] \tag{19.139}$$

and σ_v^2 denotes the variance of the acceleration errors in the model. When $\delta_k \tau_m^{-1} \leq 0.1$, the state transition matrix approaches that of NCA and [24]

$$\boldsymbol{B}_k \boldsymbol{B}_k^T \approx \frac{2\sigma_v^2}{\tau_m} \begin{bmatrix} \frac{\delta_k^5}{20} & \frac{\delta_k^4}{8} & \frac{\delta_k^3}{6} \\ \frac{\delta_k^4}{8} & \frac{\delta_k^3}{3} & \frac{\delta_k^2}{2} \\ \frac{\delta_k^3}{6} & \frac{\delta_k^2}{2} & \delta_k \end{bmatrix} \tag{19.140}$$

When $\delta_k \tau_m^{-1} \geq 0.9$, the state transition matrix approaches that of NCV and [24]

$$\boldsymbol{B}_k \boldsymbol{B}_k^T \approx \sigma_v^2 \begin{bmatrix} \frac{2\delta_k^3 \tau_m}{3} & \delta_k^2 \tau_m & \tau_m^2 \\ \delta_k^2 \tau_m & 2\delta_k \tau_m & \tau_m \\ \tau_m^2 & \tau_m & 1 \end{bmatrix} \tag{19.141}$$

The selection of σ_v^2 presents a challenge. One design method begins by setting σ_v equal to the maximum incremental change in acceleration of the target between any two measurements. Then, Monte Carlo simulations are conducted to characterize performance and refine the selection of σ_v.

19.3.4 Nearly Constant Speed Motion Model

Nearly constant speed motion is very important because it tends to characterize the motion of targets performing maneuvers with control surfaces. The high acceleration maneuvers of many targets are achieved with control surfaces and the speed remains nearly constant during maneuvers. A common approach to modeling constant speed maneuvers is to assume a constant turn rate in the horizontal plane [7] and estimate the turn rate Ω. The limitations of this approach include the requirements that the turn rate remain nearly constant and the maneuver be performed in the horizontal plane. These are two

serious limitations. This model has been extended to include both vertical and horizontal maneuvers, but the approach is rather complex and involves estimation of two parameters for the turn. An alternate approach is the use of a piecewise constant speed motion model in which the motion is characterized by incremental constant speed turns in an arbitrary plane. This approach is generally preferable. The dynamical constraint for the piecewise constant speed motion is given by (19.122) with

$$\mathbf{A}_k = \begin{bmatrix} 1 & \dfrac{\sin(\Omega_k \delta_k)}{\Omega_k} & \dfrac{1-\cos(\Omega_k \delta_k)}{\Omega_k^2} \\ 0 & \cos(\Omega_k \delta_k) & \dfrac{\sin(\Omega_k \delta_k)}{\Omega_k} \\ 0 & -\Omega_k \sin(\Omega_k \delta_k) & \cos(\Omega_k \delta_k) \end{bmatrix} \tag{19.142}$$

where

$$\Omega_k = \frac{\sqrt{\ddot{x}_k^2 + \ddot{y}_k^2 + \ddot{z}_k^2}}{\sqrt{\dot{x}_k^2 + \dot{y}_k^2 + \dot{z}_k^2}} \tag{19.143}$$

The process noise model for NCA motion is appropriate for the piecewise constant speed motion model. However, the selection of σ_v^2 continues to present a challenge. Again, σ_v can be set equal to the maximum incremental change in acceleration of the target between any two measurements. As before, Monte Carlo simulations are conducted to characterize performance and refine the selection of σ_v.

Targets that maneuver with control surfaces tend to retain a nearly constant speed through the maneuver. The use of this kinematic constraint has been investigated as a means to improve the tracking of highly maneuvering targets. The application of a kinematic constraint as a pseudo-measurement has been demonstrated to improve the tracking of constant speed, maneuvering targets [17,25].

19.4 MEASUREMENT MODELS

Radar measurements are typically in polar or spherical coordinates. For a radar measuring the target location in full Cartesian coordinates, the two angles are actually measured in two orthogonal planes, say U and V, in the aperture of the antenna [26]. In some cases, the radar measures the velocity of the target along the range vector between the target and the antenna. The general measurement equation is given by

$$\boldsymbol{Z}_k = h_k(\boldsymbol{X}_k) + \boldsymbol{w}_k \tag{19.144}$$

where

$\boldsymbol{Z}_k$ = measurement vector at time t_k.
$\boldsymbol{w}_k$ = measurement error at time t_k with $\boldsymbol{w}_k \sim \mathrm{N}(0, \mathbf{R}_k)$.

Typically, the target state estimate is maintained in a Cartesian reference frame that is stabilized (often in an inertial coordinate frame) relative to any motion of the radar antenna. In this case, an affine transform is typically used to define the relationship between the

two coordinate systems and the measurement equation is given by

$$\boldsymbol{Z}_k = h_k(\mathbf{M}_k \boldsymbol{X}_k + \boldsymbol{L}_k) + \boldsymbol{w}_k \tag{19.145}$$

where

$$\begin{aligned} \mathbf{M}_k &= \text{matrix that rotates the target state vector into the frame of the antenna at time } t_k. \\ \boldsymbol{L}_k &= \text{vector that translates the target state vector into the frame of the antenna at time } t_k. \end{aligned}$$

The typical formulation of the measurements as range, bearing, elevation, and range rate is presented first. Then, the sine space formulation of the measurements in the antenna frame is presented. The issue of unbiased converted measurements will be addressed in both sections. The measurement equation for LFM waveforms is then addressed. Finally, tracking with measurements of reduced dimension is discussed.

19.4.1 Measurements in Stabilized Coordinates

Typically, radar measurements are modeled in spherical or polar coordinates in which measurements as a function of $\boldsymbol{X}_k$ are given by

$$\boldsymbol{Z}_k = \begin{bmatrix} r_k \\ b_k \\ e_k \\ \dot{r}_k \end{bmatrix} = h_k(\boldsymbol{X}_k) + \boldsymbol{w}_k = \begin{bmatrix} h_r(\boldsymbol{X}_k) \\ h_b(\boldsymbol{X}_k) \\ h_e(\boldsymbol{X}_k) \\ h_d(\boldsymbol{X}_k) \end{bmatrix} + \begin{bmatrix} w_{rk} \\ w_{bk} \\ w_{ek} \\ w_{dk} \end{bmatrix} \tag{19.146}$$

where

$$\begin{aligned} r_k &= \text{measured range at time } t_k. \\ b_k &= \text{measured bearing at time } t_k. \\ e_k &= \text{measured elevation at time } t_k. \\ \dot{r}_k &= \text{Doppler-derived measurement of range rate at time } t_k. \\ w_{rk} &= \text{error in range measurement with } w_{rk} \sim \mathrm{N}\left(0, \sigma_{rk}^2\right). \\ w_{bk} &= \text{error in bearing measurement with } w_{bk} \sim \mathrm{N}\left(0, \sigma_{bk}^2\right). \\ w_{ek} &= \text{error in elevation measurement with } w_{ek} \sim \mathrm{N}\left(0, \sigma_{ek}^2\right). \\ w_{dk} &= \text{error in Doppler range rate measurement with } w_{dk} \sim \mathrm{N}\left(0, \sigma_{dk}^2\right). \end{aligned}$$

Also

$$h_r(\boldsymbol{X}_k) = \sqrt{x_k^2 + y_k^2 + z_k^2} \tag{19.147}$$

$$h_b(\boldsymbol{X}_k) = \begin{cases} \tan^{-1}\left(\dfrac{x_k}{y_k}\right), & |y_k| > |x_k| \\ \dfrac{\pi}{2} - \tan^{-1}\left(\dfrac{y_k}{x_k}\right), & |x_k| > |y_k| \end{cases} \tag{19.148}$$

$$h_e(\boldsymbol{X}_k) = \begin{cases} \tan^{-1}\left(\dfrac{z_k}{\sqrt{x_k^2 + y_k^2}}\right), & |\sqrt{x_k^2 + y_k^2}| > |z_k| \\ \dfrac{\pi}{2} - \tan^{-1}\left(\dfrac{\sqrt{x_k^2 + y_k^2}}{z_k}\right), & |z_k| > |\sqrt{x_k^2 + y_k^2}| \end{cases} \tag{19.149}$$

$$h_d(\boldsymbol{X}_k) = \frac{x_k\dot{x}_k + y_k\dot{y}_k + z_k\dot{z}_k}{\sqrt{x_k^2 + y_k^2 + z_k^2}} \tag{19.150}$$

where bearing b_k and elevation e_k measurements are two angles in a radar reference frame. The two cases for the bearing and elevation measurements are included to prevent singularities in the measurement functions. Note that a four-quadrant arctangent function or some other logic must be employed to ensure the bearing measurement is in the proper quadrant. While (19.147) through (19.150) represent the different kinematic measurements of a radar, many radars do not measure all four kinematic parameters. For example, most long-range surveillance radars measure only range and bearing (and possibly range rate). The kinematic state of the target is modeled in a plane that is tilted relative to the local horizontal plane and the angle of the tilt changes as the target range or altitude change.

The extended Kalman filter (EKF) for tracking with radar measurements uses a linearized model for the measurements. Thus,

$$\mathbf{H}_k = \begin{bmatrix} \dfrac{\partial h_r(\boldsymbol{X}_k)}{\partial \boldsymbol{X}_k} \\ \dfrac{\partial h_b(\boldsymbol{X}_k)}{\partial \boldsymbol{X}_k} \\ \dfrac{\partial h_e(\boldsymbol{X}_k)}{\partial \boldsymbol{X}_k} \\ \dfrac{\partial h_d(\boldsymbol{X}_k)}{\partial \boldsymbol{X}_k} \end{bmatrix}_{\boldsymbol{X}_k = \boldsymbol{X}_{k|k-1}} = \begin{bmatrix} \boldsymbol{H}_{rk} \\ \boldsymbol{H}_{bk} \\ \boldsymbol{H}_{ek} \\ \boldsymbol{H}_{dk} \end{bmatrix} \tag{19.151}$$

where the one-step ahead predicted state is given by

$$\boldsymbol{X}_{k|k-1} = \begin{bmatrix} x_{k|k-1} & \dot{x}_{k|k-1} & y_{k|k-1} & \dot{y}_{k|k-1} & z_{k|k-1} & \dot{z}_{k|k-1} \end{bmatrix}^T \tag{19.152}$$

The rows of H_k are given by

$$\boldsymbol{H}_{rk} = \begin{bmatrix} \dfrac{x_{k|k-1}}{r_{k|k-1}} & 0 & \dfrac{y_{k|k-1}}{r_{k|k-1}} & 0 & \dfrac{z_{k|k-1}}{r_{k|k-1}} & 0 \end{bmatrix} \tag{19.153}$$

$$\boldsymbol{H}_{bk} = \begin{bmatrix} \dfrac{y_{k|k-1}}{rh_{k|k-1}^2} & 0 & -\dfrac{x_{k|k-1}}{rh_{k|k-1}^2} & 0 & 0 & 0 \end{bmatrix} \tag{19.154}$$

$$\boldsymbol{H}_{ek} = \begin{bmatrix} -\dfrac{x_{k|k-1}z_{k|k-1}}{r_{k|k-1}^2 rh_{k|k-1}} & 0 & -\dfrac{y_{k|k-1}z_{k|k-1}}{r_{k|k-1}^2 rh_{k|k-1}} & 0 & \dfrac{rh_{k|k-1}}{r_{k|k-1}^2} & 0 \end{bmatrix} \tag{19.155}$$

$$\boldsymbol{H}_{dk} = \begin{bmatrix} \boldsymbol{H}_{dk}(1) & \dfrac{x_{k|k-1}}{r_{k|k-1}} & \boldsymbol{H}_{dk}(3) & \dfrac{y_{k|k-1}}{r_{k|k-1}} & \boldsymbol{H}_{dk}(5) & \dfrac{z_{k|k-1}}{r_{k|k-1}} \end{bmatrix} \tag{19.156}$$

where

$$\boldsymbol{H}_{dk}(1) = \frac{\left(y_{k|k-1}^2 + z_{k|k-1}^2\right)\dot{x}_{k|k-1} - (y_{k|k-1}\dot{y}_{k|k-1} + z_{k|k-1}\dot{z}_{k|k-1})x_{k|k-1}}{r_{k|k-1}^3} \tag{19.157}$$

$$\boldsymbol{H}_{dk}(3) = \frac{\left(x_{k|k-1}^2 + z_{k|k-1}^2\right)\dot{y}_{k|k-1} - (x_{k|k-1}\dot{x}_{k|k-1} + z_{k|k-1}\dot{z}_{k|k-1})y_{k|k-1}}{r_{k|k-1}^3} \tag{19.158}$$

$$\boldsymbol{H}_{dk}(5) = \frac{rh_{k|k-1}^2\dot{z}_{k|k-1} - (x_{k|k-1}\dot{x}_{k|k-1} + y_{k|k-1}\dot{y}_{k|k-1})z_{k|k-1}}{r_{k|k-1}^3} \tag{19.159}$$

$$r_{k|k-1} = \sqrt{x_{k|k-1}^2 + y_{k|k-1}^2 + z_{k|k-1}^2} \tag{19.160}$$

$$rh_{k|k-1} = \sqrt{x_{k|k-1}^2 + y_{k|k-1}^2} \tag{19.161}$$

Since the EKF uses a linearized output matrix for $h(\boldsymbol{X}_k)$ in the covariance update, the EKF does not provide an optimal estimate of the target state. The results of [7,27] suggest that the performance of the EKF is degraded significantly when

$$\frac{r_k \max\left\{\sigma_{bk}^2, \sigma_{ek}^2\right\}}{\sigma_{rk}} \geq 0.4 \tag{19.162}$$

Performing a debiased coordinate conversion of the spherical measurements to Cartesian measurements was proposed in [27] and refined in [28] to reduce the impacts of this limitation of the EKF. In this case, the measurements of position become direct observations of the Cartesian coordinates of the target position and the measurement equation is a simple linear function of the state. However, the EKF will be required to process the Doppler range rate measurement because it is not easily be converted to a Cartesian measurement. Other issues associated with the processing of spherical radar measurements as Cartesian observations are discussed in [29].

19.4.2 Measurements in Sine Space

The angles of a target are actually measured in two orthogonal planes, say U and V, at the aperture of the radar antenna [26]. When considering the measurements in the U-plane and the V-plane, the radar measurements (direction cosines) as a function of $\boldsymbol{X}_k$ in a Cartesian reference frame at the antenna are given by

$$\boldsymbol{Z}_k = \begin{bmatrix} r_k \\ U_k \\ V_k \\ \dot{r}_k \end{bmatrix} = \begin{bmatrix} h_r(\boldsymbol{X}_k) \\ h_U(\boldsymbol{X}_k) \\ h_V(\boldsymbol{X}_k) \\ h_d(\boldsymbol{X}_k) \end{bmatrix} + \begin{bmatrix} w_{rk} \\ w_{Uk} \\ w_{Vk} \\ w_{dk} \end{bmatrix} \tag{19.163}$$

where

U_k = measured sine of the angle of the target in the U-plane at time t_k.
V_k = measured sine of the angle of the target in the V-plane at time t_k.
w_{Uk} = error in the U_k measurement with $w_{Uk} \sim \mathrm{N}(0, \sigma_{Uk}^2)$.
w_{Vk} = error in the V_k measurement with $w_{Vk} \sim \mathrm{N}(0, \sigma_{Vk}^2)$.

Also

$$h_U(\boldsymbol{X}_k) = \frac{x_k}{\sqrt{x_k^2 + y_k^2 + z_k^2}} \tag{19.164}$$

$$h_V(\boldsymbol{X}_k) = \frac{y_k}{\sqrt{x_k^2 + y_k^2 + z_k^2}} \tag{19.165}$$

The radar measurements as a function of $\boldsymbol{X}_k$ in a radar reference frame displaced from the antenna are given by

$$\boldsymbol{Z}_k = \begin{bmatrix} r_k \\ U_k \\ V_k \\ \dot{r}_k \end{bmatrix} = h_k(M_k\boldsymbol{X}_k + \boldsymbol{L}_k) + \boldsymbol{w}_k = \begin{bmatrix} h_r(M_k\boldsymbol{X}_k + \boldsymbol{L}_k) \\ h_U(M_k\boldsymbol{X}_k + \boldsymbol{L}_k) \\ h_V(M_k\boldsymbol{X}_k + \boldsymbol{L}_k) \\ h_d(M_k\boldsymbol{X}_k + \boldsymbol{L}_k) \end{bmatrix} + \begin{bmatrix} w_{rk} \\ w_{Uk} \\ w_{Vk} \\ w_{dk} \end{bmatrix} \tag{19.166}$$

The EKF or converted measurements is commonly used for tracking the target with measurements in sine space. Implementation of the EKF requires the following

$$\mathbf{H}_k = \begin{bmatrix} \dfrac{\partial h_r(\boldsymbol{X}_k)}{\partial \boldsymbol{X}_k} \\ \dfrac{\partial h_U(\boldsymbol{X}_k)}{\partial \boldsymbol{X}_k} \\ \dfrac{\partial h_V(\boldsymbol{X}_k)}{\partial \boldsymbol{X}_k} \\ \dfrac{\partial h_d(\boldsymbol{X}_k)}{\partial \boldsymbol{X}_k} \end{bmatrix}_{\boldsymbol{X}_k = M_k\boldsymbol{X}_{k|k-1} + \boldsymbol{L}_k} = \begin{bmatrix} \boldsymbol{H}_{rk} \\ \boldsymbol{H}_{Uk} \\ \boldsymbol{H}_{Vk} \\ \boldsymbol{H}_{dk} \end{bmatrix} \tag{19.167}$$

Let

$$\boldsymbol{X}'_{k|k-1} = M_k\boldsymbol{X}_{k|k-1} + \boldsymbol{L}_k \tag{19.168}$$

and

$$\boldsymbol{X}'_{k|k-1} = \begin{bmatrix} x'_{k|k-1} & \dot{x}'_{k|k-1} & y'_{k|k-1} & \dot{y}'_{k|k-1} & z'_{k|k-1} & \dot{z}'_{k|k-1} \end{bmatrix}^T \tag{19.169}$$

The elements of $\mathbf{H}_k$ are then given by (19.153) and (19.156) with $\boldsymbol{X}_{k|k-1} = \boldsymbol{X}'_{k|k-1}$ and

$$\boldsymbol{H}_{Uk} = \begin{bmatrix} \dfrac{\left(r'_{k|k-1}\right)^2 - \left(x'_{k|k-1}\right)^2}{\left(r'_{k|k-1}\right)^3} & 0 & -\dfrac{x'_{k|k-1}y'_{k|k-1}}{\left(r'_{k|k-1}\right)^3} & 0 & -\dfrac{x'_{k|k-1}z'_{k|k-1}}{\left(r'_{k|k-1}\right)^3} & 0 \end{bmatrix} \tag{19.170}$$

$$\boldsymbol{H}_{Vk} = \begin{bmatrix} -\dfrac{x'_{k|k-1}y'_{k|k-1}}{\left(r'_{k|k-1}\right)^3} & 0 & \dfrac{\left(r'_{k|k-1}\right)^2 - \left(y'_{k|k-1}\right)^2}{\left(r'_{k|k-1}\right)^3} & 0 & -\dfrac{y'_{k|k-1}z'_{k|k-1}}{\left(r'_{k|k-1}\right)^3} & 0 \end{bmatrix} \tag{19.171}$$

where

$$r'_{k|k-1} = \sqrt{\left(x'_{k|k-1}\right)^2 + \left(y'_{k|k-1}\right)^2 + \left(z'_{k|k-1}\right)^2} \tag{19.172}$$

$$rh'_{k|k-1} = \sqrt{\left(x'_{k|k-1}\right)^2 + \left(y'_{k|k-1}\right)^2} \tag{19.173}$$

Since the EKF uses a linearized output matrix for $h(\boldsymbol{X}_k)$ in the covariance update, the EKF does not provide an optimal estimate of the target state. The results of [30] suggest that the performance of the EKF is degraded significantly when

$$r_k \frac{\max\{\sigma_{Uk}^2, \sigma_{Vk}^2\}}{\sigma_{rk}} \sqrt{\frac{3 - 3\bar{U}_{0k}^2 + \bar{U}_{0k}^4}{1 - 2\bar{U}_{0k}^2 + \bar{U}_{0k}^4}} \geq \frac{2}{3} \tag{19.174}$$

where $\bar{U}_{0k} = \sqrt{U_k^2 + V_k^2}$. Performing a nearly unbiased coordinate conversion of the measurements in sine space to Cartesian measurements is proposed in [30] to reduce the impact on this limitation of the EKF. In this case, the measurements become direct observations of the Cartesian coordinates of the target position and the measurement equation is a simple linear function of the state.

19.4.3 Measurements with LFM Waveforms

When a radar use an LFM waveform, the range measurement is coupled to the range rate induced Doppler of the target [12]. For an LFM waveform, the output function for the range measurement is given by

$$h_{rd}(\boldsymbol{X}_k) = h_r(\boldsymbol{X}_k) + \Delta t \; h_d(\boldsymbol{X}_k) \tag{19.175}$$

where

$$\Delta t = \frac{f_t \tau}{f_2 - f_1} \tag{19.176}$$

with f_t denoting the frequency of the transmitted waveform, τ denoting the duration of the transmitted pulse, f_1 denoting the initial frequency in the waveform modulation, and f_2 denoting the final frequency in the waveform modulation. The linearized output matrix is given by

$$\mathbf{H}_{rdk} = \mathbf{H}_{rk} + \Delta t \; \mathbf{H}_{dk} \tag{19.177}$$

As noted in [12] and shown analytically in [13], the range-Doppler coupling of the waveform affects the tracking accuracy. For example, an up-chirp waveform (i.e., $f_2 > f_1$ or $\Delta t > 0$) gives lower steady-state tracking errors than an equivalent down-chirp waveform (i.e., $f_2 < f_1$ or $\Delta t < 0$).

19.4.4 Surveillance Radars with Measurements of Reduced Dimension

Early warning or long range surveillance radars typically measure only the range and bearing (and possibly range rate) of the target. In this case, the radar measurements are given as a function of $\boldsymbol{X}_k$ by

$$\boldsymbol{Z}_k = \begin{bmatrix} r_k \\ b_k \\ \dot{r}_k \end{bmatrix} = h_k(\boldsymbol{X}_k) + \boldsymbol{w}_k = \begin{bmatrix} h_r(\boldsymbol{X}_k) \\ h_b(\boldsymbol{X}_k) \\ h_d(\boldsymbol{X}_k) \end{bmatrix} + \begin{bmatrix} w_{rk} \\ w_{bk} \\ w_{dk} \end{bmatrix} \tag{19.178}$$

where measured range is defined in a plane that is tilted relative to the horizontal plane. Full Cartesian estimate of the target state is not achievable under most circumstances. For tracking, the measurements are usually defined as a function in a two coordinate Cartesian system. For example, the measured range is given by $r_k = \sqrt{\bar{x}_k^2 + \bar{y}_k^2}$, where $\bar{x}_k$ and $\bar{y}_k$ are the coordinates of the target in the tilted plane. Note that the tilt angle changes as the target moves toward the radar or changes altitude. Also, note that the measured range rate is not exactly equal to the derivative to the range r_k. The measured bearing will have the same functional form of $\bar{x}_k$ and $\bar{y}_k$, while the Doppler measurement cannot be expressed solely as a function of $\bar{x}_k$ and $\bar{y}_k$ and it remain a function of z_k and $\dot{z}_k$. Thus, the processing of Doppler measurements while tracking $\bar{x}_k$ and $\bar{y}_k$ is problematic. The range and range rate are often tracked in a separate filter.

19.5 RADAR TRACK FILTERING

After the data association has been accomplished and a measurement has been assigned to a track, kinematic state estimation is performed for the track with that measurement. For most radar systems, the target motion is modeled in Cartesian coordinates, while radar measurements are typically in polar or spherical coordinates. Since the measurements of (19.144) are a nonlinear function of the state, the EKF is often employed to estimate the state [7]. The EKF is a stochastic state estimation approach that presumes an imperfect model for the target motion. In this approach, the target motion model includes a random process and a perfect estimate of the kinematic state is not possible. However, in some applications, a parametric estimation approach is taken. In this approach, a perfect model for the target motion is assumed, and the time period over which the model is applied is limited to prevent distortion of the data by violation of the model. In this approach, the covariance of the state estimate (or track) will approach zero as more data are processed. As the covariance of the track approaches zero, the gain for processing new data will likewise approach zero. Nonlinear least squares or maximum likelihood estimation are the typical methods employed for a parametric approach to track filtering, and since a window or segment of the measurements is processed as a batch, the parametric estimator is often referred to as a batch estimator.

In this section, nonlinear least squares estimation and the EKF are presented for the radar tracking problem. A few comments on the converted measurement filter are also given.

19.5.1 Nonlinear Least Squares Estimation

For a parametric or batch estimator approach to radar tracking of a target with nonlinear measurements, the measurement equation is given by (19.144) and the dynamical motion model is given by

$$\boldsymbol{X}_{k+1} = \mathbf{F}_k \boldsymbol{X}_k \tag{19.179}$$

where $\boldsymbol{X}_k$ is the state vector for the target at time t_k. This estimator is often referred to as a *sliding window estimator* or *batch estimator*. The name "sliding window estimator" is derived from the idea that the estimate is based on a window of the N most recent measurements and that window slides along with time. Note that estimates based on

fewer measurements will have a higher variance, but the distortions of the underlying true trajectory will be smaller.

Using (19.179) and (19.144), the measurement at t_N can be rewritten as

$$\boldsymbol{Z}_N = h(\boldsymbol{X}_N) + \boldsymbol{w}_N = h(\mathbf{F}_{N-1}\mathbf{F}_{N-2}\ldots\mathbf{F}_1\boldsymbol{X}_1) + \boldsymbol{w}_N \tag{19.180}$$

Given N measurements between t_1 and t_N, an augmented measurement equation can be written in terms of $\boldsymbol{X}_1$ as

$$\bar{\boldsymbol{Z}}_1^N = \begin{bmatrix} \boldsymbol{Z}_1 \\ \boldsymbol{Z}_2 \\ \vdots \\ \boldsymbol{Z}_{N-1} \\ \boldsymbol{Z}_N \end{bmatrix} = \begin{bmatrix} h_1(\boldsymbol{X}_1) \\ h_2(\mathbf{F}_1\boldsymbol{X}_1) \\ \vdots \\ h_{N-1}(\mathbf{F}_{N-2}\mathbf{F}_{N-3}\ldots\mathbf{F}_1\boldsymbol{X}_1) \\ h_N(\mathbf{F}_{N-1}\mathbf{F}_{N-2}\ldots\mathbf{F}_1\boldsymbol{X}_1) \end{bmatrix} + \begin{bmatrix} \boldsymbol{w}_1 \\ \boldsymbol{w}_2 \\ \vdots \\ \boldsymbol{w}_{N-1} \\ \boldsymbol{w}_N \end{bmatrix} = \bar{h}_N(\boldsymbol{X}_1) + \boldsymbol{W}_N \tag{19.181}$$

where

$$\mathrm{E}\{\boldsymbol{W}_N\} = 0 \tag{19.182}$$

$$\bar{\mathbf{R}}_N = \mathrm{E}\{\boldsymbol{W}_N\boldsymbol{W}_N^T\} = \begin{bmatrix} \mathbf{R}_1 & \mathbf{0} & \ldots & \mathbf{0} \\ \mathbf{0} & \mathbf{R}_2 & \ldots & \vdots \\ \vdots & & \ddots & \\ \mathbf{0} & \ldots & \mathbf{0} & \mathbf{R}_N \end{bmatrix} \tag{19.183}$$

In this case, $\bar{\mathbf{R}}_N$ is a block diagonal matrix because the measurement errors between any two times are assumed to be zero mean and independent. Had the errors included correlation across time, off-diagonal elements of the matrix would be nonzero. One of the advantages of parametric estimation is the ease of including correlation of the measurement errors at different times. The weighted nonlinear least-squares estimate (NLSE) [7] of $\boldsymbol{X}_1$ given measurements from t_1 to t_N is found through an iterative process given by

$$\boldsymbol{X}_{1|N}^{(i+1)} = \boldsymbol{X}_{1|N}^{(i)} + \left(\left(\bar{\mathbf{H}}_N^{(i)}\right)^T\bar{\mathbf{R}}_N^{-1}\bar{\mathbf{H}}_N^{(i)}\right)^{-1}\left(\bar{\mathbf{H}}_N^{(i)}\right)^T\bar{\mathbf{R}}_N^{-1}\left[\bar{\boldsymbol{Z}}_1^N - \bar{h}_N\left(\boldsymbol{X}_{1|N}^{(i)}\right)\right] \tag{19.184}$$

where

$$\mathbf{H}_N^{(i)} = \left.\frac{\partial\bar{h}_N(\boldsymbol{X}_1)}{\partial\boldsymbol{X}_1}\right|_{\boldsymbol{X}_1=\boldsymbol{X}_{1|N}^{(i)}} \tag{19.185}$$

The initialization of the iterative process can be achieved by using converted measurements and a linear least squares estimate with the first M measurements. The covariance of the estimate is given by

$$P_{1|N} = \left(\bar{\mathbf{H}}_N^T\bar{\mathbf{R}}_N^{-1}\bar{\mathbf{H}}_N\right)^{-1} \tag{19.186}$$

where $\bar{\mathbf{H}}_N$ is the partial derivative of $\bar{h}_N(\boldsymbol{X}_1)$ evaluated at the final estimate. Note that the covariance will reflect only the actual errors in the state estimate to the degree that the kinematic model (19.179) is accurate and the measurements errors are zero-mean Gaussian with covariance $\bar{\mathbf{R}}_N$. The $\boldsymbol{X}_{1|N}$ and $\mathbf{P}_{1|N}$ are smoothed estimates. For a state estimate and

covariance at time t_j, $t_1 < t_j \leq t_N$,

$$\boldsymbol{X}_{j|N} = \mathbf{F}_{j-1} \ldots \mathbf{F}_1 \boldsymbol{X}_{1|N} \tag{19.187}$$

$$\mathbf{P}_{j|N} = \mathbf{F}_{j-1} \ldots \mathbf{F}_1 \mathbf{P}_{1|N} \mathbf{F}_1^T \ldots \mathbf{F}_{j-1}^T \tag{19.188}$$

For the Gaussian errors, $\boldsymbol{X}_{j|N}$ is also the ML estimate of $\boldsymbol{X}_j$. For the parametric approach, constant velocity and constant acceleration motion are the two most common assumptions for the motion of the target. However, more complicated models are typically used for applications like ballistic missile defense.

19.5.2 Extended Kalman Filter

For a stochastic state estimation for radar tracking with nonlinear measurements, the measurement equation is given by (19.144) and the dynamical motion model is given by

$$\boldsymbol{X}_{k+1} = \mathbf{F}_k \boldsymbol{X}_k + \mathbf{G}_k \boldsymbol{v}_k \tag{19.189}$$

where $\mathbf{G}_k$ is the input matrix for the target motion at time t_k, and $\boldsymbol{v}_k$ is the white noise error in the state process with $v_k \sim \mathrm{N}(0, \mathbf{Q}_k)$. The EKF for target state estimation with nonlinear measurements is given by the following equations:

State prediction:

$$\boldsymbol{X}_{k|k-1} = \mathbf{F}_{k-1} \boldsymbol{X}_{k-1|k-1} \tag{19.190}$$

$$\mathbf{P}_{k|k-1} = \mathbf{F}_{k-1} \mathbf{P}_{k-1|k-1} \mathbf{F}_{k-1}^T + \mathbf{G}_{k-1} \mathbf{Q}_{k-1} \mathbf{G}_{k-1}^T \tag{19.191}$$

State update with the measurement:

$$\boldsymbol{X}_{k|k} = \boldsymbol{X}_{k|k-1} + \mathbf{K}_k \widetilde{\boldsymbol{Z}}_k \tag{19.192}$$

$$\widetilde{\boldsymbol{Z}}_k = \boldsymbol{Z}_k - h_k(\boldsymbol{X}_{k|k-1}) \tag{19.193}$$

$$\mathbf{P}_{k|k} = [\mathbf{I} - \mathbf{K}_k \mathbf{H}_k] \mathbf{P}_{k|k-1} \tag{19.194}$$

$$\mathbf{K}_k = \mathbf{P}_{k|k-1} \mathbf{H}_k^T \mathbf{S}_k^{-1} \tag{19.195}$$

$$\mathbf{S}_k = \mathbf{H}_k \mathbf{P}_{k|k-1} \mathbf{H}_k^T + \mathbf{R}_k \tag{19.196}$$

In these equations, $\widetilde{\boldsymbol{Z}}_k$ is the filter residual at time t_k and

$$\mathbf{H}_k = \left[\frac{\partial h_k(\boldsymbol{X}_k)}{\partial \boldsymbol{X}_k} \right]_{\boldsymbol{X}_k = \boldsymbol{X}_{k|k-1}} \tag{19.197}$$

Since the measurements are a nonlinear function of the state and the EKF uses a linearized output matrix for $h_k(\boldsymbol{X}_k)$ in the covariance update, the EKF does not provide an optimal estimate of the target state. When the criteria of (19.162) are satisfied for radar measurements in spherical coordinates or the criteria of (19.174) is satisfied for measurements in sine space, the performance of the EKF is expected to be poor, and either converted measurements [28,30] or the measurement covariance adaptive extended Kalman filter (MCAEKF) [30] should be employed to reduce the impacts of the nonlinearities in the measurements on tracking performance.

Typically, the target state estimate is maintained in a Cartesian reference frame that is stabilized relative to any motion of the radar antenna. In this case, an affine transform

is typically used to define the relationship between the two coordinate systems and the measurement equation is given in (19.145). The measurement update portion of the EKF for target state estimation with nonlinear measurements at a remote reference frame is given by the following:

Update of the state estimate with the measurement:

$$\boldsymbol{X}_{k|k} = \boldsymbol{X}_{k|k-1} + \mathbf{K}_k[\boldsymbol{Z}_k - h_k(\mathbf{M}_k\boldsymbol{X}_{k|k-1} + \boldsymbol{L}_k)] \tag{19.198}$$

$$\mathbf{P}_{k|k} = [\mathbf{I} - \mathbf{K}_k\mathbf{H}_k\mathbf{M}_k]\mathbf{P}_{k|k-1} \tag{19.199}$$

$$\mathbf{K}_k = \mathbf{P}_{k|k-1}\mathbf{M}_k^T\mathbf{H}_k^T\mathbf{S}_k^{-1} \tag{19.200}$$

$$\mathbf{S}_k = \mathbf{H}_k\mathbf{M}_k\mathbf{P}_{k|k-1}\mathbf{M}_k^T\mathbf{H}_k^T + \mathbf{R}_k \tag{19.201}$$

where

$$\mathbf{H}_k = \left[\frac{\partial h_k(\boldsymbol{X}_k)}{\partial \boldsymbol{X}_k}\right]_{\boldsymbol{X}_k=\mathbf{M}_k\boldsymbol{X}_{k|k-1}+\boldsymbol{L}_k} \tag{19.202}$$

19.5.3 Converted Measurement Filter

One of the attractions to the converted measurement filter is the nice linear relationship between the state and the measurements. For the converted measurement filter in Cartesian space, the measurement equation is given as a function of $\boldsymbol{X}_k$ by

$$\boldsymbol{Z}_k = \begin{bmatrix} x_k^m \\ y_k^m \\ z_k^m \end{bmatrix} = \begin{bmatrix} 1 & 0 & 0 & 0 & 0 & 0 \\ 0 & 0 & 1 & 0 & 0 & 0 \\ 0 & 0 & 0 & 0 & 1 & 0 \end{bmatrix} \boldsymbol{X}_k + \begin{bmatrix} w_{xk} \\ w_{yk} \\ w_{zk} \end{bmatrix} = \mathbf{H}\boldsymbol{X}_k + \boldsymbol{W}_k \tag{19.203}$$

where

x_k^m = measured x coordinate at time t_k.
y_k^m = measured y coordinate at time t_k.
z_k^m = measured z coordinate at time t_k.
w_{xk} = error in x-coordinate measurement at time t_k.
w_{yk} = error in y-coordinate measurement at time t_k.
w_{zk} = error in z-coordinate measurement at time t_k.

The converted measurements (x_k^m, y_k^m, z_k^m) are computed from the spherical or sine space measurements, and one should take care to use the unbiased transform as needed [28,30]. The measurement errors (w_{xk}, w_{yk}, w_{zk}) are cross-correlated and non-Gaussian, and one must be careful to use the covariance from the unbiased transform as needed. Since the measurement errors are non-Gaussian, the Kalman filter will not be optimal in a general sense. The Kalman filter will be the best linear estimator given that the measurements are unbiased and the measurement covariance is correct.

19.6 | MEASUREMENT-TO-TRACK DATA ASSOCIATION

All detections, or threshold exceedances, are processed to produce measurements that include an estimate of range and two angles that correspond to the location of a potential target. That measurement could be the result of a false alarm due to receiver noise or an echo

from clutter. If the measurement originated from a target, it could be from a target currently under track or a newly found target. When tracking multiple closely spaced targets, the measurement could have originated with any of the targets. Furthermore, if any of the targets are employing countermeasures to electronic attack, the measurement may not correspond directly to the position of any target. Thus, the problem of accurate and reliable measurement-to-track association is very challenging, and it is the crux of the multitarget tracking problem. However, in this section, the measurement-to-track association problem is restricted to the problem of tracking a single target to limit the scope and length of the material to an appropriate level for this text.

The first step in the measurement-to-track association is validation of the candidate measurements. The measurements are compared with the predicted measurement based on the state estimate of the track. The comparison is usually achieved by computing the difference between the measurements and the predicted measurement and comparing that difference with the sum of the covariances of the measurement and the predicted measurement. Let the set of validated measurements for the target under track be denoted by

$$\boldsymbol{Z}_k^{1,m_k} = \left\{ \boldsymbol{Z}_k^i, \mathbf{R}_k^i, \Re_{ok}^i \right\}_{i=1}^{m_k} \tag{19.204}$$

where $\boldsymbol{Z}_k^i$ is the i-th validated measurement, $\mathbf{R}_k^i$ is the covariance of the i-th measurement, and $\Re_{ok}^i$ is the observed signal-to-noise (i.e., signal-plus-noise-to-noise) ratio.

The second step in the measurement-to-track association is the processing of the validated measurements to update the track state estimate. Some techniques such as *statistical nearest neighbor* (NN) or *strongest neighbor* (SN) select one of the validated measurements to update the track and the standard Kalman filter equations are used to update the state estimate and covariance as if the selection is correct. Other techniques such as the *probabilistic data association filter* (PDAF) use all of the measurements in the validation gate to update the state estimate and covariance. In the case of the PDAF, the uncertainty in the origin of the measurements is captured in the filtering process and the covariance reflects this uncertainty.

The gating and measurement update process is illustrated in Figure 19-25. Note that in this example one measurement has been determined to be invalid with the use of a rectangular gate. Rectangular gates are computationally efficient to implement and computational efficient methods for classifying measurements as valid or invalid are critical to the successful implementation of real-time tracking algorithms. Note in Figure 19-25 that two measurements have been validated by the ellipsoidal gate that is the result of a likelihood test. The border of the ellipse represents a constant contour of the likelihood. Thus, any two measurements on the border of the ellipse will have the same likelihood. The statistical NN measurement is found by drawing a line from the center of the ellipse through each measurement to the border. The measurement with the smallest fraction of the distance to the border is the statistical NN. On the other hand, the PDAF processes both validated measurements with the additional hypothesis that the target was not detected and both measurements are false alarms. The PDAF can be thought to be processing a pseudo-measurement that is a result of blending the two validated measurements and the predicted measurement.

In the remainder of this section, the process of taking an initial, isolated detection to a firm track is discussed, and that is followed by a discussion of measurement validation and gating. Then, the equations for the NN filter, the SN filter, and PDAF are presented.

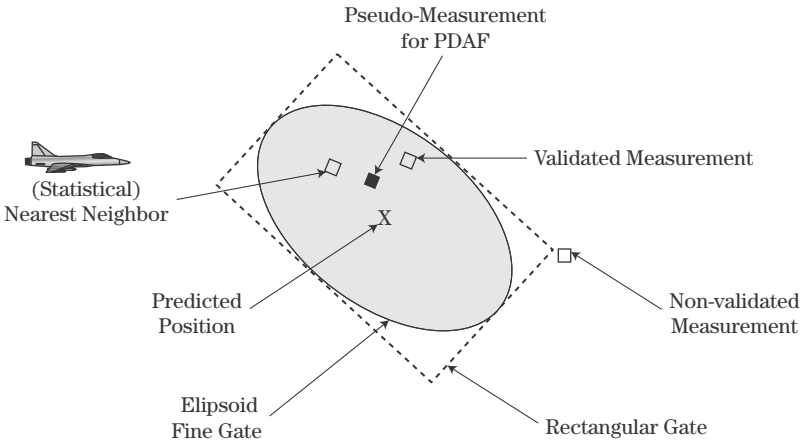

FIGURE 19-25 ■ Measurement validation, gating, and processing for multiple measurements.

- Conventional approach uses statistical nearest neighbor measurement for filtering.
- PDAF uses all validated measurements for filtering, which is conceptually equivalent to using a single pseudo-measurement with inflated covariance.
- PDAF does not directly support threat discriminqation in ballistic missile defense or combat identification in air defense.

19.6.1 Formation of a New Track

When a measurement is formed and it does not associate with any existing track, the measurement is first considered for association to any of the unassociated measurements from the previous scan. The measurements are usually converted to Cartesian coordinates for this assessment. If the distance between the measurement and an unassociated measurement from the previous scan is less than the maximum speed of the target times the scan period, then a tentative track is formed from the two measurements by setting the position estimate to the position of the latest measurement and the velocity estimate to the vector difference between the two measurements divided by the scan period. For rotating targets, the scan period is usually on the order of a few seconds, and the entire surveillance region is observed between the two measurements. The long scan period and large region observed between the two measurements can result in a rather challenging data sorting and management problem. If M measurements of the next the N scans (e.g., 5 of 7) associate to the track, the newly formed tentative track is promoted to a confirmed track.

For phased array radars with electronic scanning, an unassociated detection is usually followed by a confirmation dwell within a fraction of a second after the original detection. Since the scan period is small and the search region covered by a single dwell is also small, the data sorting and management is rather straightforward. Typically, if the confirmation dwell does not find a candidate measurement, the candidate track is dropped. If a measurement is found on the confirmation dwell and it associates to the measurement from the previous scan, a sequence of dwells is scheduled and if M measurements of the next N dwells are associated with the track, then the tentative track is promoted to a firm track.

19.6.2 Measurement Validation and Gating

Any real-time algorithm should include code that verifies the inputs as reasonable and statistically feasible. A computer program will process unreasonable data and produce unreasonable results, and those unreasonable results may drive an operator display, combat identification system, or a weapon system. For tracking, these functions are referred to as *measurement validation* and *gating*, and these functions are critical elements of any real-time tracker. The developers of advanced MTT algorithms such as *multiple hypothesis tracking* (MHT) or *multiple frame assignment* (MFA) often cite efficient and effective gating as critical to a successful implementation of a real-time tracker [2].

Consider a radar system with 1,000 active tracks and a radar dwell that results in five measurements. A brute force approach to the gating would require 5,000 tests or decisions. Since a radar performs a dwell every few milliseconds, a brute force approach is not a reasonable use of computational resources. Measurement gating is typically implemented as a sequence of tests of increasing computational complexity. Coarse gating is typically performed first and it should be a computationally efficient method for eliminating nearly all of the tracks from consideration for association to the measurement. Coarse gating techniques include segmentation of the surveillance space and track partitioning. *Segmentation* involves dividing the surveillance space into contiguous regions and mapping each new measurement into a region or regions. The measurement is then gated with only the tracks identified within that region. *Track partitioning* involves separating the tracks into groups of tracks that can be isolated from all other groups of tracks. The coarse gating is then performed with the centriod of the partition instead of the individual tracks.

Rectangular gating usually follows the coarse gating. Rectangular gating is simple in that it is usually performed in measurement space and involves a series of inequality tests on the individual coordinates of the difference between the measurement and track. Once an inequality test is failed, the track is rejected and no further testing is needed. For radar tracking, the range coordinate eliminates most of the measurement-to-track hypotheses and is often performed first.

The fine or ellipsoidal gating is the final test and performed only for measurement-to-track hypotheses that pass the rectangular gating process. The border of the ellipse as shown in Figure 19-25 represents the location of measurements with equal likelihood, and ellipsoidal gating is a likelihood test of the measurement-to-track hypothesis. Moving the focus back to the single target tracking problem of this section, the likelihood test is evaluated with a *Mahalanobis distance* between measurement i, and it is given by

$$d_k^i = \left(\widetilde{\mathbf{Z}}_k^i\right)^T \left(\mathbf{S}_k^i\right)^{-1} \widetilde{\mathbf{Z}}_k^i \tag{19.205}$$

where $\widetilde{\mathbf{Z}}_k^i$ is the residual of (19.193) between measurement i and the track, and $\mathbf{S}_k^i$ is the covariance of the residual in (19.196) between measurement i and the track and given by

$$\mathbf{S}_k^i = \mathbf{H}_k \mathbf{P}_{k|k-1} \mathbf{H}_k^T + \mathbf{R}_k^i \tag{19.206}$$

If measurement i originated from the target corresponding to the track, then d_k^i is chi-square distributed with n_Z degrees of freedom, where n_Z is the dimension of the measurement. Tables such as Table 1.5.4-1 in [7] for the chi-square distribution are used to select a gating threshold d_{th} for d_k^i with a given probability of gating P_G. Thus, $1 - P_G$ is the probability that measurement i is rejected for the track, given that measurement i originated from the target. That is, $1 - P_G$ is the probability of discarding the correct measurement due

TABLE 19-1 ■ Typical Threshold Values d_{th} for Gating

n_Z	$P_G = 0.995$	$P_G = 0.999$
1	7.88	10.8
2	10.6	13.8
3	12.8	16.3

to failure of the gating test. Some typical gating thresholds d_{th} are given in Table 19-1 for measurement dimensions of one, two, and three. If $d_k^i < d_{th}$, the measurement i is accepted as a validated measurement.

19.6.3 Nearest Neighbor Filter

The NN filter selects the most likely measurement from a group of validated measurements and performs the track filtering as if no uncertainty exists in the selection of the correct measurement. Thus, the state error covariance produced by the NN filter is often optimistic in that it does not reflect the data association errors in the state estimate. The measurement selection of the NN filter is given by

$$NN_k = \underset{1 \le i \le m_k}{\text{argmin}} \left\{ d_k^i \right\} \tag{19.207}$$

where d_k^i is given by (19.205) and the NN_k represents the index of the statistically nearest neighbor measurement at time t_k and argmin{} denotes the argument (i.e., i in this case) that provides the minimum. Then, the NN filter is given by standard equations for prediction or time update and the following equations for the measurement update:

$$\boldsymbol{X}_{k|k} = \boldsymbol{X}_{k|k-1} + \mathbf{K}_k \left[\boldsymbol{Z}_k^{NN_k} - h_k(\boldsymbol{X}_{k|k-1}) \right] \tag{19.208}$$

$$\mathbf{P}_{k|k} = [\mathbf{I} - \mathbf{K}_k \mathbf{H}_k] \mathbf{P}_{k|k-1} \tag{19.209}$$

$$\mathbf{K}_k = \mathbf{P}_{k|k-1} \mathbf{H}_k^T \left(\mathbf{S}_k^{NN_k} \right)^{-1} \tag{19.210}$$

where $\mathbf{S}_k^{NN_k}$ is the residual measurement covariance given by (19.206) for measurement NN_k and $\mathbf{H}_k$ is the linearized output matrix given in (19.197). Note that the measurement update equations do not reflect any uncertainty in the selection of the measurement from a group of m_k validated measurements.

19.6.4 Strongest Neighbor Filter

The SN filter selects the measurement with the highest signal-plus-noise-to-noise ratio (i.e., $\Re_{oi}$) from a group of validated measurements and performs the track filtering as if no uncertainty exists in the selection of the correct measurement. Thus, the state error covariance produced by the SN filter is often optimistic in that it does not reflect the data association errors in the state estimate. The measurement selection of the SN filter is given by

$$SN_k = \underset{1 \le i \le m_k}{\text{argmax}} \left\{ \Re_{ok}^i \right\} \tag{19.211}$$

where $\Re_{ok}^i$ is the observed SNR for measurement i, and SN_k represents the index of the strongest neighbor at time t_k and argmax{} denotes the argument (i.e., i in this case) that provides the maximum. Then, the SN filter is given by standard equations for prediction

or time update and the following equations for the measurement update:

$$\boldsymbol{X}_{k|k} = \boldsymbol{X}_{k|k-1} + \mathbf{K}_k\left[\boldsymbol{Z}_k^{SN_k} - h_k(\boldsymbol{X}_{k|k-1})\right] \tag{19.212}$$

$$\mathbf{P}_{k|k} = [\mathbf{I} - \mathbf{K}_k\mathbf{H}_k]\mathbf{P}_{k|k-1} \tag{19.213}$$

$$\mathbf{K}_k = \mathbf{P}_{k|k-1}\mathbf{H}_k^T\left(\mathbf{S}_k^{SN_k}\right)^{-1} \tag{19.214}$$

where $\mathbf{S}_k^{SN_k}$ is the residual measurement covariance given by (19.206) for measurement SN_k. Note that the measurement update equations do not reflect any uncertainty in the selection of the measurement from a group of m_k validated measurements.

19.6.5 Probabilistic Data Association Filter (PDAF)

The PDAF uses all validated measurements and performs the track filtering while accounting for the uncertainty in the origin of the validated measurements. Thus, one of the most beneficial characteristics of the PDAF is that its state error covariance is nearly consistent and reflects the uncertainty in the measurement-to-track association when tracking a single target. In the PDAF, a measurement update from the Kalman filter is performed for each validated measurement, and the resulting hypothesized tracks are blended with the probability that each is true. Let β_k^i, $1 \le i \le m_k$, denote the probability that measurement i originated from the target. Also, let β_k^0 denote the probability that none of the validated measurements originated from the target. Then

$$\beta_k^i = \begin{cases} \dfrac{e_k^i}{b_0 + \sum_{i=1}^{m_k} e_k^i}, & 1 \le i \le m_k \\ \dfrac{b_0}{b_0 + \sum_{i=1}^{m_k} e_k^i}, & i = 0 \end{cases} \tag{19.215}$$

where

$$e_k^i = \frac{P_D V_k}{m_k\sqrt{|2\pi S_k^i|}}\exp\left[-\frac{1}{2}d_k^i\right] \tag{19.216}$$

$$b_0 = 1 - P_D P_G \tag{19.217}$$

d_k^i is given by (19.205), P_G is the probability of gating the target-originated measurement with the track, P_D is the probability of detection of the target under track, and V_k is the volume of the validation gate.

The PDAF is given by the standard equations for prediction or time update and the following equations for the measurement update.

$$\boldsymbol{X}_{k|k} = \boldsymbol{X}_{k|k-1} + \boldsymbol{U}_k \tag{19.218}$$

$$\mathbf{P}_{k|k} = [\mathbf{I} - \bar{\mathbf{K}}_k H_k]\mathbf{P}_{k|k-1} + \sum_{i=1}^{m_k}\beta_k^i\left[\mathbf{K}_k^i\boldsymbol{\varepsilon}_k^i\right]\left[\mathbf{K}_k^i\boldsymbol{\varepsilon}_k^i\right]^T - \boldsymbol{U}_k\boldsymbol{U}_k^T \tag{19.219}$$

$$\mathbf{K}_k^i = \mathbf{P}_{k|k-1}\mathbf{H}_k^T\left(\mathbf{S}_k^i\right)^{-1} \tag{19.220}$$

where

$$\boldsymbol{U}_k = \mathbf{P}_{k|k-1}\mathbf{H}_k^T\sum_{i=1}^{m_k}\beta_k^i\left(\mathbf{S}_k^i\right)^{-1}\boldsymbol{\varepsilon}_k^i \tag{19.221}$$

$$\boldsymbol{\varepsilon}_k^i = \boldsymbol{Z}_k^i - h_k(\boldsymbol{X}_{k|k-1}) \tag{19.222}$$

$$\bar{\mathbf{K}}_k = \mathbf{P}_{k|k-1}\mathbf{H}_k^T\sum_{i=1}^{m_k}\beta_k^i\left(\mathbf{S}_k^i\right)^{-1} \tag{19.223}$$

The PDAF is often presented in the literature for measurements with covariance that is uniform across all of the validated measurements. Thus, $\mathbf{R}_k^i = \mathbf{R}_k,\ 1 \le i \le m_k$, which implies for radar measurements that $\Re_{ok}^i = \Re_{ok},\ 1 \le i \le m_k$. While this assumption is typically invalid for a set of radar measurements, it does greatly simplify the PDAF equations when made. The measurement update equations for the PDAF with uniform measurement covariances are given by the following equations:

$$\boldsymbol{X}_{k|k} = \boldsymbol{X}_{k|k-1} + \mathbf{K}_k[\bar{\boldsymbol{Z}}_k - h_k(\boldsymbol{X}_{k|k-1}] \tag{19.224}$$

$$\mathbf{P}_{k|k} = \left[\mathbf{I} - \left(1 - \beta_k^0\right)\mathbf{K}_k\mathbf{H}_k\right]\mathbf{P}_{k|k-1} + \mathbf{K}_k\left[\sum_{i=1}^{m_k}\beta_k^i\left[\boldsymbol{\varepsilon}_k^i\right]\left[\boldsymbol{\varepsilon}_k^i\right]^T - \bar{\boldsymbol{\varepsilon}}_k\bar{\boldsymbol{\varepsilon}}_k^T\right]\mathbf{K}_k^T \tag{19.225}$$

$$\mathbf{K}_k = \mathbf{P}_{k|k-1}\mathbf{H}_k^T(\mathbf{S}_k)^{-1} \tag{19.226}$$

where

$$\bar{\boldsymbol{Z}}_k = \sum_{i=0}^{m_k}\beta_k^i\boldsymbol{Z}_k^i \tag{19.227}$$

$$\boldsymbol{Z}_k^0 = h_k(\boldsymbol{X}_{k|k-1}) \tag{19.228}$$

$$\boldsymbol{\varepsilon}_k^i = \boldsymbol{Z}_k^i - h_k(\boldsymbol{X}_{k|k-1}) \tag{19.229}$$

$$\bar{\boldsymbol{\varepsilon}}_k = \sum_{i=1}^{m_k}\beta_k^i\boldsymbol{\varepsilon}_k^i \tag{19.230}$$

19.7 | PERFORMANCE ASSESSMENT OF TRACKING ALGORITHMS

Performance assessment of MTT algorithms is very much an outstanding research problem. The metrics are rather complex and involve such items as track completeness, track switches, track breaks, spurious tracks, and redundant tracks as well as the standard metrics of track accuracy and covariance consistency used in this chapter [31]. One of the major challenges in the assessment of MTT algorithms is the track-to-truth assignment problem [32] that is required to compute any of these metrics. However, performance metrics for tracking a single target are much simpler and track-to-truth assignment is not required, because only one target is present and only one track is generated by the tracker. The discussion of this section is restricted to the accuracy metrics for single target tracking.

Typically, for a Monte Carlo simulation, the kinematic trajectory for the truth object is fixed and the sensor measurement errors are randomized between experiments. The first step for computing the performance metrics involves setting the scoring times (i.e., identifying the times of the scenario when the track filter will be requested to report its best estimate of the kinematic state) throughout the entire scenario or truth trajectory. For each experiment, the squared errors for position and velocity are computed at each scoring time. These errors at each scoring time are averaged across the Monte Carlo experiments giving the RMSEs.

Let the error in the reported track state on the i^{th} Monte Carlo experiment at time t_k be given by

$$\boldsymbol{\varepsilon}_k^{(i)} = \boldsymbol{X}_{k|j}^{(i)} - \boldsymbol{X}_k \tag{19.231}$$

where $\boldsymbol{X}_{k|j}^{(i)}$ is the state estimate at time t_k for experiment i given the most recent measurements at time t_j, $t_j \leq t_k$, and $\boldsymbol{X}_k$ is the true kinematic state at time t_k. Let $\boldsymbol{\varepsilon}_k^{(i)}(n)$ denote the n-th component of $\boldsymbol{\varepsilon}_k^{(i)}$. Then, $[\boldsymbol{\varepsilon}_k^{(i)}(1), \boldsymbol{\varepsilon}_k^{(i)}(3), \boldsymbol{\varepsilon}_k^{(i)}(5)]$ denotes the position vector, and $[\boldsymbol{\varepsilon}_k^{(i)}(2), \boldsymbol{\varepsilon}_k^{(i)}(4), \boldsymbol{\varepsilon}_k^{(i)}(6)]$ denotes the velocity vector. The RMSEs in position and velocity at t_k for M experiments are given by

$$RMSE_k^{pos} = \sqrt{\frac{1}{M}\sum_{i=1}^{M}\left[\left(\boldsymbol{\varepsilon}_k^{(i)}(1)\right)^2 + \left(\boldsymbol{\varepsilon}_k^{(i)}(3)\right)^2 + \left(\boldsymbol{\varepsilon}_k^{(i)}(5)\right)^2\right]} \tag{19.232}$$

$$RMSE_k^{vel} = \sqrt{\frac{1}{M}\sum_{i=1}^{M}\left[\left(\boldsymbol{\varepsilon}_k^{(i)}(2)\right)^2 + \left(\boldsymbol{\varepsilon}_k^{(i)}(4)\right)^2 + \left(\boldsymbol{\varepsilon}_k^{(i)}(6)\right)^2\right]} \tag{19.233}$$

The NEES is used the to measure the quality or consistency of the covariance produced by the estimator. The NEES is a Mahalanobis distance between the estimated state and the true kinematic state and it should reflect the true errors in the estimate relative to the covariance produced by the estimator. A chi-square test is performed to assess the correctness of the covariance matrices. For $\boldsymbol{X}_{k|j}$ of dimension N and M experiments, the NEES is given by

$$C_k = \frac{1}{NM}\sum_{i=1}^{M}\left(\boldsymbol{\varepsilon}_k^{(i)}\right)^T \mathbf{P}_{k|j}^{(i)}\boldsymbol{\varepsilon}_k^{(i)} \tag{19.234}$$

where $\mathbf{P}_{k|j}^{(i)}$ is the state covariance for experiment i at time t_k given the most recent measurements at time t_j. Under the case that the errors in the state estimate are zero-mean Gaussian with covariance $\mathbf{P}_{k|j}^{(i)}$, C_k is chi-square distributed with NM degrees of freedom. For example, consider a track filter the provides state estimates with $N = 6$ and a Monte Carlo simulation with $M = 50$ experiments. Thus, if errors in that state estimate are zero-mean Gaussian and the covariance is accurate, then C_k will be chi-square distributed with 300 degrees of freedom at each time t_k. From Table 1.5.4-1 of [7], C_k should be between 0.87 (261/300) and 1.14 (341/300) 90% of the time. If C_k is greater than 1.14, then the covariance underrepresents the errors in the state estimate, and if C_k is less than 0.87, then the covariance overrepresents the errors.

19.8 FURTHER READING

Further applications of the track filtering concepts of this chapter are discussed in [8]. Some topics include multiplatform-multisensor track filtering, tracking in the presence of electronic attack and electronic protection, modeling radars for assessing tracking performance, and an engineering guide to the IMM estimator. Another topic of interest in radar is tracking with monopulse measurements in the presence of sea-surface induced multipath [33–35]. Advanced track filtering techniques such as particle filters are addressed nicely in [36]. The book includes an introduction to nonlinear filters and particle filters and gives numerous applications. A good introduction to multitarget tracking and measurement-to-track association is given in [5]. The book includes much of the mathematical details that are needed by a novice. Practical insights into the application of

tracking techniques without the mathematical details are presented in [2]. Thus, this book is a good source for those who can add the mathematics on their own. Since all radar tracking problems are actually MTT problems, additional reading about the metrics for performance assessment of MTT algorithms is recommended. One of the greatest challenges to performance assessment of MTT algorithms is the track-to-truth assignment. In other words, in MTT, the tracks in a good simulation do not necessarily map uniquely to the truth objects. The methodologies of assigning tracks-to-truth objects are addressed in [32]. Many of the metrics associated with MTT are presented in [31].

19.9 REFERENCES

[1] Bar-Shalom, Y., and Li, X.R., *Multitarget-Multisensor Tracking: Principles and Techniques*, YBS Publishing, Storrs, CT, 1995.

[2] Blackman, S.S., and Popoli, R., *Design and Analysis of Modern Tracking Systems,* Artech House, Norwood, MA, 1999.

[3] Morris, G., and Harkness, L., (Eds.), *Airborne Pulsed Doppler Radar,* 2d ed., Artech House, Norwood, MA, 1996.

[4] Blair, W.D., Register, A.H.,and West, P.D., "Multiple Target Tracking," W. L. Melvin, Ed., *Principles of Modern Radar Systems*, vol. II, forthcoming.

[5] Bar-Shalom, Y., and Li, X.R., *Estimation and Tracking: Principles, Techniques and Software*, Artech House, Dedham, MA, 1993. (reprinted by YBS Publishing, 1998).

[6] Blair, W.D., and Bar-Shalom, Y., "Tracking Maneuvering Targets with Multiple Sensors: Does More Data Always Mean Better Estimates?" *IEEE Trans. Aerospace and Electronic Systems*, vol. AES-32, no. 1, pp. 822–825, January 1996.

[7] Bar-Shalom, Y., Li, X.R., and Kirubarajan, T., *Estimation with Applications to Tracking and Navigation: Theory, Algorithms, and Software*, John Wiley & Sons, Inc., New York, 2001.

[8] Bar-Shalom, Y., and Blair, W.D. (Eds.), *Multitarget-Multisensor Tracking: Applications and Advances,* vol. 3, Artech House, Dedham, MA, 2000.

[9] Blair, W.D., "Design of Nearly Constant Velocity Filters for Tracking Maneuvering Targets," *Proceedings of the 11th International Conference on Information Fusion*, Cologne, Germany, July 2008.

[10] Kalata, P.R., "The Tracking Index: A Generalized Parameter for Alpha-Beta-Gamma Target Trackers," *IEEE Trans. on Aerospace and Electronic Systems*, vol. AES-20, no. 2, pp. 174–182, March 1984.

[11] Gray, J.E., and Murray, W., "The Response of the Transfer Function of an Alpha-Beta Filter to Various Measurement Models," in *Proc. of 23th IEEE Southeastern Symposium on System Theory,* pp. 389–393, March 1991.

[12] Fitzgerald, R.J., "Effects of Range-Doppler Coupling on Chirp Radar Tracking Accuracy," *IEEE Trans. Aerospace and Electronic Systems*, vol. AES-10, No. 3, pp. 528–532, July 1974.

[13] Wong, W., and Blair, W.D., "Steady-State Tracking with LFM Waveforms," *IEEE Trans. on Aerospace and Electronic Systems*, vol. AES-36, no. 1, pp. 701–709, April 2000.

[14] Bar-Shalom, Y., Chang, K.C., and Blom, H.A.P., "Tracking Maneuvering Targets Using Input Estimation Versus the Interacting Multiple Model Algorithm," *IEEE Trans. Aerospace and Electronic Systems*, vol. AES-25, no. 2, pp. 296–300, March 1989.

[15] Blair, W.D., Watson, G.A., et al., *Information-Based Radar Resource Allocation: FY96 Test-of-Concept Experiment (TOCE),* Technical Report No. NSWCDD/TR-97/22, Naval Surface Warfare Center, Dahlgren Division, Dahlgren, VA, February 1997.

[16] Blom, H.A.P., and Bar-Shalom Y., "The Interacting Multiple Model Algorithm for Systems with Markovian Switching Systems," *IEEE Trans. on Automatic Control Systems*, vol. AC-33, no. 8, pp. 780–783, August 1988.

[17] Watson, G.A., and Blair, W.D., "IMM Algorithm for Tracking Targets That Maneuver Through Coordinate Turns," pp. 236–247 in *Signal and Data Processing of Small Targets 1992* SPIE vol. 1698, ed. O.E. Drummond, 1992.

[18] Watson, G.A., and Blair, W.D., "Multiple Model Estimation for Control of a Phased Array Radar," pp. 275–286 in *Signal and Data Processing of Small Targets 1993,* SPIE vol. 1954, ed. E.O. Drummond, 1993.

[19] Kirubarajan, T., and Bar-Shalom, Y., "Kalman Filter Versus IMM Estimator: When Do We Need the Latter?" *IEEE Trans. on Aerospace and Electronic Systems*, vol. AES-39, no. 4, pp. 1452–1457, October 2003.

[20] Stromberg, D., "Scheduling of Track Updates in Phased-Array Radars," *Proc. of the 1996 IEEE National Radar Conference,* Ann Arbor, MI, pp. 214–219, May 13–16, 1996.

[21] Kirubarajan, T., Bar-Shalom, Y., Blair, W.D., and Watson, G.A., "IMMPDA Solution to Benchmark for Radar Resource Allocation and Tracking in the Presence of ECM," *IEEE Trans. on Aerospace and Electronic Systems*, vol. AES-34, no. 4, pp. 1115–1133, October 1998.

[22] Blair, W.D., *Fixed-Gain, Two-Stage Estimators for Tracking Maneuvering Targets,* Technical Report No. NSWCDD/TR-92/297, Naval Surface Warfare Center Dahlgren Division, Dahlgren, VA, 1992.

[23] Li, X.R., and Jilkov, V.P., "Survey of Maneuvering Target Tracking - Part I: Dynamic Models," *IEEE Trans. Aerospace and Electronic Systems*, vol. AES-39, no. 4, pp. 1333–1364, October 2003.

[24] Blackman, S.S., *Multiple Target-Target Tracking with Radar Applications,* Artech House, Dedham, MA, 1986.

[25] Alouni, A.T., and Blair, W.D., "Use of Kinematic Constraint in Tracking Constant Speed, Maneuvering Targets," *IEEE Trans. Automatic Control,* pp. 1107–1111, July 1993.

[26] Mehra, R.K., "A Comparison of Several Nonlinear Filters for Reentry Vehicle Tracking," *IEEE Trans. on Automatic Control*, vol. 16, no. 3, pp. 307–319, March 1971.

[27] Lerro, D., and Bar-Shalom, Y., "Tracking With Debiased Consistent Converted Measurements Versus the EKF," *IEEE Transactions on Aerospace and Electronic Systems*, vol. AES-29, no. 3, pp. 1015–1022, July 1993.

[28] Mo, L., Song, X., Zhou, Y., Sun, Z.K., and Bar-Shalom, Y., "Unbiased Converted Measurements for Tracking," *IEEE Transactions on Aerospace and Electronic Systems*, vol. AES-34, no. 3, pp. 1023–1027, July 1998.

[29] Daum, F.E., and Fitzgerald, R.J., "Decoupled Kalman Filters for Phased Array Radar Tracking," *IEEE Trans. Automatic Control*, vol. AC-28, no. 3, pp. 269–283, March 1983.

[30] Tian, X., and Bar-Shalom, Y., "Coordinate Convertion and Tracking for Very Long Range Radars," *IEEE Trans. on Aerospace and Electronic Systems*, vol. AES-45, no. 3, pp. 1073–1088, July 2009.

[31] Rothrock, R.L., and Drummond, O., "Performance Metrics for Mulitple-Sensor Multiple-Target Tracking," pp. 521–531 in *Signal and Data Processing of Small Targets 1999,* SPIE vol. 4048, ed. Drummond, 2000.

[32] Drummond, O., "Methodology for Performance Evaluation of Multitarget Multisensor Tracking," pp. 355–369 in *Signal and Data Processing of Small Targets 1999,* SPIE vol. 3809, ed. O.E. Drummond, 1999.

[33] Bruder, J.A., and Saffold, J.A., "Multipath Effects on Low-angle Tracking at Millimetre-wave Frequencies," *IEE Proceedings F,*, vol. 138, no. 2, pp. 172–184, April 1991.

[34] Blair, W.D., and Keel, B.M., "Radar Systems Modeling for Target Tracking," in *Multitarget-Multisensor Tracking: Advanced and Applications,* vol. 3, ed. Y. Bar-Shalom and W.D. Blair, Artech House, Dedham, MA, 2000.

[35] Blair, W.D., and Brandt-Pearce, M., "Statistics of Monopulse Measurements of Rayleigh Targets in the Presence of Specular and Diffuse Multipath," *Proc. of the 2001 IEEE Radar Conference*, Atlanta, GA, pp. 369–375, May 2001.

[36] Ristic, B., Arulampalam, S., and Gordon, N., *Beyond the Kalman Filter: Particle Filters for Tracking Applications,* Artech House, Boston, MA, 2004.

19.10 PROBLEMS

1. *Process observations of a stationary object*. Let the state equation be given by $x_{k+1} = x_k$ and the measurement equation be given by $y_k = x_k + w_k$, with w_k being a Gaussian random process with $E\{w_k\} = 0$ and $E\{w_k^2\} = \sigma_w^2$. Derive the formulas for the LSE and covariance for the state of a stationary object as function of N measurements.

2. *Derive the alpha filter gain for tracking a stationary random process*. Let the state equation be given by $x_{k+1} = x_k + \frac{T^2}{2} v_k$, with v_k being a Gaussian random process with $\mathrm{E}\{v_k\} = 0$ and $\mathrm{E}\{v_k^2\} = q$. Let the measurement equation be given by $y_k = x_k + w_k$, with w_k being a Gaussian random process with $\mathrm{E}\{w_k\} = 0$ and $\mathrm{E}\{w_k^2\} = \sigma_w^2$. Derive expressions for steady-state gain α and covariance for the alpha filter for tracking this stationary random process.

3. *Develop a gain schedule for track initiation*. Use $\mathbf{K}_k = \mathbf{P}_{k|k}\mathbf{H}_k^T\mathbf{R}_k^{-1}$ and the covariance of the LSE from Problem 1 to develop the Kalman gain for the alpha filter of Problem 2 for processing the k-th measurement. The result of this processing is a LSE through the k^{th} measurement.

4. *Derive the sensor noise only (SNO) variance*. Given the measurement noise variance σ_w^2, derive the SNO variance for the alpha filter derived in Problem 2. Hint: Write the current filtered state estimate $(k|k)$ of the alpha filter as a linear difference equation in terms of the previous filtered state estimate $(k-1|k-1)$ and the measurement. Then let the input be zero-mean white noise and compute the variance of the output in terms of the variance of the input.

5. *Derive the filter bias for a moving target*. Given a constant velocity target of velocity V_0, derive the lag or bias in the position estimates relative to the true values for the alpha filter derived in Problem 2. Hint: Write the alpha filter as a linear difference equation in terms of the previous filtered state and the measurement as a kTV_0 and use a z transform.

6. *Derive the bounds for the process noise variance*. Given targets that maneuver as much as 30 m/s^2, a sensor measurement rate of 2 s, and measurement variance of 1600 m^2 for the nearly constant velocity filter with discrete white noise acceleration acceleration (DWNA), find the minimum acceptable process noise variance and the process noise variance that minimizes the maximum mean squared error (MMSE).

7. *Compute the MMSE*. Compute the MMSE for the position and velocity estimates for the maximum acceleration of target and both values of the process noise variance found in Problem 6.

8. *Find the number of measurements required*. Given a sensor measurement rate of 1 s and measurement variance of 625 m^2, find the minimum number of measurements required to achieve a variance of the velocity estimate that is less than than 100 m^2/s^4.

9. *Derive the LSE and covariance for tracking with LFM waveforms*. Derive the formulas for the LSE and covariance for the state of a constant velocity object as function of N measurements. Let the state and measurement equations be defined by

$$\begin{aligned} \boldsymbol{X}_k &= [\, r_k \quad \dot{r}_k \,]^T \\ \mathbf{F}_k &= \mathbf{F} = \begin{bmatrix} 1 & T \\ 0 & 1 \end{bmatrix} \\ \mathbf{H}_k &= \mathbf{H} = [\, 1 \quad \Delta t \,] \\ R_k &= R = \sigma_r^2 \end{aligned}$$

where r_k and $\dot{r}_k$ are the range and range rate of the target, respectively, σ_w^2 is the variance of the measurement errors, T is the sample period between measurements, and Δt is the range-Doppler coupling coefficient.

10. *Develop a gain schedule for track initiation*. Use the covariance of the LSE from Problem 9 to develop a gain schedule for processing the k-th measurement with the alpha-beta filter for tracking with LFM waveforms. The result of this processing is a LSE through the k-th measurement.

11. *Investigate the need for an unbiased transform*. Consider a target at a range of 1,000 km and bearing of zero. Thus, the Cartesian position of the target is $(x, y) = (1000, 0)$ km. Consider a radar that measures the bearing with errors of standard deviation of 3 mrad and range with errors of standard deviation of 25 m. For this radar-target scenario, use the criteria in (19.162) to assess the need for an unbiased transform of spherical to Cartesian coordinates in this case. Simulate 2,000 measurements of range and bearing by adding Gaussian errors to the true range and bearing of the target. Convert the measurements to Cartesian x and y, and plot the converted measurements. Compute the sample mean and sample covariance of the measurements in Cartesian space. The sample covariance is computed by subtracting the sample mean from each sample and forming the outer product of it with itself and then computing a sample average. Next, compute the measurements directly in Cartesian space as Gaussian errors in the x coordinate with standard deviation of 25 m and Gaussian errors in the y coordinate with standard deviation of 3,000 m. Plot these measurements. Do the two distributions of the measurements appear similar in Cartesian space? Repeat the above for a radar measuring range with a standard deviation of 1 m.

12. *Investigate the PDAF for a single validated measurement*. Consider the case of processing a single measurement with the PDAF. Consider a radar that measures the bearing with errors of standard deviation of 2 mrad and range with errors of standard deviation of 10 m. Consider a target at a range of 100 km and bearing of zero. Let the covariance of the predicted position in Cartesian coordinates be a diagonal matrix with standard deviations of 20 m in the x coordinate and 200 m in the the y coordinate. From the chi-squared tables, what is the gating threshold for a probability of gating of 0.999? For probabilities of detection of 0.5, 0.75, and 0.95, compute and plot β_k^1 versus the Mahalanobis distance (i.e., d_k^1) from 0 to the gating threshold. For a validated measurement near the edge of the gate and $P_D = 0.5, 0.75$, and 0.95, how much will the effect of the Kalman gain be reduced by the consideration that a false alarm may have been detected in place of the actual target?

13. *Design and analyze a radar tracking algorithm*. Consider a surveillance radar that measures range and bearing and scans with a period of 4 s. The radar measures range with standard deviation of 25 m and bearing with standard deviation of 0.02 degree. Targets that perform maneuvers with acceleration as much as 30 m/s^2 are expected. Use the design techniques of Section 19.2.2.1 to find process noise covariances for tracking in range and cross-range. Make a small angle assumption to approximate the cross-range errors in Cartesian space. The process noise covariance for tracking in cross-range will be a function of the range of the target. The radar is to track targets at ranges from 5 km to 400 km. (a) Recommend a single process noise covariance tracking targets at all ranges in the field of regard. (b) Recommend a range dependent function for selecting the process noise covariance for both coordinates for tracking.

(c) Develop a formulation of the process noise covariance that accounts for a different process noise variances in the range and cross range coordinates. It will be a function of the bearing of the target. (d) Assume target maneuvers are restricted to 30 m/s^2 perpendicular to the velocity vector of the target and 10 m/s^2 along the velocity vector. Extend the results of (c) to include these limitations on the target acceleration in the selection of the process noise covariance. (e) Consider a target starting at (250, 250) km and moving with a velocity of (−150, −150) m/s. After 100 s, the target maneuvers with acceleration of (−7, −7) for 15 s. At 200 s, the target starts maneuvering with acceleration of (20, −20) m/s^2 and the acceleration is orthogonal to the velocity for 16 s. At 300 s, the target starts maneuvering with acceleration of 24 m/s^2 orthogonal to the velocity for a right turn for 16 s. At 400 s, the target slows down at 10 m/s^2 for 15 s. The scenario ends at 500 s. Simulate the target and radar and compare the performances of the four track filter designs with 200 Monte Carlo runs. (f) Implement an IMM estimator with two NCV filters and compare its performance with that of the NCV filters. Use the NCV filter formulation of (d) and use the process noise covariance the minimizes the MMSE as the maneuver model.